

# **Building skin as energy supply:**

## **Prototype development of a wooden prefabricated BiPV wall**

Laura Maturi



UNIVERSITÀ DEGLI STUDI DI TRENTO

Dipartimento di Ingegneria Civile,  
Ambientale e Meccanica

Department of Civil,  
Environmental and Mechanical Engineering

in cooperation with



Institute for Renewable Energy

**2013**

Supervisors:  
Prof. Paolo Baggio,  
Ing. Roberto Lollini,  
Ing. Wolfram Sparber



Doctoral thesis in Environmental Engineering, XXV cycle

Faculty of Engineering, University of Trento

Academic year 2012/13

Supervisors: Prof. Paolo Baggio, University of Trento

Ing. Roberto Lollini, Eurac

Ing. Wolfram Sparber, Eurac

University of Trento

Trento, Italy

2013





*To Francesco  
and Agostino  
-With love-*



## Acknowledgements

The author would like to thank the following people for their assistance and contribution during the course of this study:

My promoters Prof. Paolo Baggio, Ing. Roberto Lollini, Ing. Wolfram Sparber who have supported and guided my activities.

The Network Chi Quadrato with FESR for the realization of the prototype, and IEA Task 41 “Solar Energy and Architecture” experts.

My colleagues at EuracTec, who contributed actively in supporting my activities, without whom this work would not exist: Roberto Lollini again, for his constant and active presence during all the thesis development, Paolo Baldracchi for his essential help in all fields (energy simulations, test in laboratory, data elaboration), David Moser for the precious support to improve the results of this work and for revising the thesis in a very effective way [see Lollini-Moser plot], Stefano Avesani and Alessia Giovanardi for their contribution during the test and for all interesting discussions, Ludwig Kronthaler for his smart way to always find proper solutions to any problem during the test in SoLaRE-PV lab, Walter Bresciani for the nice electrical cabinet, Giorgio Belluardo for the “ABD data”, Ulrich Filippi for the “mathematical discussions”, Radko Brock for the experiments suggestions, David Cennamo for the software elaboration, Matteo Del Buono for his inputs and suggestions, Siegfried from Stahlbau Pichler for the precious technical support, Alessandra Colli for her enthusiasm in encouraging me and for the many international contacts she managed to create and bring in our group, Lorenzo Fanni for the help with resistors and many issues, Miglana Dimitrova for the discussions and support. All my colleagues and former colleagues at Eurac, who have created a warm and friendly working environment: Francesco<sup>2</sup> of course, Patrizia, Gabriella, Cristiana, Alexa, Francesca, Chiara, Giulia, Annamaria, Elisabetta, Marco, Roberto V., Hannes, Davide, Matteo D., Dagmar, Federico, Monika, Marina, Alexandra, Filippo, Roberto F., Daniele, Adriano, Philip, Simon, Anton, Alice, Alessio, Florian, Markus.

My special friends Federica, Silvia, Maria, Serena and Michele.

Finally, special thanks to my parents, to Francesca with Roberto and Fabiano with Claudia. Grazie!



---

# TABLE OF CONTENTS

TABLE OF CONTENTS .....	i
LIST OF FIGURES.....	vi
LIST OF TABLES .....	xiii
LIST OF SYMBOLS.....	xv
ABSTRACT.....	xvii
<b>CHAPTER 1 Introduction .....</b>	<b>1</b>
1.1 Introduction.....	3
1.2 Thesis structure .....	5
References .....	7
<b>CHAPTER 2 State of the art .....</b>	<b>9</b>
2.1 PV technological integration into the envelope.....	11
2.2 PV topological integration into the envelope .....	13
2.2.1 Roof integration .....	13
2.2.2 Façade integration.....	16
2.2.3 Façade vs roof integration.....	18
2.3 Limitations, needs and IEA Task 41 recommendations.....	19
References .....	21
<b>CHAPTER 3 Prototype development.....</b>	<b>23</b>
3.1 Introduction.....	25
3.2 Development process methodology .....	26



---

3.3	Concept.....	28
3.3.1	Integration concept.....	29
3.3.2	Multi-functionality concept .....	30
3.3.3	Sustainability concept.....	31
3.3.4	Prefabrication concept.....	32
3.4	Theoretical study .....	33
3.4.1	PV technology and integration issues.....	33
3.4.2	PV performance .....	41
3.4.3	Building performance .....	53
3.5	Prototype design .....	63
3.6	Prototype application .....	64
	References .....	68
	<b>CHAPTER 4 Experimental campaign.....</b>	<b>73</b>
4.1	Introduction.....	75
4.2	INTENT Lab.....	77
4.2.1	Measurement sensors.....	79
4.3	SoLaRE-PV Lab.....	80
4.3.1	Measurement sensors.....	81
4.4	The use of INTENT and SoLaRE-PV Labs (phase 2&3).....	82
4.5	The specimen .....	83
4.5.1	Specimen construction drawing .....	83
4.5.2	Specimen construction: the industrial collaboration.....	84
4.6	Phase 1: “Bi” characterization.....	85
4.6.1	Aim of the test .....	85
4.6.2	Experimental setup .....	87

---

4.6.3	Results .....	88
4.7	Phase 2: “PV” characterization.....	89
4.7.1	Aim of the test .....	89
4.7.2	Experimental setup .....	90
4.7.3	PV module preconditioning.....	90
4.7.4	Results .....	93
4.8	Phase 3: “PV in Bi” characterization .....	97
4.8.1	Aim of the test .....	97
4.8.2	Experimental setup .....	98
4.8.3	Results .....	102
	References .....	111
	<b>CHAPTER 5 Test results and discussion.....</b>	<b>113</b>
5.1	Introduction.....	115
5.2	“Bi” performance .....	116
5.3	PV” performance .....	117
5.3.1	BiPV façade system: Ex-Post Building.....	117
5.3.2	BiPV roof system: Milland Church .....	120
5.3.3	Ground mounted PV system: ABD PV plant .....	123
5.3.4	BiPV wall prototype.....	127
5.3.5	Performance comparison with BiPV wall prototype .....	129
5.3.6	Generalization of results over one year time period.....	132
5.4	Further PV performance improvement due to fins application.....	137
5.4.1	Generalization of results to other PV technologies.....	139
5.4.2	Generalization of results over one year time period.....	145
	References .....	149

---

<b>CHAPTER 6 Summary, conclusions and future development .....</b>	<b>151</b>
6.1 Summary.....	153
6.1.1 Concept.....	153
6.1.2 Theoretical study .....	154
6.1.3 Prototype design and application .....	156
6.1.4 Experimental campaign .....	156
6.2 Conclusions.....	160
6.2.1 General achievement.....	160
6.2.2 Experimental approach .....	160
6.2.3 “Bi” performance .....	161
6.2.4 Effectiveness of the BiPV prototype configuration .....	161
6.2.5 Influence of “PV” on “Bi” and of “Bi” on “PV” .....	163
6.2.6 Explicit correlation for façade integrated PV operating temperature .....	164
6.2.7 NOCT model vs experimental data .....	165
6.2.8 Factors influencing effectiveness of fins application .....	165
6.2.9 Effectiveness of fins application in the prototype.....	166
6.2.10 Estimated effectiveness of fins application for different PV technologies .....	167
6.3 Research limitations and future developments .....	168
<b>BIBLIOGRAPHY .....</b>	<b>171</b>
<b>ANNEXES .....</b>	<b>181</b>
Annex A.....	183
Drawing of INTENT calorimeter.....	186
Sensors positioning -phase 1- .....	187

---

Sensors positioning -phase 3- .....	189
Measurements of phase 2 .....	191
Annex B .....	195
Outdoor temperature coefficients of six different technologies ....	197
Annex C .....	199
IEA Task 41 project “Solar Energy and Architecture” .....	201
FP7 project “Solar Design - On-the-fly alterable thin-film solar modules for design driven applications” .....	207

---

## LIST OF FIGURES

Figure 2.1: Solar laminate integrated into metal roof system.....	13
Figure 2.2: Left: Schüco façade SCC 60 and its application. Right: Schüco façade module ProSol TF and its application, © Schüco.....	13
Figure 2.3: roof systems: Solar tile © SRS Sole Power Tile, Solar slate © Megaslate, Solar slate © Sunstyle Solaire France .....	14
Figure 2.4: Left: special rack system for flexible laminate on stainless steel substrate, © Unisolar. Centre: Powerply monocrystalline module with plastic substrate © Lumeta, Right: Biohaus, Germany, plastic substrate, © Flexcell. ....	15
Figure 2.5: semi-transparent skylights. Left: Community Center Ludesch, Austria, Herman Kaufmann: semi-transparent modules with crystalline cells © Kaufmann. Right: Würth Holding GmbH HQ: semi-transparent thin film modules © Würth Solar. ....	16
Figure 2.6: PV facade cladding solutions. Left: Solteature Solartechnik GmbH, Berlin, Germany, © Solteaturel. Right: Paul-Horn Arena, Tübingen, Germany, Alman-Sattler-Wappner, © Sunways. ....	17
Figure 2.7: warm façade solution. Zara Fashion Store, Cologne, Germany, Architekturbüro Angela und Georg Feinhals: opaque monocrystalline cells combined with transparent glazing in post-beam curtain wall structure, © Solon. ....	17
Figure 2.8: Left: Schott Headquarter Mainz, translucent thin film module, © Schott; right: GreenPix Media Wall, Beijing, China, Simone Giostra & Partners, frameless modules with spider glazing system, © Simone Giostra & Partners/Arup. ....	18
Figure 2.9: How the orientation affects BiPV installation in Europe [2.1].....	19
Figure 2.10: Comparison of the monthly sun radiation available on a 33° south exposed optimal tilted surface vs. a vertical south exposed surface in Zurich, Switzerland (Middle Europe latitude). ....	19
Figure 3.1: Process that guided the development of the BiPV prototype, from the concept to the construction.....	27

---

Figure 3.2: Conceptual schema of the four key concepts that originated the prototype development. ....	28
Figure 3.3: multi-layering concept: the prototype is conceived as a wall package made of several layers with several functions. ....	30
Figure 3.4: Conceptual schema: the building envelope could be conceived not only as a passive component which provides protection from the outside conditions, but also as an active system able to produce energy. ....	31
Figure 3.5: Example of prefabricated wooden panels during manufacturing phase (on the left) and installation on site (on the right, [source: Promolegno]) .....	32
Figure 3.6: Colour palette for monocrystalline cells, © System Photonics .....	38
Figure 3.7: Multicrystalline silicon wafers; first the blue antireflective standard color with the best efficiency, the second is the original wafer without reflective layer, then cells with other colours that have different anti-reflective layers, © Sunways .....	38
Figure 3.8: Coloured thin film modules in reddish brown, chocolate-brown, hepatic and sage green colour, © Rixin .....	38
Figure 3.9: Different PV module typologies, which originate different textures [source: Eurac, ABD experimental PV plant] .....	39
Figure 3.10: Horizontal section of three wooden prefabricate wall types .....	40
Figure 3.11: multifunctional characteristics of the BiPV prototype, based on [3.13] reccomandations.....	41
Figure 3.12: Vertical section of the specimen with the schema of the natural ventilation concept: the air in the gap cools the PV modules.....	44
Figure 3.13: examples of CPU heat-sinks. On the right: a fan-cooled heat sink on the processor of a personal computer with a smaller heat sink cooling another integrated circuit of the motherboard .....	45
Figure 3.14: different geometry configurations of the air gap behind the PV module, as investigated by Friling et al. [3.28] and Tonui et al. [3.14] ..	46
Figure 3.15: the zoom shows the L shape of the aluminium fin attached to the back side of the PV modules .....	47
Figure 3.16: The pictures show the fins applied on a 6mm glass. ....	48

---

Figure 3.17: temperature distribution of the PV module simulated with the FEM software THERM (developed by Lawrence Berkeley National Laboratory). .....	49
Figure 3.18: temperature distribution of the PV module simulated with the FEM software THERM (developed by Lawrence Berkeley National Laboratory) .....	51
Figure 3.19: The images show the temperature distribution of the PV module with and without attached metal fin, simulated with the FEM software THERM (developed by Lawrence Berkeley National Laboratory) in average summer conditions (as described in Table 3.2). .....	52
Figure 3.20: The images show the temperature distribution of the PV module with and without attached metal fin, simulated with the FEM software THERM (developed by Lawrence Berkeley National Laboratory) in average winter conditions (as described in Table 3.2). .....	52
Figure 3.21: the U-value (i.e. thermal transmittance) calculated considering the prototype with and without PV modules. ....	56
Figure 3.22: dimensions of each layer of the prototype.....	58
Figure 3.23: schema of the considered sections a, b, c and d.....	59
Figure 3.24: Schema of the considered resistances to calculate the upper limit of the total thermal resistance .....	59
Figure 3.25: schema of the considered layers of the prototype.....	61
Figure 3.26: Schema of the considered resistances to calculate the lower limit of the total thermal resistance .....	61
Figure 3.27: design of the frontal view and horizontal section of the prototype. The horizontal section is made of the following layers : .....	63
Figure 3.28: preliminary hypothesis for the BiPV wall prototype positioning. ..	65
Figure 3.29: Visibility: module aesthetical perception vs observer position. ...	66
Figure 3.30: Rendering of the elementary school that was designed as a prototypical building within the project “Chi Quadrato” .....	66
Figure 3.31: architectural drawings and details of the BiPV wall prototype integrated in the elementary school design. ....	67
Figure 4.1: The diagram shows the organization of the experimental campaign, which is divided into three phases.....	76

---

Figure 4.2: INTENT Lab at Eurac: the calorimeter with the sun simulator and the hydraulic circuit.....	78
Figure 4.3: general schema of INTENT lab, which is made of. ....	78
Figure 4.4: PV-SoLaRE Lab at Eurac: the sun simulator and the climatic chamber .....	81
Figure 4.5: The diagram shows the concept behind the organization of the experimental campaign related to phase 2 and 3. ....	82
Figure 4.6: frontal view and horizontal section of the specimen (see annex A for further details).....	83
Figure 4.7: The specimen built by two enterprises belonging to the network Chi-Quadrato. ....	84
Figure 4.8: guarded hot box as foreseen by the UNI EN ISO 8990 [3.1], where: 1 is the metering box, 2 is the guarded box, 3 is the cold chamber and 4 is the specimen. ....	85
Figure 4.9: calibration and surrounding panel in the frame of the guarded hot-box .....	86
Figure 4.10: drawing of the calorimeter with the specimen during test of phase 1. ....	87
Figure 4.11: Normalized Pmax (i.e. normalized to the value of Pmax at M1, before light soaking) against light-soaking cycles referred to the no-fins CIGS module (NF) and the CIGS module with fins (WF). ....	92
Figure 4.12: Surface that interpolate the measured maximum power point values of the module without fins (NF) at different temperature and Irradiance conditions. ....	94
Figure 4.13: Measured maximum power point values of the module with fins (WF) at different temperature and Irradiance conditions. ....	94
Figure 4.14: Pmppt values of the module no fins at 1000W/sqm (AM 1.5) as function of the device temperature (over a range of 50°C) with a least-squares-fit curve through the set of data. ....	95
Figure 4.15: $\gamma$ and $\gamma_{rel}$ of the NF and WF modules are plotted for each irradiance value (AM 1.5) from the measured Pmppt values .....	97
Figure 4.16: test devices used during experiments of phase 3 .....	100
Figure 4.17: Positioning of the temperature, air velocity and irradiance sensors during the third phase of the experimental campaign .....	101



---

Figure 4.18: Measured average values of modules temperature (NF and WF) at twenty different set point conditions of air temperature and irradiance. ....	102
Figure 4.19: I-V characteristic curve of the WF module (above, on the left), the NF module (above, on the right) and of both modules connected in series (below) measured with a peak power measuring device with I-V-Curve tracer at an irradiance of 797W/sqm. ....	103
Figure 4.20: Measured average values of modules temperature (NF and WF) and resulting $\Delta T$ between them at twenty different set point conditions of air temperature and irradiance, after applying the filtering procedure to eliminate transient points.....	104
Figure 4.21: test boundary conditions of air velocity, air temperature and irradiance kept in the calorimeter cold chamber during the experiment.....	105
Figure 4.22: test boundary conditions of air temperature and air velocity measured in the air gap between the modules and the wooden wall during the experiment. ....	105
Figure 4.23: Approximated surface through the average T measured values of the two modules depending on $T_{air}$ and Irradiance.....	106
Figure 4.24: Approximated surface through the $\Delta T$ measured data depending on $T_{air}$ and Irradiance.....	108
Figure 4.25: AM1.5 spectrum and corresponding spectral response of different solar cell materials. The spectral response of various materials is indicated by the boxes [4.12].....	109
Figure 5.1: Schema linking the two test phases. ....	115
Figure 5.2: Pictures of Ex Post Building with a schema of the building plant showing the pictures point of view [source of pictures: www.expost.it].....	117
Figure 5.3: mounting system of the modules integrated in the Ex Post building façade [source: Elpo] .....	118
Figure 5.4: Module ( $T_{mod}$ ) and air ( $T_{air}$ ) temperature difference against Irradiance values and least-squares-fit line through the set of data (with additional constraint $T_{mod}-T_{air}=0$ when $Irr=0$ ), referred to Ex-Post BiPV system .....	119

---

Figure 5.5: Picture of the roof integrated PV system of the Milland Church in Bressanone (North of Italy).....	120
Figure 5.6: On the left: picture of the BiPV system highlighting the inlet and outlet air gap sections. On the right: zoom which shows the reduced air gap section.....	121
Figure 5.7: Module ( $T_{mod}$ ) and air ( $T_{air}$ ) temperature difference against Irradiance values and least-squares-fit line through the set of data (with additional constraint $T_{mod}-T_{air}=0$ when $Irr=0$ ), referred to Milland Church BiPV system.....	122
Figure 5.8: ABD PV Plant. Experimental plant on the left and commercial part on right .....	123
Figure 5.9: meteo station at ABD PV Plant .....	124
Figure 5.10: The analysed PV systems at ABD: mono-crystalline back-contact technology [source:Eurac].....	125
Figure 5.11: schema of the positioning of the two PT100 on the back side of the modules [source:Eurac]. .....	125
Figure 5.12: Module ( $T_{mod}$ ) and air ( $T_{air}$ ) temperature difference against Irradiance values and least-squares-fit line through the set of data (with additional constraint $T_{mod}-T_{air}=0$ when $Irr=0$ ), referred to the mono-crystalline back-contact technology at ABD plant. ....	126
Figure 5.13: Module ( $T_{mod}$ ) and air ( $T_{air}$ ) temperature difference against Irradiance values and least-squares-fit line through the set of data (with additional constraint $T_{mod}-T_{air}=0$ when $Irr=0$ ), referred to the NF module of the BiPV wall prototype. ....	127
Figure 5.14: Module ( $T_{mod}$ ) and air ( $T_{air}$ ) temperature difference against Irradiance values and least-squares-fit line through the set of data (with additional constraint $T_{mod}-T_{air}=0$ when $Irr=0$ ), referred to the WF module of the BiPV wall prototype. ....	128
Figure 5.15: plots of Equation 5.1, Equation 5.2, Equation 5.4 and Equation 5.5. ....	129
Figure 5.16: plots of Equation 5.3, Equation 5.4 and Equation 5.5.....	131
Figure 5.17: plots of Equation 5.1, Equation 5.2, Equation 5.3, Equation 5.4 and Equation 5.5. ....	132

---

Figure 5.18: average monthly values of irradiance onto a vertical south facing façade for the two locations Agrigento and Bolzano.....	134
Figure 5.19: Schema of the reference South facing BiPV façade simulated with the commercial software PV-SOL. ....	135
Figure 5.20: interpolation surface of $\Delta P_{NF-WF}$ (as absolute value) in different condition of $T_{air}$ and $Irr$ , as calculated by Equation 5.10 .....	138
Figure 5.21: Outdoor temperature coefficients evaluated with the methodology explained in the previous paragraph, referred to a-Si (on the left, Module 3) and a-Si/ $\mu$ c-Si (on the right, Module 5) technologies. ....	143
Figure 5.22: $\Delta P_{NF-WF}$ distribution over 1 year referred to the prototype positioned South facing (azimuth = $0^\circ$ , tilt = $90^\circ$ ) in Bolzano. ....	146
Figure 5.23: $\Delta P_{NF-WF}$ distribution over 1 year referred to the prototype positioned South facing (azimuth = $0^\circ$ , tilt = $90^\circ$ ) in Agrigento.....	147
Figure 6.1: (from chapter 3) Process that guided the development of the BiPV prototype, from the concept to the experimental campaign. ....	153
Figure 6.2: energy yield and module life-time, normalized by values referred to integration type 1 referred to the climate of Agrigento. ....	163

---

## LIST OF TABLES

Table 3.1: some examples of the cell types available on the market for the two main PV types, i.e. crystalline silicon and thin film. ....	36
Table 3.2: the table shows average values at 12 o'clock for the city of Bolzano (North of Italy) of: global irradiation on a vertical South-oriented surface, air temperature and air velocity. ....	51
Table 3.3: Coefficient of thermal conductivity of each layer (W/mK), referred to numbered items of Figure 3.27.....	56
Table 3.4: L is the reference number of each layer referred to Figure 3.25, s is the thickness (m), $\lambda$ is the thermal conductivity (W/m K), $R_i$ is the resistance of each homogeneous layer (sqm K/W) .....	57
Table 3.5: indoor and outdoor surface resistance calculation.....	57
Table 3.6: Calculation of the upper limit of the total thermal resistance .....	60
Table 3.7: Calculation of the lower limit of the total thermal resistance.....	61
Table 4.1: Technical characteristics of the calorimeter of INTENT Lab .....	78
Table 4.2: Technical characteristics of the climatic chamber of SoLaRE-PV Lab .....	81
Table 4.3: Measured values registered during the test, required by the UNI EN ISO12567-1 [4.2] for the assessment of the thermal transmittance. ...	88
Table 4.4: this table summarizes the main average values measured during the steady conditions used for the thermal transmittance calculation according to the UNI EN ISO12567-1 [4.2] .....	88
Table 4.5: no fins module: power temperature coefficients ( $\gamma$ ) and relative power temperature coefficients ( $\gamma_{rel}$ ), calculated for each irradiance value (AM 1.5) from the measured $P_{mppt}$ values at different temperatures over a range of 50°C (25°C-75°C) .....	96
Table 4.6: with fins module: power temperature coefficients ( $\gamma$ ) and relative power temperature coefficients ( $\gamma_{rel}$ ), calculated for each irradiance value (AM 1.5) from the measured $P_{mppt}$ values at different temperatures over a range of 45°C (30°C-75°C) .....	96

---

Table 4.7: Isc values of the two modules connected in series for different conditions. The values are taken from the measurements of the NF module..... 99

Table 4.8: Voc values of the two modules connected in series for different conditions. The values are calculated multiplying by two the measurements of the NF module. .... 99

Table 5.1: outdoor temperature coefficients as function of irradiance for each PV technology, referred to the installed nominal power  $P_n$ ..... 142

## LIST OF SYMBOLS

Symbol	Definiton
<b>NF</b>	No Fins (refers to the module without fins)
<b>WF</b>	With Fins (refers to the module with fins)
<b><math>P_{mppt}</math></b>	Power at the maximum power point
<b><math>I_{sc}</math></b>	Short circuit current
<b><math>V_{oc}</math></b>	Open circuit voltage
<b><math>\gamma</math></b>	Temperature coefficient of $P_{mppt}$
<b><math>\gamma_{rel}</math></b>	Relative temperature coefficient of $P_{mppt}$
<b><math>T_{mod}</math></b>	PV module temperature
<b><math>T_{air}</math></b>	Air temperature
<b>Irr</b>	Irradiance
<b><math>V_{air}</math></b>	Air velocity
<b>C-Si</b>	Crystalline silicon
<b>m-Si</b>	Mono-crystalline silicon
<b>p-Si</b>	Poly-crystalline silicon
<b>a-Si</b>	Amorphous silicon
<b>a-Si/a-Si</b>	Single junction amorphous silicon
<b>a-Si/<math>\mu</math>c-Si</b>	amorphous/microcrystalline
<b><math>h_{cv\ i}</math></b>	Convective coefficient in the air gap - PV module side-
<b><math>h_{cv\ out}</math></b>	Outdoor convective coefficient -PV module external side-
<b><math>T_i</math></b>	Air temperature in the air gap
<b><math>T_{out}</math></b>	Outdoor air temperature
<b><math>\epsilon_i</math></b>	PV module emissivity - air gap side
<b><math>\epsilon_o</math></b>	PV module emissivity - outdoor side
<b><math>\Delta T_{NF-WF}</math></b>	Average working temperature difference between NF and WF modules [°C]
<b><math>\Delta P_{NF-WF}</math></b>	Power production difference between NF and WF modules, according to $\Delta T_{NF-WF}$ [W]
<b><math>\Delta T_{EX-POST-WF}</math></b>	Average working temperature difference between Ex-Post modules and WF module [°C]
<b><math>\Delta P_{EX-POST-WF}</math></b>	Power production difference between Ex-Post modules and WF modules, according to $\Delta T_{EX-POST-WF}$ [W]
<b><math>\Delta E_{NF-WF}</math></b>	Annual energy production difference between NF and WF modules due to $\Delta T_{NF-WF}$ [kWh/(kWp y)]
<b><math>\Delta E_{EX-POST-WF}</math></b>	Annual energy production difference between Ex-Post and WF modules due to $\Delta T_{EX-POST-WF}$ [kWh/(kWp y)]
<b><math>T_{mod,Ex-Post}</math></b>	Average temperature of the back side of the Ex-Post module
<b><math>T_{mod,Milland}</math></b>	Average temperature of the back side of the Milland Church module
<b><math>T_{mod,m-Si}</math></b>	Average temperature of the back side of the m-Si module at ABD-PV Plant
<b><math>T_{mod,CIGS}</math></b>	Average temperature of the back side of the CIGS module at ABD-PV Plant
<b><math>T_{mod,NF}</math></b>	Average temperature of the back side of the NF module integrated in the prototype
<b><math>T_{mod,WF}</math></b>	Average temperature of the back side of WF module integrated in the prototype

---

---

## ABSTRACT

In the perspective of “nearly zero energy buildings” as foreseen in the EPBD 2010/31/EU [1.3], herein a prototype of a wooden prefabricated BiPV wall is conceived, designed, built and tested.

The prototype key concepts, identified according to the recommendations of the IEA Task 41 project [see annex C], are: multi-functionality, prefabrication, sustainability and integration.

The prototype design is the result of a theoretical study which takes into account both architectural integration aspects and energy performance issues. The latter in particular, is based on the evaluation and improvement of both PV and building-related aspects, through the investigation and implementation of low-cost passive strategies to improve the overall BiPV performance.

A modular specimen of the prototype was built thanks to an industrial collaboration and tested through an experimental approach, based on the combination of several phases performed in two test facilities (i.e. INTENT lab and SoLaRE-PV lab) by means of original experimental set-up.

The effectiveness of the proposed BiPV prototype configuration is proven by comparing the results of the experiments with monitored data of two BiPV systems (a roof and a façade system) located in South Tyrol (North of Italy).

The experimental results are then generalized, providing significant data and experimental expressions for a deeper understanding of BiPV systems energy performance.



---

# CHAPTER 1

## Introduction



## 1.1 Introduction

Present European energy demand is growing continuously, together with the related CO<sub>2</sub> gas emissions in the atmosphere resulting from the use of non-renewable energies.

The building sector accounts for over 40% of the European total primary energy use and 24% of greenhouse gas emissions [1.1],[1.2].

A combination of making buildings more energy-efficient and using a larger fraction of renewable energy is therefore a key issue to reduce the non-renewable energy use and greenhouse gas emissions.

European policy is fostering the use of renewable energies in buildings, setting ambitious goals for the next coming years as foreseen in two strategic directives: the EPBD (energy performance building directive) recast 2010/31/EU [1.3], which states that all new buildings after 2021 will have to be nearly zero-energy and the RES Directive (Renewable Energy Sources) 2009/28/CE [1.4], that requires minimum levels of RES use in all new buildings after 2015.

The essential role of the renewable energies in the building sector is also part of the national (Italian) strategy which recently implemented the RES European Directive in the “RES national action plan” (June 2010) [1.5], foreseeing to introduce a minimum requirement of electric power from RES in the building sector after 2011.

A recent study by the Italian Association Confartigianato [1.6] shows that in 2009 all the residential electrical demand was covered by RES in Italy, underlining the importance of this sector which is growing despite the current economic crisis.

Among renewables in particular, solar energy is an enormous resource considering that the sun is a clean, unlimited and almost infinite energy source, providing each hour on earth as much energy as the whole world needs in a year [1.1].

Within solar technologies, the greatest role is played by photovoltaic systems and promising developments are expected in the BiPV (Building Integrated Photovoltaic) sector (J. Bloem 2008). Numerous market studies (e.g. BiPV Report Global Data, 2011, Frost and Sullivan) suggest that BiPV will be the

fastest growing segment of the whole PV market for the next years. Base case scenarios project that the BiPV market in Europe alone will jump over 2,5 billion Euros until 2015. Furthermore, many European countries are altering their feed-in tariffs in favour of BiPV.

On the other hand, a large portion of the potential to utilize PV systems in buildings still remains unused and it is clear that solar energy use can be an important part of the building design and the building's energy balance to a much higher extent than it is today [1.10].

The reasons for this condition can be ascribed to several aspects: economic factors (such as investment costs and maintenance costs), technical knowledge factors (such as lack of knowledge among decision makers and architects, as well as a general reluctance to "new" technologies) and architectural-aesthetic factors (solar technologies for building use have an important impact on the building's architecture).

An international survey among architects and designers carried out in the context of IEA Task 41 [1.10] (see annex C on IEA Task 41 Project) underlines that one of the main barriers which obstacle the spread of PV systems integrated in buildings is the lack of suitable products developed to satisfy the architects and engineers needs for high quality, formal and conceptual architectural integration.

In this context, the concept of an innovative BiPV prototype has been conceived and developed, with the aim to make available to engineers, architects, manufacturers and clients a new multifunctional façade component able to provide both passive and active functions.

It is a prefabricated wooden façade component with integrated PV, conceived as a multifunctional component able to provide mechanical resistance, thermal insulation, water-tightness and to produce electricity.

The prototype has been designed as a multifunctional prefabricated product, as encouraged by the Task 7 of the IEA PV Power Systems Program [1.7], which identified in standardisation, prefabrication and "low cost" the greatest opportunities for new product developments.

The design of the prototype has been driven by considering both architectural integration aspects and energy performance issues.

The latter in particular regarded both energy saving (i.e. thermal characteristics related to the building envelope) and producing aspects (i.e. electricity production); In fact, the concurrent consideration of these two aspects (saving and producing) is a crucial point for BiPV concept, to evaluate the overall energy performance (considering the “Bi” and “PV” part).

The prototype of such a component has been developed, built with the collaboration of a network of enterprises (Chi Quadrato [1.8]) and tested at the EURAC laboratory (INTENT Lab and SoLaRE Lab [1.9]).

## 1.2 Thesis structure

Chapter 2 gives an overview on the state of the art regarding BiPV systems and presents several examples of current products available on the market.

After this review, the main limitations of current BiPV products are highlighted and the related recommendations for new product development defined in IEA Task 41 project are reported.

Chapter 3 presents the development process which, according to the above mentioned recommendations, lead to the prototype design of a BiPV prefabricated wooden wall. The methodology used and all the steps needed to reach this aim are described: from the definition of the concept, through a theoretical study, to the final prototype design. The possible application of this prototype in the design of a prototypical elementary school is also presented.

Chapter 4 describes the experimental campaign performed on a sample of the designed BiPV wooden wall, which was built thanks to an industrial collaboration with a network of enterprises.

A new experimental approach (based on three phases) is applied and new test set-ups are defined to explore the overall energy performance of the BiPV prototype (both “Bi”, i.e. building and “PV”, i.e. photovoltaic characteristics). Each one of the three experimental phases is described and the single results are reported in this chapter.

In chapter 5, the results obtained from the whole experimental campaign are analysed and discussed. The output of all test phases are linked together and general outcomes are provided regarding the “Bi” and the “PV” performance.

The last chapter, summarizes the main steps of the prototype development process and presents the main related outcomes and conclusions.

Finally, the research limitations, which could represent the starting point for future developments of this work, are highlighted.

## References

- [1.1] Oliver Morton, 2006. Solar energy: A new day dawning?: Silicon Valley sunrise. *Nature* 443, 19-22. doi:10.1038/443019a
- [1.2] IEA Promoting Energy Efficiency Investments - case studies in the residential sector, Paris 2008. ISBN 978-92-64-04214-8
- [1.3] Directive 2010/31/EU of the European Parliament and of the Council of 19 May 2010 on the Energy Performance of Buildings (EPBD)
- [1.4] Directive 2009/28/CE the European Parliament and of the Council of 23 April 2009 on renewable energy sources (RES)
- [1.5] Piano di Azione Nazionale per le Energie Rinnovabili (with reference to Directive 2009/28/CE), Ministero dello sviluppo economico
- [1.6] <http://www.ecologiae.com/energie-rinnovabili/18808/>
- [1.7] T. Schoen, et al, 2001. Task 7 of the IEA PV power systems program- achievements and outlook, Proceedings of the 17th European Photovoltaic Solar Conference.
- [1.8] <http://www.chiquadrato.org/>
- [1.9] <http://www.eurac.edu/en/research/institutes/renewableenergy/default.html>
- [1.10] K. Farkas, M. Horvat et al., 2012. Report T.41.A.1: Building Integration of Solar Thermal and Photovoltaics - Barriers, Needs and Strategies. (available at: <http://members.iea-shc.org/publications/task.aspx?Task=41>)





## CHAPTER 2

### State of the art

#### *Abstract*

This chapter gives an overview on the state of the art regarding BiPV systems. Many examples of products currently available on the market are presented and categorized according to their technological and topological integration characteristics.

After this review, which includes both roof and façade systems, the main limitations of the current systems are highlighted and the related recommendations for new product development defined in IEA Task 41 project are reported.



## 2.1 PV technological integration into the envelope

According to a technological integration classification, PV systems can be divided in two main groups: BaPV (i.e. Building Added Photovoltaics), and BiPV systems (i.e. Building Integrated Photovoltaics).

In the first case, PV modules are simply applied on top of the building skin and they are thus commonly considered just as technical devices added to the building, without any specific technical or architectural function. An example of add-on system could be a typical frame-mounted system attached above an existing roof without any architectural design and not providing any additional function to the existing roof.

As for BiPV systems instead, the PV modules are integrated into the envelope constructive system, being an integral part of the building. PV modules in this case, replace traditional building components and are able to fulfill other functions required by the building envelope (e.g. providing weather protection, heat insulation, sun protection, noise protection, modulation of daylight and security).

BiPV products could be thus seen as multifunctional building components able to produce energy rather than dissipating it.

### **Concept of gradual levels of integration**

Three progressive levels of integrability can be defined according to IEA Task 41 guidelines for BiPV system developments (see annex C on IEA Task 41 project) [2.3]: basic, medium and advanced, which are defined as follows:

#### **Basic level of integrability** (module formal flexibility)

The “basic level” refers to solar systems which are conceived to be adaptive to specific contexts and buildings (both new and retrofits), being able to provide flexibility on a maximum of module characteristics affecting building appearance, such as module shape and size (i.e. offer of a maximum dimensional freedom to cope with the great variability of building dimensional constraints), jointing (i.e. offer of an appropriate selection of jointing to interact correctly with the building envelope), colours and surface finishing.

#### **Medium level of integrability** (non-active elements)

The further integration step refers to the possibility to associate to the PV modules, some non-active elements (called “dummies”), similar to the modules, but fulfilling only the added envelope function; they are conceived to help position and dimension of the whole system field according to building composition needs.

Advanced level of integrability (complete roof/façade system)

The maximum integrability is reached when a complete active envelope system is offered by providing also all the needed complementary elements (jointing/finishing/building functions).

According to [2.3], to develop such integral solar roof/façade systems, two approaches can be considered:

- Start from the module and complete the system by designing all the interface elements around it. This path gives the maximum freedom to designers and might offer some additional functionality to the non-active elements, but at the extensive cost of developing a whole roof/façade concept.
- Start from the roof/façade system. This approach means to adapt the new multifunctional module to an already existing roof/façade system. This option can require some modifications to the module’s initial design and to the original roof/façade system, but in most cases it will be quicker to develop and more cost effective, while offering access to an existing market.

The second approach was recently taken by the several façade and roof manufacturers, i.e. Rheinzink and Schüco. The former, developed a Solar PV Standing Seam and Click Roll Cap roof system using flexible Unisolar thin film laminates, conceived to be compatible with the already existing Rheinzink Standing Seam and Click Roll Cap roof covering system (Figure 2.1). The curtain wall manufacturer Schüco integrated thin film PV into their glazing to be used in ventilated cladding (Façade SCC 60, Figure 2.2) and in thermal insulated glass of windows and curtain wall façades (ProSol TF, Figure 2.2).



Figure 2.1: Solar laminate integrated into metal roof system.  
Left: Click roll cap jointing, Center: Standing seam jointing, Right: Standing Seam System on a curved roof, © Rheinzink



Figure 2.2: Left: Schüco façade SCC 60 and its application. Right: Schüco façade module ProSol TF and its application, © Schüco

## 2.2 PV topological integration into the envelope

The topological integration concept refers to the placement of the PV system in the building envelope. According to this classification, PV modules can be integrated into different parts of the building fabric and it is possible to group them into two macro-categories: facade systems (which include curtain wall products, spandrel panels, glazings etc.) and roof systems (which include tiles, shingles, standing seam products, skylights etc.).

Between these two categories, mixed configurations are also possible, as in the case of many contemporary architectures, where a clear distinction between roof and façade do not exists anymore.

### 2.2.1 Roof integration

According to different levels of technological integration as defined in paragraph 2.1, a PV component can be added on the roof, it can substitute the external layer of the roof system (i.e. PV as a cladding), or it can also

substitute the whole technological sandwich (i.e. semitransparent glass-glass modules as skylights). Depending on the layer(s) the PV component substitutes, it has to meet different requirements that influence the choice of the most suitable PV component.

In the following a general overview of the way PV can be used in roofs will be presented, according to the review performed by IEA Task 41 experts [2.5].

### Opaque - Tilted roof

Building added PV systems have been very common on tilted roofs especially in case of integration into existing buildings. Using this solution there is a need for an additional mounting system and in most cases the reinforcement of the roof structure due to the additional loads.



Figure 2.3: roof systems: Solar tile © SRS Sole Power Tile, Solar slate © Megaslate, Solar slate © Sunstyle Solaire France

The building added PV systems systems on roof have been highly criticized for their aesthetics that urged the market to provide building integrated products replacing all types of traditional roof claddings. There are products both with crystalline and thin film technologies for roof tiles, shingles and slates that formally match with common roof products (Figure 2.3). Several metal roof system manufacturers (standing seam, click-roll-cap, corrugated sheets) developed their own PV products with the integration of thin film solar laminates (Figure 2.1). Moreover there are also prefabricated roofing systems (insulated panels) with integrated thin film laminates available [2.5]. Depending on the insulating features, these PV “sandwiches” can be suitable for any kind of building (i. e. industrial or residential).

### **Opaque - Flat roof**

In the case of flat opaque roofs, the most commonly used systems are: added systems with rack supporting standard glass-Tedlar modules, or specific tilted rack system with thin film laminates (Figure 2.4, on the left).

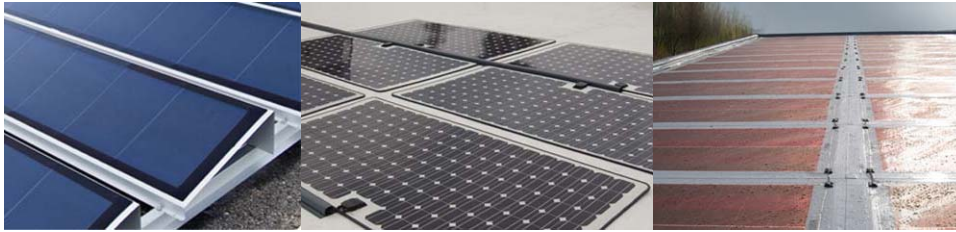


Figure 2.4: Left: special rack system for flexible laminate on stainless steel substrate, © Unisolar. Centre: Powerply monocrystalline module with plastic substrate © Lumeta, Right: Biohaus, Germany, plastic substrate, © Flexcell.

There is also a possibility to use crystalline modules with plastic substrates allowing a seamless integration on the roof with an adhesive backing (Figure 2.4, in the centre). Thin film technologies also offer different flexible laminates, with plastic or stainless steel substrates, that can be easily mounted on flat roofs (Figure 2.4, on the right). A recent trend for flat roof is using the waterproof membrane as a support on which flexible amorphous laminates are glued, providing a simple and economic integration possibility.

### **Semi-transparent roofs**

The PV system can also become the complete roof covering, fulfilling all its functions. Most commonly semi-transparent crystalline or thin film panels are used in skylights (Figure 2.5). These solutions provide controlled day lighting for the interior, while simultaneously generating electricity. Semi-transparent crystalline modules are sometimes custom-made. In this case it could happen that the architect have no technical information and data about the performance of the component from the manufacturer. A simulation or a special test or measurement should then be asked for [2.6],[2.7].

However standard semi-transparent modules have more detailed datasheets with this information.



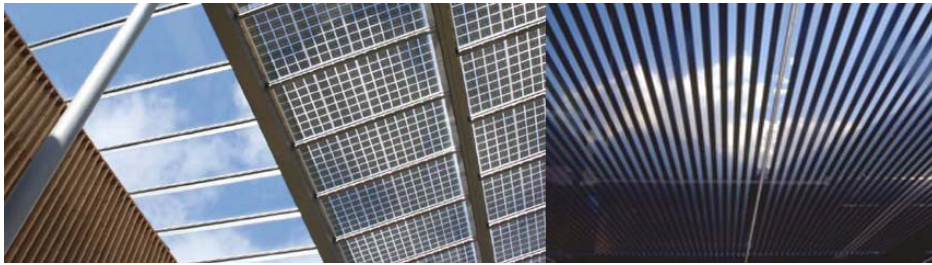


Figure 2.5: semi-transparent skylights. Left: Community Center Ludesch, Austria, Herman Kaufmann: semi-transparent modules with crystalline cells © Kaufmann. Right: Würth Holding GmbH HQ: semi-transparent thin film modules © Würth Solar.

### 2.2.2 Façade integration

According to different levels of technological integration as defined in paragraph 2.1, a PV component can substitute the external layer of the façade (i.e. PV as a cladding of a cold façade), or it can substitute the whole façade system (i.e. curtain walls - opaque or translucent) [2.8]. Depending on the layer(s) the PV component substitutes, it has to meet different requirements that influence the choice of the most suitable PV component.

In the following a general overview of the way PV can be used in façades will be presented, according to the review performed by IEA Task 41 experts [2.5].

#### Opaque - cold facade

Photovoltaic modules can be used in all types of façade structures. In opaque cold façades, the PV panel is usually used as a cladding element, mounted on an insulated load-bearing wall.

In these cases, the PV integration should be carefully evaluated since PV performance could be affected by temperature increasing if the design do not foresee adequate retro-ventilation.

Some fastening systems have been developed for façade cladding, for specific PV modules (Figure 2.6).

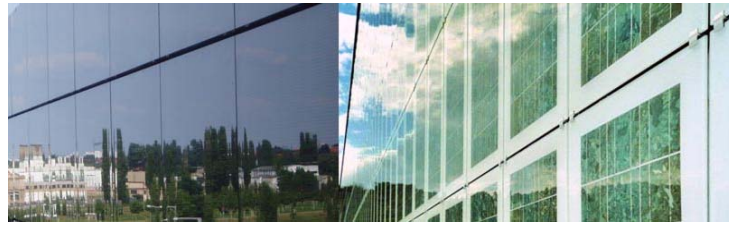


Figure 2.6: PV facade cladding solutions. Left: Soltecture Solartechnik GmbH, Berlin, Germany, © Soltecturel. Right: Paul-Horn Arena, Tübingen, Germany, Alman-Sattler-Wappner, © Sunways.

### **Opaque - non-insulated glazing and warm facade**

Curtain wall systems with single glazing (for non-insulated facades) or double glazing modules (Figure 2.7) also offer opportunities for PV integration. These can be either opaque or semi-transparent/translucent. In these cases, the PV integration should be carefully evaluated since problems with indoor comfort and overheating could occur.



Figure 2.7: warm façade solution. Zara Fashion Store, Cologne, Germany, Architekturbüro Angela und Georg Feinhals: opaque monocrystalline cells combined with transparent glazing in post-beam curtain wall structure, © Solon.

### **Semi-transparent and translucent facade parts**

Semi-transparent PV modules can be integrated in translucent parts of the façade. With crystalline cells, the distance among each cell inside the module can be freely defined, controlling transparency and aesthetical effect (Figure 2.8, on the right).

Also a single crystalline cell can be semi-transparent (due to grooved holes in the cell), but this solution is rarely used for its costs.

With thin-film modules, transparency is created by additional grooves perpendicular to the cell strip, creating a finely checked pattern that gives the

thin-film modules a neutrally coloured transparency (Figure 2.8, on the left).



Figure 2.8: Left: Schott Headquarter Mainz, translucent thin film module, © Schott; right: GreenPix Media Wall, Beijing, China, Simone Giostra & Partners, frameless modules with spider glazing system, © Simone Giostra & Partners/Arup.

When working with a semi-transparent PV in façades, the PV integration should be carefully evaluated since problems with indoor comfort and overheating could occur.

### 2.2.3 Façade vs roof integration

The great majority of BiPV systems have been developed and used for roof integration (see product review in [2.5]).

Roof is in fact considered as the natural location for PV integrated systems in order to optimize the energy efficiency due to the system tilt (see Figure 2.9 and Figure 2.10) and to minimize the aesthetic disturbance.

In fact Figure 2.9 and Figure 2.10 show that in central Europe (e.g. Zurich, Switzerland) the annual solar irradiation of a PV system placed in a south vertical surface is almost constant, and it is reduced by about 30% compared to optimal slope.

However, in the near future, exploitation of roof surface for capturing solar irradiance won't be enough to meet the ambitious goals set by the European policy as for nearly zero energy buildings [2.9],[2.10].

Many studies ([2.12],[2.13],[2.14],[2.15],[2.16]) show that it is crucial to start looking at façade surfaces, which represent a huge potential for solar technologies integration, considering that, as shown in [2.2] about  $\frac{1}{4}$  of the total EU BiPV area potential is attributed to façades.

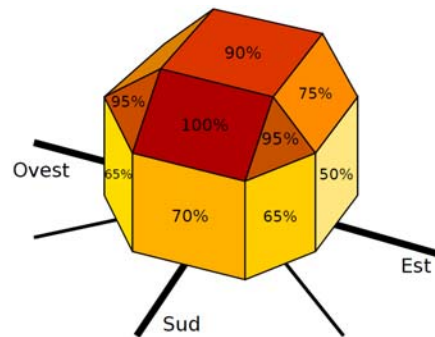


Figure 2.9: How the orientation affects BiPV installation in Europe [2.1]

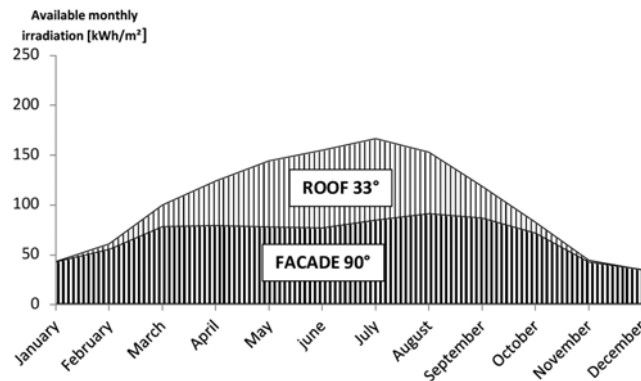


Figure 2.10: Comparison of the monthly sun radiation available on a 33° south exposed optimal tilted surface vs. a vertical south exposed surface in Zurich, Switzerland (Middle Europe latitude). Data elaborated on monthly database of PVGIS [2.1]

### 2.3 Limitations, needs and IEA Task 41 recommendations

Despite the variety of special PV components available on the market to match building integration needs (see previous paragraphs and a BiPV products review in [2.5]), only very few among architects, engineers and designers are using PV technologies in their current architectural practice on a regular basis [2.11].

In order to identify the reasons for this situation and to investigate architects' needs for increased/better use of active solar in their architecture, an international survey was conducted within IEA Task 41 project.

The web-based survey involved about 600 architects/engineers from 14 different countries and it was translated into 10 languages.

According to the survey results, three main topics are here highlighted and are considered as main recommendations for this thesis development:

- Barriers and needs of using active solar systems in architecture:

The results of the survey showed that economic issues are the main driving forces for photovoltaic integration issue: 73% of the interviewed architects identified in high cost the main barrier to overcome and consequently in cost reduction the most important strategy to consider for new product development.

- Satisfaction with actual product offers:

the overall results of this survey regarding the current offer of products that are suitable for successful architectural integration that, although considerable advancements have been made in the development of innovative BiPV systems, there is still quite a lot of room for improvements for new products especially, as architects are still finding it difficult to find suitable products on the current market.

According to what discussed in paragraph 2.2.3, there is a lack of available products especially with regard façade systems despite the huge potential offered by facades for PV integration.

- Integration level requirements:

Regarding the integration level, the survey results showed that building integration is becoming of increasing interest, especially in Europe. Accordingly, IEA Task 41 experts developed possible approaches (as presented in paragraph 2.1) for the development of innovative integral solar roof/façade systems (advanced level of integration concept) [2.3].

These main aspects, resulting from IEA Task 41 project, lead to the definition of the concept for the new prototype developed in this thesis.

The concept is presented in detail in the next chapter.

## References

- [2.1] A. Giovanardi, 2012. Integrated solar thermal facade component for building energy retrofit. PhD thesis, Doctoral School in Environmental Engineering Università degli Studi di Trento.
- [2.2] Marcel Gutschner et al., 2002. Report IEA-PVPS T7-4, Potential for building integrated photovoltaic. IEA Task 7 PVPS “Photovoltaic Power Systems in the Built Environment”
- [2.3] Report T.41.A.3, 2013. Designing photovoltaic systems for architectural integration -Criteria and guidelines for product and system developers, in press.
- [2.4] A. Scognamiglio, P. Bosisio, V. Di Dio, 2009. Fotovoltaico negli edifici, Edizioni Ambiente, ISBN 978-88-96238-14-1.
- [2.5] MC Munari Probst, C Roecker et al., 2012. Report T.41.A.2: IEA SHC Task 41 Solar energy and Architecture. Solar energy systems in architecture - Integration criteria and guidelines. (available at: <http://members.iea-shc.org/publications/task.aspx?Task=41>)
- [2.6] F. Frontini, 2009. Daylight and Solar Control in Buildings: General Evaluation and Optimization of a New Angle Selective Glazing, PhD Thesis, Politecnico di Milano, Fraunhofer Verlag, ISBN 978-3839602386.
- [2.7] F. Frontini, T.E. Kuhn, 2010. A new angle-selective, see-through BiPV façade for solar control. In proceedings of Eurosun Conference 2010, Graz.
- [2.8] C. Schittich et al., 2001. Building Skins - Concepts, Layers, Materials, Birkhauser (2001) Edition Detail, pp.8-27.
- [2.9] Karsten Voss, Eike Musall, 2012. Net zero energy buildings, Detail Green Book, ISBN 978-3-920034-80-5.
- [2.10] Directive 2010/31/EU of the European Parliament and of the Council of 19 May 2010 on the Energy Performance of Buildings (EPBD)
- [2.11] K. Farkas, M. Horvat et al., 2012. Report T.41.A.1: Building Integration of Solar Thermal and Photovoltaics - Barriers, Needs and Strategies. (available at: <http://members.iea-shc.org/publications/task.aspx?Task=41>)
- [2.12] T.T. Chow et al., 2007. An experimental study of façade-integrated photovoltaic/water-heating system. Applied Thermal Engineering 27 (1), 37-45. DOI: 10.1016/j.applthermaleng.2006.05.015

[2.13] G. Quesada et al., 2012. A comprehensive review of solar facades. Transparent and translucent solar facades. *Renewable and Sustainable Energy Reviews* 16, 2643-2651.

[2.14] A. Guardo et al., 2009. CFD approach to evaluate the influence of construction and operation parameters on the performance of Active Transparent Facades in Mediterranean climates. *Energy and Buildings* 41, 534-42.

[2.15] S.P. Corgnati et al., 2007. Experimental assessment of the performance of an active transparent facade during actual operating conditions. *Solar Energy* 81,993-1013.

[2.16] D.Infield D et al., 2004. Thermal performance estimation for ventilated PV facades. *Solar Energy* 76, 93-8.

## CHAPTER 3

# Prototype development

### *Abstract*

This chapter presents the development process which lead to the prototype design of a BiPV prefabricated wooden wall.

The methodology and all the steps needed to reach this aim are described: from the definition of the concept, through a theoretical study involving architectural integration issues as well as photovoltaic and building performance, to the final prototype design.

The last paragraph presents the possible integration of this prototype in a real case study for the design of a prototypical elementary school following an IDP approach (integrated design process).





### 3.1 Introduction

Given the recommendations provided by the IEA Task 41 project for the development of new BiPV products related to architects and designers' needs (as highlighted from the results of an international survey which involved about 600 architects/designers [3.1]), an innovative BIPV façade component is conceived and developed.

This chapter describes the development process which lead to the configuration of such a prototype, from the concept to its realization.

The development process starts with the identification of the main concepts which constitute the motivation and background for this prototype development. After that, a theoretical study is carried out to define the prototype configuration. The theoretical study is based on the evaluation of both photovoltaic and building energy performance.

This approach, focussed on the contemporary consideration of both "PV" and "Bi" aspects, is essential for a successful development of BiPV systems.

Often in the actual practice, one or the other aspects are under-evaluated [3.7].

In addition, a FEM energy simulation campaign is carried out to assist the design phase in order to improve the thermal behaviour of the prototype.

The formal architectural integration issue is also an essential factor which was taken into account during the design phase, as described in detail in paragraph 3.4.1.

## 3.2 Development process methodology

The process that guided the development of the prototype, from the concept to the construction, is synthetically shown in Figure 3.1 and described below.

- Analysis of the context: European and National policies

As already mentioned in the first chapter, two important European Directives such as the Energy Performance Building Directive (2010/31/EU) and the Renewable Energy Sources Directive (2009/28/CE), are paving the way for the development of new ways to conceive the building envelope: from a merely passive system to an active multi-functional system.

At national level, Italy is also supporting and promoting the use of renewable energies in buildings through the Renewable Energy Sources national action plan and the special incentives foreseen for innovative PV integrated systems in the scheme of “conto energia” (5<sup>th</sup> conto energia, DM 507 agosto 2012, at the time of the thesis writing. Also in former Conto Energia, special incentives were foreseen for building integrated PV)

- State of the art: existing BIPV products and limitations

A review of the state of the art of BIPV systems, their problematic and opportunities, is described in the second chapter.

- Concept

The above mentioned steps lead to the definition of the concept, which is described in the next paragraph.

- From theoretical study to experimental campaign

The theoretical study, as described in paragraph 3.4, leads to the configuration of the prototype which is improved through an energy simulation campaign and preliminary tests until the complete definition of the prototype characteristics in the executive design.

Based on the executive design, a specimen of the prototype is then built, thanks to an industrial collaboration, by a network of enterprises called “Chi Quadrato”, that is a consortium gathered together through a local research project (province of Trento L. 6 scheme) entitled “CHI QUADRATO - costruire strutture in bioedilizia certificate per attività

formative” (“Chi Quadrato: construction building of certified green buildings designed for training activities”).

The last step of the development project is an experimental campaign on the specimen, carried out with the Eurac testing facilities, to characterise through experimental data the BiPV system performance and to identify its limits and suggestions for future adjustments, needed before facing an industrialization phase.

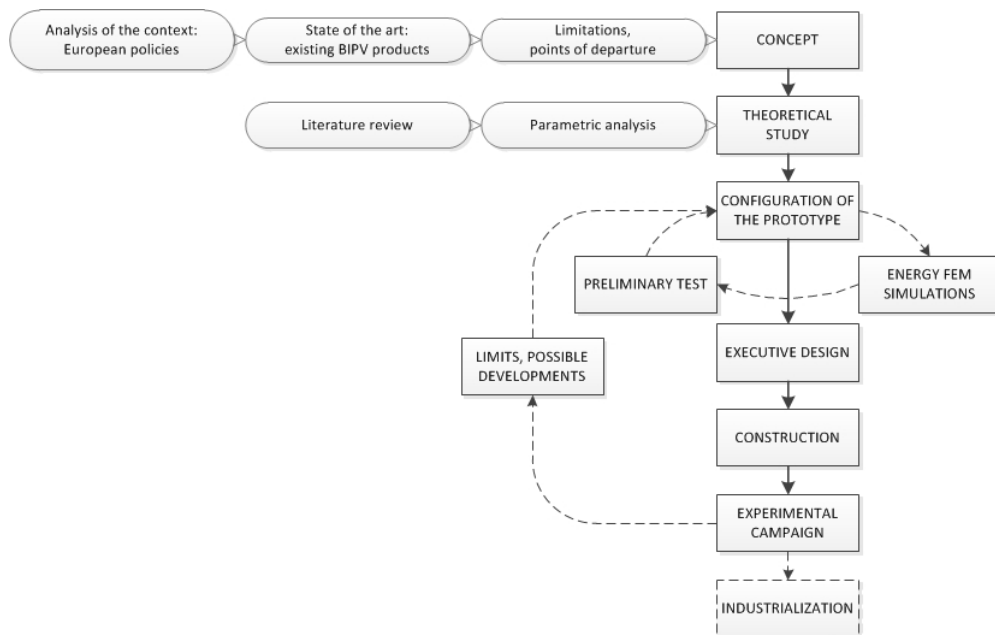


Figure 3.1: Process that guided the development of the BiPV prototype, from the concept to the construction.

### 3.3 Concept

The analysis of the context (in terms of European policies and trends) and of the state of the art on BiPV systems, lead to the definition of the main concepts which are listed below:

- multi-functionality concept: the prototype is conceived to satisfy several building requirements and to produce electricity;
- sustainability concept: the prototype foresees the coupling of the PV technology, which exploits a renewable energy source, with wood, which is an autochthonous material considering the Alpine region where it has been developed;
- integration concept: the PV system is not conceived as an element added as an additional layer to the building envelope, but as a part of it;
- prefabrication concept: to allow a costs reduction, implementation effectiveness, lean construction site and quality enhancement.

Each concept is described in more detail in the next paragraphs.

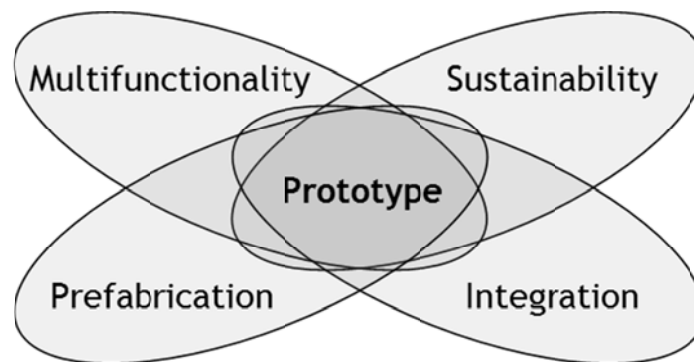


Figure 3.2: Conceptual schema of the four key concepts that originated the prototype development.

### 3.3.1 Integration concept

As already mentioned in paragraph 2.3, three progressive levels of integrability can be defined according to Task 41 guidelines for BiPV system developments [3.6]: basic, medium and advanced.

- Basic level of integrability (module formal flexibility)

The “basic level” refers to solar systems which are conceived to be adaptive to specific contexts and buildings (both new and retrofits), being able to provide flexibility on a maximum of module characteristics affecting building appearance, such as module shape and size (i.e. offer of a maximum dimensional freedom to cope with the great variability of building dimensional constraints), jointing (i.e. offer of an appropriate selection of jointing to interact correctly with the building envelope), colours and surface finishing.

- Medium level of integrability (non-active elements)

The further integration step refers to the possibility to associate to the PV modules, some non-active elements (called “dummies”), similar to the modules, but fulfilling only the added envelope function; they are conceived to help position and dimension of the whole system field according to building composition needs.

- Advanced level of integrability (complete roof/façade system)

The maximum integrability is reached when a complete active envelope system is offered by providing also all the needed complementary elements (jointing/finishing/building functions).

Because the prototype developed in this thesis is conceived from the beginning as a “BiPV” system, it aims to reach the “advanced level of integrability”, developing a “multi-functional façade system” which allows architects/designers to use a complete system where the “integration” issues are already solved and which is characterized both from the building and the photovoltaic point of view.

### 3.3.2 Multi-functionality concept

The commonly shared definition of “BiPV system” states that the main characteristic of such a system is the multi-functionality.

The acronym BiPV in fact refers to systems and concepts in which the photovoltaic element takes, in addition to the function of producing electricity, the role of a building element. This concept opposes to the definition of BaPV (i.e. Building added PV) systems, which refers instead to applications where the PV module is simply added to the building envelope as an additional layer which do not substitute any building material (see BiPV and BaPV definitions in chapter 2).

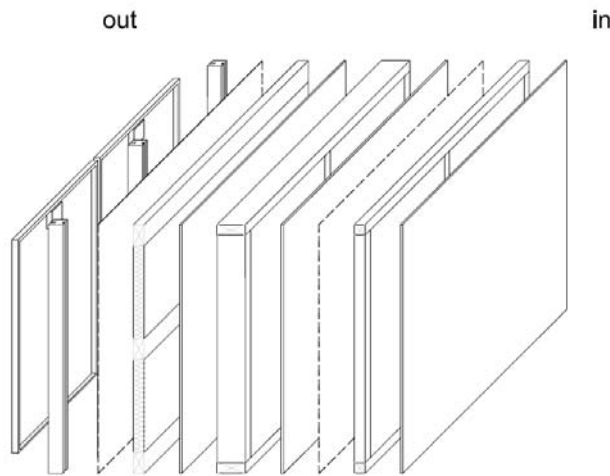


Figure 3.3: multi-layering concept: the prototype is conceived as a wall package made of several layers with several functions. Within this wall package, the PV modules provide the double function to produce electricity and to provide weather protection (replacing the traditional cladding)

This BiPV prototype is conceived as a “multilayer façade system”, in which each layer provides part of the building required functions.

Within this wall package, the PV modules provide the double function to produce electricity and to provide weather protection, thus replacing the traditional cladding.

The final multi-layer package provides the “traditional” functions related to building requirements such as mechanical resistance, thermal insulations, air

and water tightness, weather protection, moisture/condensation protection as well as the “additional” function of producing electricity.

Currently, production of energy is not considered a requirement for building envelope components, but in the next future this concept could represent an option to cover part of a building energy consumption.

In the future in fact, a new approach will be required for building design since buildings will have to be able to produce a part of the energy they consume using renewable energies. Europe is setting ambitious goals for the next coming years to promote the use of renewable energies in the building sector: the EPBD (energy performance building directive) recast 2010/31/EU [3.36] states that all new buildings by 2021 will have to be nearly zero-energy and the RES Directive (Renewable Energy Sources) 2009/28/CE [3.37] requires minimum levels of RES use in all new buildings after 2015.

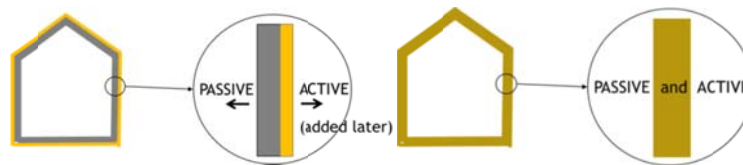


Figure 3.4: Conceptual schema: the building envelope could be conceived not only as a passive component which provides protection from the outside conditions, but also as an active system able to produce energy.

The prototype is thus conceived as a passive and active system which incorporates several functions able to fulfil current and future building requirements.

### 3.3.3 Sustainability concept

The main part of the prototype is made by wood, which is an autochthonous material in the Alpine region where it has been developed. In the region of Trentino Alto Adige in fact, wood represents a leading resource of the local economy because of its copious presence in the territory (the same is for the neighbouring areas such as Tyrol, Vorarlberg and Bavaria). The structural frame is made of wood and the selected insulation materials are based on wood fibres. All materials which constitute the prototype are certified with the European quality mark “Natureplus” [3.33] and “FSC” certification [3.34] [3.38]



[3.39] which guarantee environmentally-friendly production, protection of limited natural resources and suitability of application.

### 3.3.4 Prefabrication concept

An international survey carried out among about 600 architects/designers in the context of IEA Task 41 project (as described in chapter 2) [3.7] highlights that costs are still identified as one of the main barriers which obstacle the use of PV systems in architecture. In fact, even if promising developments are expected in the integration of PV technology in buildings [3.10], costs represent still a barrier for the use of PV as a common building material [3.9].

The prefabrication of an envelope component that integrates a PV system could reduce the installation costs and, at the same time, enhance the overall architectural quality and the energy performance.

The prototype has thus been conceived as a prefabricated product, as also encouraged by the Task 7 of the IEA PV Power Systems Program [3.11], which identified in standardisation, prefabrication and “low cost” the greatest opportunities for new product developments.

All the constituting components are in fact standardized products currently available, which could enhance the production efficiency and accelerate the market penetration. The BiPV product has been conceived to be assembled in the factory under controlled and industrial conditions, with a high degree of automation and high level of accuracy, in order to guarantee high standard quality. The “prefabrication concept” also implies less and faster activities at the construction site carried out by less actors (moving complexity towards farm site), making costs reduction possible and reducing the whole times of completion.

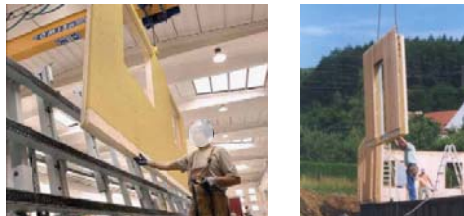


Figure 3.5: Example of prefabricated wooden panels during manufacturing phase (on the left) and installation on site (on the right, [source: Promolegno])

### 3.4 Theoretical study

The configuration of the prototype is the result of a theoretical study which takes into account both architectural integration aspects (as described in paragraph 3.4.1) and energy performance issues (paragraph 3.4.2 and 3.4.3).

The latter in particular, is based on the evaluation and improvement of both PV and building-related aspects.

In fact, since it is a BiPV prototype, its energy behaviour regards both the energy production of electricity (paragraph 3.4.2) and the thermal characteristics related to the building envelope (paragraph 3.4.3).

The “Bi” and the “PV” performances are investigated through four main factors: ventilation of the air gap, thickness of the air gap, heat exchange features and materials applied.

The “PV” performance is improved taking into consideration passive strategies to keep the module temperature as low as possible and the “Bi” performance is evaluated taking into account the thermal transmittance value of the whole BiPV system, which is assessed in accordance with the UNI EN ISO 6946 [3.1].

#### 3.4.1 PV technology and integration issues

Three main aspects are taken into account for the choice of the PV technology: formal-architectural integration issues, cost and energy performance.

Following these criteria, a standard module based on thin film technology (CIGS) was selected.

The choice of this PV module is the result of the considerations described in this paragraphs, including the above mentioned three criteria, but where the main role is played by formal-architectural concerns.

The latter influences in an essential way the public acceptance of such a prototype, which, being part of a building, is supposed to have an important impact on the building architecture.

The international project IEA Task 41 [3.4] highlights how public acceptance of solar energy systems integrated in architecture is one of the main obstacles to their diffusion and underlines, as a provocation, that a “less performing” solar device installed (or integrated) is better than an “optimal performing” solar

device not installed (or integrated). Thus, the public acceptance of these systems, is one of the main obstacles that need to be overcome.

### **Cost considerations**

Since the prototype is planned to be a prefabricated component and the price reduction plays an important role, it was decided to use a “standard” module, rather than a custom-made product in order to be coherent with the concept of standardization to reduce costs.

Dimensions were thus a key point for the selection of the most suitable module, which had to fit the standard measures foreseen by the structural prefabricated part of the prototype, composed itself by standardised components.

### **Energy performance considerations**

It is not possible to assess which is the “optimal” choice of PV technology for a specific application just from an energy perspective, but some general concerns can be considered.

The use of a thin film technology was preferred to a crystalline one as, in general, they fit better for BiPV applications. This is due to their lower temperature coefficient (see definition below) and their often reported better low light response, which are positive aspects considering the operating conditions of the modules integrated in the façade.

The relative temperature coefficient  $\gamma_{P_{mppt}}$  is defined as follows:

$$\gamma_{P_{mppt}} = \frac{1}{P_{mppt}} \frac{\partial P_{mppt}}{\partial T}$$

Equation 3.1

Where,  $P_{mppt}$  is the power at the maximum power point and  $T$  is the temperature. The temperature coefficient  $\gamma_{P_{mppt}}$  indicates how the value of  $P_{mppt}$  behaves by changing the temperature.

Considering the datasheets temperature coefficients, the selected module presents a relative temperature coefficient of  $-0,36\%/^{\circ}\text{C}$ , which is lower compared with a crystalline module (typically around  $-0,5\%/^{\circ}\text{C}$ ) [3.40] [3.42] [3.41].

### **Architectural integration and PV module**

The PV module aesthetical appearance is an essential aspect for a successful formal-architectural integration of a PV system, and the architectural (aesthetic) integration is an essential issue for the public acceptance of every BiPV system, considering that it has an important impact on the building architecture.

Several PV solutions based on different cell technologies are available on the market, offering a variety of design possibilities, as described below. Table 3.1 lists some examples of the cell types available on the market for the two main PV types, i.e. crystalline silicon and thin film.

The main characteristics of the two main PV types are described below.

#### **Crystalline silicon**

Crystalline silicon (c-Si) modules, which account for about 85% of the cells used worldwide [3.32], are subdivided in two main categories: single crystalline (sc-Si) and multi-crystalline (mc-Si).

Crystalline silicon cells are typically produced in a complex manufacturing process. Mono-crystalline cells are produced from silicon wafers; these wafers are cut from an ingot of single crystal silicon, resulting in slices of approximately 0.2 mm thick. This produces square (most common, even if also circular and quadrilateral exist) cells of 100 to 150 mm sides with a homogeneous structure and a dark blue / blackish colour appearance.

For poly-crystalline cells, the melted silicon is cast into square ingots where it solidifies into a multitude of crystals with different orientations (frost-like structure), which gives the cells their spotted and shiny surface (see Table 3.1).

Crystalline modules present front contacts (usually visible) constituted by several thin individual lines (contact fingers, about 0.1 mm to 0.2 mm thick) and two collector contact lines (busbars, about 1.5mm to 2.5 mm thick), which run across the thin contact fingers.

### Thin film

Thin-film solar cells (also called “second generation” solar cells) are usually categorized according to the photovoltaic material used, the three main technologies being amorphous silicon (a-Si), Copper Indium Gallium (Di)Selenide (CIS or CIGS) and Cadmium Telluride (CdTe).

In general, thin-film modules have a more homogeneous surface appearance with respect to wafer based crystalline technology, ranging from brown/orange to purple and black, with parallel lines more or less marked (see Table 3.1).

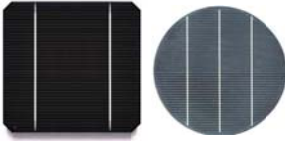

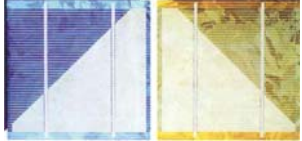



	Cell type	Appearance	Image
CRYSTALLINE SILICON CELLS	Monocrystalline Silicon Cell	Standard: Dark blue to black Custom-made: Different colours available (see Figure 3.6)	
	Polycrystalline Silicon Cell	Standard: blue custom-made: Different colours available (Figure 3.7)	
	Polycrystalline semitransparent Silicon Cell	The same as above (with transparency)	
THIN FILM CELLS	Amorphous silicon Cell	Red-brown to black	
	Copper indium diselenide Cell (CIS)	Black/dark blue	
	Cadmium telluride Cell (CdTe)	Dark red/brown to black	

Table 3.1: some examples of the cell types available on the market for the two main PV types, i.e. crystalline silicon and thin film.

An analysis of the standard products available on the market was carried out and a thin film module based on CIGS technology was selected. The aim was in fact to find a PV module presenting an homogenous surface, as coherent as possible with the common building cladding materials, taking into consideration guidelines and criteria provided by the IEA project Task 41 “Solar Energy and Architecture” [3.5]. In particular, the IEA Task 41 project reports three main criteria for the evaluation of architectural integration of solar systems (as proposed for the selection of the best case studies that are uploaded on the Task 41 web-site [3.5]), i.e. the overall global composition, the detailed composition of surface and materials (e.g. PV colour and PV pattern/texture) as well as the added values and function. The first criteria (i.e. overall global composition) is not eligible for this analysis since it refers to the global composition of a whole architecture and thus cannot be used for the evaluation of a single building component (i.e. the prototype of the BiPV wall). This criteria has to be taken into consideration by the architects who would use this prototype as part of their composition.

The other two criteria (i.e. surface and materials, added values and function) were instead considered during the prototype development and are described below.

#### Surface and materials: PV colour considerations

Most of standard PV modules are in the dark range of colours (black, blue, purple, green).

The use of coloured cells is also possible for almost all kind of PV technologies, as shown in Figure 3.6, Figure 3.7 and Figure 3.8.

Despite the widely-spread idea that the possibility to choose among different cell colours would push architects to make a larger use of PV systems in their architectures, it seems that these options were not so appreciated so far and “coloured modules” seem not to be the key solution for the use of solar systems in architecture.

Of course this is primary due to their low efficiency and high cost but, surprisingly, other reasons may exist which are directly connected to the formal quality.

Results of a web survey conducted among European architects (1500 distributed, 170 fully completed questionnaires) with the aim to objectively define the formal quality of building integrated solar technologies [3.2], surprisingly shows that architects prefer black/dark solar modules for many examples of integration better than coloured modules.

This does not imply that architects in general do not like coloured modules, but it demonstrates that the latter do not necessarily represent a key solution to increase the formal quality of a system integrating solar energy systems.

Given these considerations, together with the economical aspect, it was decided to use a standard black module for the prototype integration. The chosen module also has an anodized-aluminium black frame and a black cells background which provide an homogeneous appearance to the whole PV module.



Figure 3.6: Colour palette for monocrystalline cells, © System Photonics



Figure 3.7: Multicrystalline silicon wafers; first the blue antireflective standard color with the best efficiency, the second is the original wafer without reflective layer, then cells with other colours that have different anti-reflective layers, © Sunways



Figure 3.8: Coloured thin film modules in reddish brown, chocolate-brown, hepatic and sage green colour, © Rixin

#### Surface and materials: PV pattern/texture considerations

Contrarily to crystalline silicon modules, the most of which present an inhomogeneous surface due to the “pixelling effect” of the strict quadratic grid of cells connected by visible metal contacts, the pattern of thin film modules

present a much more homogeneous aspect without visible cell contacts or “pixelling effect” [3.3].

Thin-film solar cells and their contacts are deposited directly on large area substrates, such as glass, metal or polymeric panels.

Thin films module surface have a more homogeneous appearance with respect crystalline technology.

Thin film laminates currently have a particular surface texture and two empty lateral areas where the substrate is visible. The choice of a thin film module, as in the case of this prototype, with a substrate having the same colour as the active material, guarantees a complete homogeneous appearance, as coherent as possible with a traditional building cladding.



Figure 3.9: Different PV module typologies, which originate different textures [source: Eurac, ABD experimental PV plant]

From top left to bottom right: m-Si with visible contact fingers, s-Si with visible contact fingers, s-Si with back contact technology, s-Si on dark substrate without frame, a-Si without frame, CIGS (i.e. the selected module for the prototype), a-Si/a-Si.

### Added value and function

Given the different definition between BAPV (building added photovoltaic) and BiPV (building integrated photovoltaic) systems, it is clear that a PV system, in



order to be considered as “integrated” and not just as “added”, has to provide an additional function to the building component. The PV system integrated in this prototype is conceived from the beginning as part of the building prefabricated wall, substituting the traditional external cladding of wooden prefabricated walls.

Figure 3.10 shows the schematic horizontal section of traditional wooden prefabricate wall types (option 1 and 2) and of the conceived innovative prototype (option 3). It is clearly visible that, according to option 3, the PV module is conceived as a multifunctional element, which substitutes the traditional cladding (option 1 and 2).

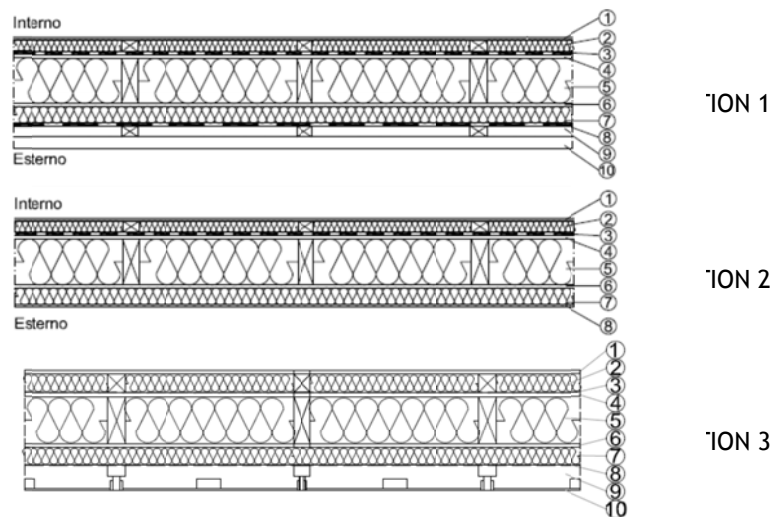


Figure 3.10: Horizontal section of three wooden prefabricate wall types

1. Gypsum fiber panels
2. thermal insulation (between the wooden frame)
3. Vapor retarder
4. OSB
5. thermal insulation (between the wooden frame)
6. OSB (Oriented Strand Board)
7. Thermal insulation

OPTION 1 -traditional-

8. Waterproof barrier
9. Air gap
10. wooden planking

OPTION 2 -traditional-

8. finishing coat

OPTION 3 -innovative-

8. Waterproof barrier
9. Air gap
10. PV module

The BiPV prefabricated prototype as a whole is conceived as a multifunctional building component, able to fulfil the building needs, such as weather protection, insulation and to also produce electricity.

In particular, the prototype is configured according to the recommendation provided by the outcomes of the research project MULTIELEMENT-PV elements in building services engineering [3.13]. This project, which involved 15 partners from research institutions industry and economy, defined several functions that a BiPV system should provide with the aim to reduce the cost by systematically including multifunctionality [Figure 3.11].

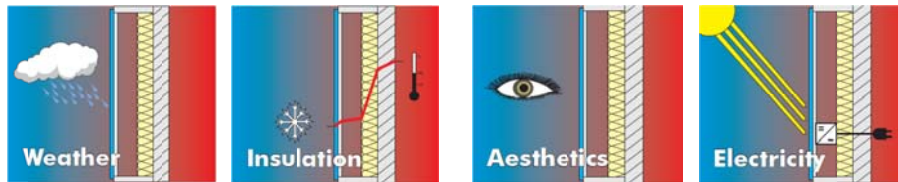


Figure 3.11: multifunctional characteristics of the BiPV prototype, based on [3.13] recommendations

The BiPV prototypal prefabricated wall, as recommended in [3.13], is conceived to provide the following functions:

- Weather protection, including impermeability against rain and wind, resistance against weather changes (see Figure 3.31);
- Thermal insulation, achieved through the multi-layered of module configuration as well as the thermal insulation of the wooden structure;
- Aesthetics design, as shown in the previous paragraphs;
- Electrical energy production, generating power for direct use in the building or to feed into the grid.

### 3.4.2 PV performance

#### Ventilation of the air gap

An essential aspect for the correct integration of PV modules in the building envelope is the presence of an air gap to guarantee a ventilation between the PV modules' back surface and the building envelope structure.

In fact, when the module is integrated, the increase of the operating temperature, as already mentioned in chapter 2, is one of the critical points with regard of BiPV systems performance [3.14].

B.V. Kampen [3.24] shows that a BiPV façade system without ventilation can reach temperature peaks of 85°C (at max ambient temperatures of 40°C, in Lugano -Switzerland- ), which could affect the PV power output up to 30% with respect to PV temperature conditions of 25°C, depending on the PV technology. Other experiences in monitoring of BIPV façades in Northern Italy show that, without ventilation, peaks of around 60°C are easily reached causing losses of 15.4 % in power production [3.29].

Especially it has to be underlined that it is during the most productive hours that the PV temperature is the highest, i.e. when the PV surface is reached by the peak irradiance. In fact, the maximum production conditions (MPC, i.e. the ambient conditions in which the most power production occurs) appear usually at high temperature levels, as shown in [3.25] for two PV plants in Central and South Italy (MPC Bolzano: 50°C, MPC Catania: 45°C), which means that most of the energy is produced when the PV system operates at high temperatures (high with respect to STC conditions, which are never met).

In order to avoid significant PV power losses, it is thus crucial to properly design and to carefully consider the integration characteristics. This aspect is in fact very often underestimated by designers and architects.

Air circulation in the air gap to cool the PV array can be triggered either by forced or natural flow. Forced circulation is more efficient than natural circulation owing to increase convective heat transfer, but the required fan power reduces the net electricity gain [3.15].

Moreover, natural air circulation constitutes a simpler and lower cost method to remove heat from PV modules and to keep the electrical efficiency at an acceptable level [3.16], representing an opportunity for the development of a prefabricated BIPV component where the cost is an issue. In addition, considering that the BIPV component has to fulfil also the building standards, the maintenance aspects represent another key point.

Henceforth, natural ventilation instead than the mechanical one was preferred for this prototype.

Natural ventilation foresees that the movement of the air in the gap behind the PV module is governed by a combination of natural convection (or stack effects, i.e. the warming of the air in the duct induces an upward flow), and wind induced flow (i.e. local wind at the inlet and outlet apertures of the air gap causes pressure differences between those two points, which induce a flow that can assist or oppose to the stack effect) [3.18].

Design for natural ventilation behind the BIPV elements can enable a temperature reduction of up to 20°C [3.17].

B.J. Brinkworth & M.Sandberg [3.19] found that, even for moderate solar irradiance (i.e. 600W/sqm), the average temperature rise of a PV array integrated into a façade specimen, is reduced by the presence of an air gap behind the modules by 11°C in still air and by 14°C when the wind speed is just 2 m/s.

Natural ventilation could thus enhance the PV performance and it could also provide other advantages from the building point of view, as shown by Ji et al. [3.22]: they studied numerically the energy performance of a BIPV façade with a ventilating air gap behind the PV modules in a high-rise building of Hong Kong. In this case it was found that the provision of the free airflow gap affects not only the electrical performance but it is also able to reduce the heat gains through the PV façade during the summer, helping to avoid the internal space overheating. Yang et al. [3.23] carried out a similar study based on the weather conditions of three cities in China: Hong Kong (at 22.3\_N), Shanghai (at 31.2\_N) and Beijing (at 39.9\_N). It was found that the ratio of space cooling load reduction owing to the airflow behind the PV modules ranges from 33% to 52% on typical days.

The literature review led thus to the choice to include a naturally ventilated air gap in the prototype with the main aim to cool the PV operating temperature. In addition the air gap could lead to other advantages such as avoiding overheating of the building during summer, as shown in [3.22] [3.23].

The characteristics of this air gap are discussed in the following paragraphs.

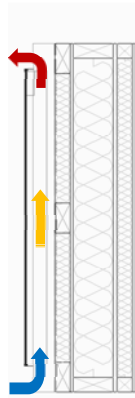


Figure 3.12: Vertical section of the specimen with the schema of the natural ventilation concept: the air in the gap cools the PV modules

### **Thickness of the air gap**

Several studies in the past have been carried out on the optimisation of the air gap thickness to lower the PV temperature as much as possible in condition of natural ventilation.

According to Brinkworth et al. [3.19],[3.20] there is an optimum value of this design variable to minimize the PV module working temperature, such that for an array of length  $L$  the minimum temperature occurs when the ratio between  $L$  and  $D_{eq}$  (i.e. the equivalent hydraulic diameter) is among 15 and 20. This formula, can be considered as a “rule of thumb” for the design of cooling air gaps behind PV modules integrated into facades.

The existence of this optimum value was originally found by Brinkworth et al. during repeated simulations involving computer modelling of the heat transfer and fluid mechanical behaviour of the flow in the ducts and then validated through an experimental campaign on a façade specimen [3.21] [3.19].

The robustness of this “rule of thumb” and its theoretical foundation is further demonstrated in [3.20], where it is also shown that this optimum proportion is practically independent of the slope of the array, and thus it can be considered a valid rule for both façade and roof applications.

Considering the prototype dimensions, this results in an optimal value of 10 cm for the air gap thickness to minimise efficiency loss due to temperature rise.

### **Heat exchange improvement**

As stated in the paragraph above, temperature increase of the PV operating temperature causes significant power production drops that, for a correct integration into building, has to be minimized as much as possible.

Therefore, it is crucial to develop strategies and solutions to reduce the working module temperature.

In this thesis, a passive low-cost strategy is experimented and investigated, with the aim to further enhance the advantages provided to the PV module performance by the ventilation in terms of PV temperature decreasing.

The idea rises from the necessity to develop a technique as passive, low cost and simple as possible (for coherency with the prototype prefabrication concept), implementing in the PV sector a strategy which is very often used in the ICT sector for electronic device cooling.

In fact, in electronic systems it is a very common practice to include a heat sink which works as passive heat exchanger to cool a device by dissipating heat into the surrounding air.

For example, in computers, heat sinks are used to cool central processing units (CPU) or graphics processors.

In general, heat sinks are often used with high-power semiconductor devices, such as power transistors and optoelectronic devices, such as lasers and light emitting diodes (LEDs), wherever the heat dissipation ability of the basic device package is insufficient to control its temperature.



Figure 3.13: examples of CPU heat-sinks. On the right: a fan-cooled heat sink on the processor of a personal computer with a smaller heat sink cooling another integrated circuit of the motherboard

This concept is scaled up to the PV module dimensions, resulting in a proposed solution which is first evaluated through FEM simulations, then measured and quantified through an experimental campaign presented in the next chapter.

The concept results in a technical modification of the PV module, foreseeing the applications of metal fins attached on the back side of the module itself (as shown in Figure 3.15).

The heat coming from the PV module is transferred to the heat sink (i.e. the fins) by conduction and from the heat sink to the ambient air by natural convection [3.26][3.1].

The role of the metal fins is to increase the heat transfer surface area in the air channel, working as a heat sink and thus dissipating an higher quantity of heat produced by the PV modules.

Furthermore, Tonui & Tripanagnostopoulos [3.14] showed that presence of fins in a naturally ventilated duct behind the PV modules create an higher stack effect leading to a better PV cooling. Similar results were found by Friling et al. [3.28]. In those cases, the fins were attached on the wall to the opposite side of the PV modules [as shown in Figure 3.14], but the same concept could be extended for the case of fins attached on the module.

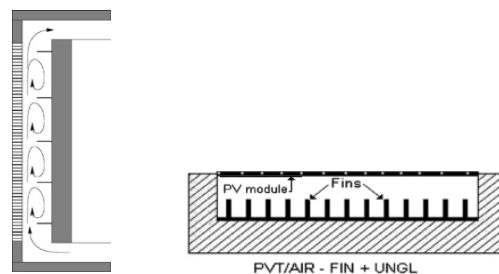


Figure 3.14: different geometry configurations of the air gap behind the PV module, as investigated by Friling et al. [3.28] and Tonui et al. [3.14]

No much literature was found by the author about experimental data regarding the application of heat sinks directly on the PV module. Some data are reported for a module with aluminium finned substrate in [3.31] but no information are provided about the characteristics of the fins and their application on the module. This configuration is thus investigated in this thesis to evaluate and quantify its effectiveness, also through an experimental campaign (as reported in chapters 4 and 5).

In order to define the configuration of the system module-heat sink, because no much experimental data or examples are available, several energy simulations with finite elements method are carried out.

The material chosen for the fins is aluminium (i.e. a material largely used in façade systems), since it is a cheap and light material with high conductivity properties, and it is the same material as the module frame to avoid possible corrosion effects.

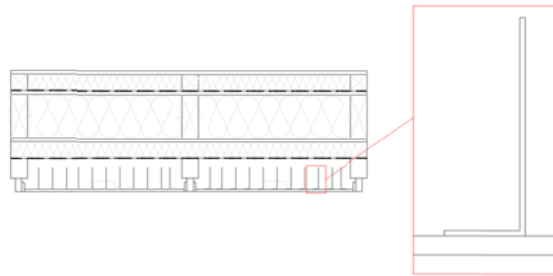


Figure 3.15: the zoom shows the L shape of the aluminium fin attached to the back side of the PV modules

The next paragraphs report the results of some energy simulations and first rough experiments that were carried out to define the way to incorporate the heat sink on the module, and in particular: the characteristics of the thermal compound layer between the fins and the module as well as the fins dimensions.

#### Fin-module heat transfer: the thermal compound layer

Metal fins are attached on the back side of the PV module in the vertical direction.

It is necessary to include a thermal conductive compound layer between the fins and the module to guarantee a perfect contact between them (avoiding the presence of any air) and to permit the heat transmission through conduction from the PV module to the fins.

Several kind of such thermal compound are evaluated to find the most suitable and economical solution for this application.

Two options are in particular compared: one foresees the application of the fins through a thermal conductive (non-adhesive) compound ensuring the mechanical joint with additional fixing to the module frame, and the other one considering only the presence of a thermo conductive adhesive.



Both options are tested through first rough experiments: two fins are applied on a 6mm glass (the same thickness as the PV module which is a glass-glass kind) through one commercially available thermal compound and one commercially available thermal adhesive, as shown in the following pictures.

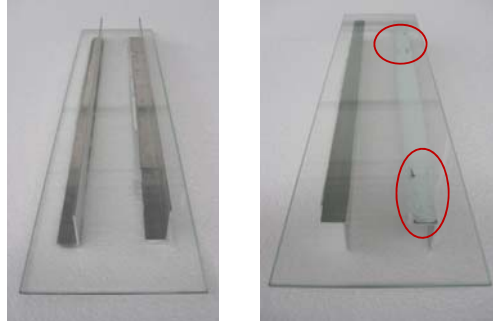


Figure 3.16: The pictures show the fins applied on a 6mm glass. The right-hand image, which shows the backside of the glass, displays the air holes (as marked in the red circles) in the thermal compound used to attach the fin on the right. The fin on the left is instead attached with a thermo conductive adhesive, which gives better results from the contact point of view.

Therefore, the alternative with the adhesive is selected as the best, since it allows to avoid additional mechanical fixing thus reducing time in the component construction and also because it presents better characteristics in its distribution, avoiding air holes between the glass and the fins (as shown in Figure 3.16) which could significantly affect the thermal transmittance.

Among the commercially available thermal conductive adhesives, two different kinds are considered: a thermal compound based on Epoxy technology (with a thermal conductivity coefficient of 1.4 W/mK, based on ISO 8302) and a thermal compound based on Silver technology (with a thermal conductivity coefficient of 8.89 W/mK).

The latter presents an higher value of conductivity and thus could be considered as best option, nevertheless it has a much higher price.

Some energy simulations are thus carried out to quantify the different performances of the two compounds to evaluate the best option balancing between performance and costs.

The FEM energy simulations results reported in Figure 3.17 show that there is no need of an higher thermal conductivity coefficient, since there is no significant change in the module temperature distribution considering the two thermal compound types. This can be due to the fact that the thermal

conductivity of the first compound, even if it is lower than the second, is higher than that of the module glass where it is applied (which is 1 W/mK).

The first image of Figure 3.17 plots the isotherms expressed in °C, considering the thermal compound based on Epoxy technology (with a thermal conductivity coefficient of 1,4 W/mK) between the module and the fin; the second one considers a thermal compound based on Silver technology (with a thermal conductivity coefficient of 8,89 W/mK).

The considered boundary conditions for the simulations are:

$T_i = 30^\circ\text{C}$ ,  $h_{cv\ i} = 2.5\ \text{W}/(\text{sqmK})$ ,  $\varepsilon_i = 0.84$ ,  $T_{out} = 25^\circ\text{C}$ ,  $h_{cv\ out} = 8\ \text{W}/(\text{sqmK})$ ,  $\varepsilon_o = 0.84$ , constant heat flux = 1000W/sqm, hp of black body radiation.  $h_{cv}$  coefficients (i.e. convective coefficients) are calculated according to UNI EN ISO 6946.

Considering the results of the simulations, the cheapest solution (a structural adhesive based on epoxy technology with a coefficient of thermal conductivity (ISO 8302) of 1.4 W/(mK)) is thus selected as the best option for this application.

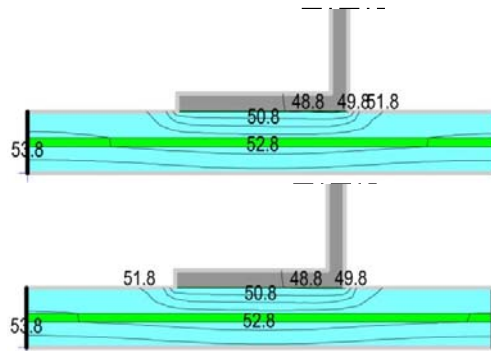


Figure 3.17: temperature distribution of the PV module simulated with the FEM software THERM (developed by Lawrence Berkeley National Laboratory). The first image plots the isotherms expressed in °C, referred to the epoxy technology compound; the second one considers a thermal compound based on Silver technology

It is important to underline that these simulations are focussed on the heat sink thermal performance of different possible configurations.

The considered boundary conditions in fact refer to hypothetical conditions (no measured data are available at this stage) and thus, the temperatures shown in Figure 3.17 have to be considered significant not as absolute values but as relative values, which are of interest for this study.

### Fin-module heat transfer: the fins dimensions

In order to improve the heat transfer between the PV module and the air in the gap, several FEM energy simulations are carried out considering different fin dimensions.

The considered boundary conditions are:

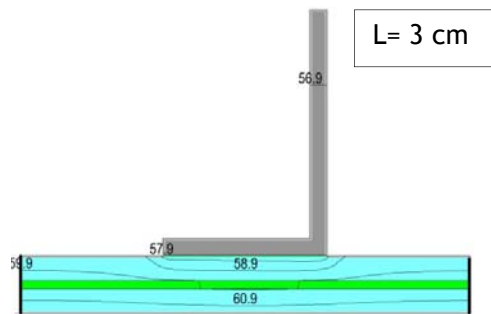
$T_i = 30^\circ\text{C}$ ,  $h_{cv\ i} = 2.5\ \text{W}/(\text{sqmK})$ ,  $\epsilon_i = 0.84$ ;  $T_{out} = 25^\circ\text{C}$ ,  $h_{cv\ out} = 8\ \text{W}/(\text{sqmK})$ ,  $\epsilon_{out} = 0.84$ , constant heat flux =  $1000\ \text{W}/\text{sqm}$ ; hp of black body radiation.

$h_{cv}$  coefficients (i.e. convective coefficients) are calculated according to UNI EN ISO 6946.

Three values of fin length (L) are considered, and the results show that the longest is the one that manages to dissipate the largest amount of heat.

Considering “top conditions” (according to the hypothesis given above), the cell temperature (see Figure 3.18) is around  $60,9^\circ\text{C}$  for the first case (L=3cm), it is around  $56,6^\circ\text{C}$  for the second case (L=5 cm) and it is around  $52,7^\circ\text{C}$  for the last case (L=8cm). A 8 cm-long fin could thus decrease the cell temperature of  $8,2^\circ\text{C}$  with respect to a 3 cm-long fin, which means, in the considered conditions (as previously listed), an increase in the PV power output of about 3% (considering the temperature coefficient of power as reported on the CIGS modules datasheet  $\gamma = -0.36\%/^\circ\text{C}$ ).

Given these simulation results, the fin length of 8 cm is thus selected for the prototype, i.e. the maximum possible length considering the configuration of the prototype and the available space in the air gap.



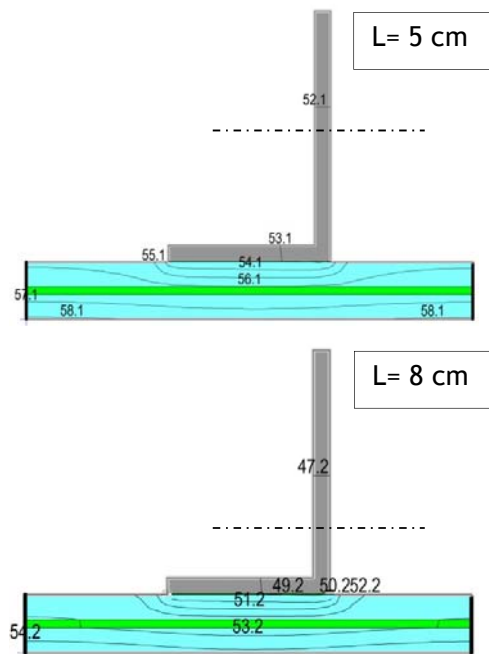


Figure 3.18: temperature distribution of the PV module simulated with the FEM software THERM (developed by Lawrence Berkeley National Laboratory), given the boundary conditions listed above. The first image plots the isotherms expressed in °C, considering respectively: a 3 cm-long fin, a 5 cm-long fin and a 8 cm-long fin.

#### Preliminary evaluation of the fins effect

Several FEM simulations are carried out to evaluate the effect of the fins application on the PV module temperature distribution.

The simulation results reported in Figure 3.19 and in Figure 3.20 show how the PV temperature changes considering the situation with and without fins in average meteorological conditions referred to the city of Bolzano (North of Italy) at 12:00 for summer and winter (as described in Table 3.2).

Average Values at 12:00			
	global irradiation	air temperature	air velocity
	W/sqmK	°C	m/s
<b>WINTER</b>	358	6	1,2
<b>SUMMER</b>	340	25	2,5

Table 3.2: the table shows average values at 12 o'clock for the city of Bolzano (North of Italy) of: global irradiation on a vertical South-oriented surface, air temperature and air velocity. The values were calculated considering the meteorological data base

of the Swiss software Meteororm. Values are divided in winter conditions (December 21st-March 21st ) and summer conditions (June 21st - September 21st )

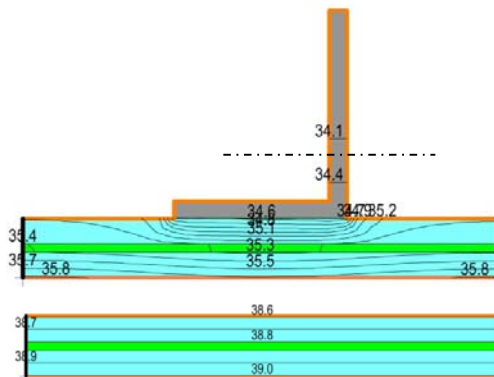


Figure 3.19: The images show the temperature distribution of the PV module with and without attached metal fin, simulated with the FEM software THERM (developed by Lawrence Berkeley National Laboratory) in average summer conditions (as described in Table 3.2).

Figure 3.19 shows that, in the considered conditions ( $T_i = 30^\circ\text{C}$ ,  $h_{cv\ i} = 2.5\ \text{W}/(\text{sqm K})$ ,  $\epsilon_i = 0.84$ ;  $T_{out} = 25^\circ\text{C}$ ,  $\epsilon_{out} = 0.84$ , constant heat flux =  $340\ \text{W}/\text{sqm}$ ,  $h_{cv\ out} = 14\ \text{W}/(\text{sqm K})$ , which was evaluated in accordance with the UNI EN ISO 6946 considering the air velocity of  $2.5\ \text{m/s}$ ; hp of black body radiation), the presence of the fins allows a decrease of around  $3.5\ ^\circ\text{C}$  in the cell temperature, which would mean an increase of the PV power output of  $1.3\%$ , considering a constant power temperature coefficient of  $-0.36\ \%/^\circ\text{C}$  (as reported on the module datasheet).

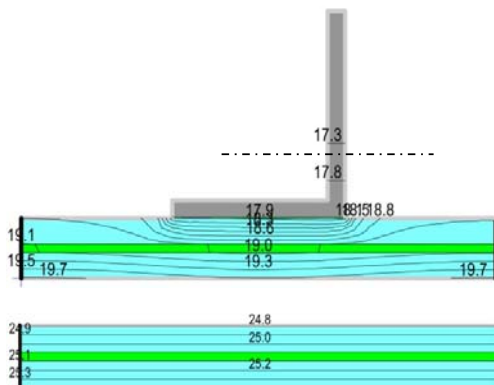


Figure 3.20: The images show the temperature distribution of the PV module with and without attached metal fin, simulated with the FEM software THERM (developed by Lawrence Berkeley National Laboratory) in average winter conditions (as described in Table 3.2).

Figure 3.20 shows that, in the considered conditions ( $T_i = 11^\circ\text{C}$ ,  $h_{cv\ i} = 2.5\ \text{W}/(\text{sqm K})$ ,  $\varepsilon_i = 0.84$ ;  $T_{out} = 6^\circ\text{C}$ ,  $\varepsilon_{out} = 0.84$ , constant heat flux =  $358\ \text{W}/\text{m}^2$ ,  $h_{cv\ out} = 8.8\ \text{W}/(\text{sqm K})$ , which was evaluated in accordance with the UNI EN ISO 6946 considering the air velocity of  $1.2\ \text{m}/\text{s}$ ; hp of black body radiation), the presence of the fins leads to a decrease of around  $6^\circ\text{C}$  in the cell temperature, which would mean an increase of the PV power output of 2.2%, considering a constant power temperature coefficient of  $-0.36\ \%/^\circ\text{C}$  (as reported on the module datasheet). According to these simulations, application of fins leads to a slight enhancement of the PV power production (+1.3% in typical summer conditions, +2.2% in typical winter conditions) in the considered average working conditions.

These values are expected to be higher during peak working conditions, i.e. when the power production is at the top, providing an increase in the PV power production up to 6.2% [3.27].

These simulations show that application of fins on the PV module has a positive influence on the PV performance and could thus represent a passive and low cost strategy to further improve the performance of BiPV systems.

However, in order to comprehensively quantify the influence of fins on the performance of the PV module integrated in a façade, further investigation were carried out. An experimental campaign was thus performed as described in chapter 4, providing monitored data to describe this phenomena in an exhaustive and reliable way.

### 3.4.3 Building performance

The prototype energy performance, in terms of “building performance” is strictly linked with two main variables: the choice of materials (i.e. their thermal characteristics) and the thickness of each material layer.

The latter is mainly related to the fact that the prefabricated prototype is supposed to have adequate resistance to static and dynamic loads and safety against structural collapse and inadmissible deformations.

The thickness of the prototype frame is thus a fixed parameter, which is given by structural requirements.

Accordingly, the thickness of the main insulation layer becomes a fixed parameter because it is inserted in the same plane of the structural frame.

The only design variable is thus related to the choice of insulation materials, which is discussed in the next paragraph.

### **Materials**

Four commercially available insulation materials, which are typically used in the light wooden buildings, are considered and compared:

- 1) Flexible thermal insulation made from natural wood fibres ( $\lambda = 0.042$  W/mK)
- 2) Flexible thermal insulation made from hemp ( $\lambda = 0.044$  W/mK)
- 3) Mineral wool thermal insulation ( $\lambda = 0.042$  W/mK)
- 4) Extruded polystyrene ( $\lambda = 0.039$  W/mK)

All insulation materials present similar thermal conductivity values. In order to quantify the influence of the choice of the different materials on the overall prototype thermal transmittance, the total prototype resistance is evaluated for the four options, according to the UNI EN ISO 6946.

The calculated resistance values, considering the four materials are respectively:

- 1)  $R = 5.31$  sqm\*K/W
- 2)  $R = 5.23$  sqm\*K/W
- 3)  $R = 5.31$  sqm\*K/W
- 4)  $R = 5.44$  sqm\*K/W

Extruded polystyrene is the material which provides the highest thermal resistance ( $R = 5.44$  sqm\*K/W), while insulation made from hemp is the one which perform in the poorest way ( $R = 5.23$  sqm\*K/W).

However, it has to be considered that the extruded polystyrene is a synthetic polymer made from the monomer styrene, a liquid petrochemical, which does not fit very well with the overall prototype concept of sustainability and use of natural local materials.

The other two materials (based respectively on natural wood fibres and mineral wool) provide a resistance which do not differ in a significant way from the extruded polystyrene (i.e. 2% less).

Given these considerations, the flexible thermal insulation made from natural wood fibres is selected as the best option for this prototype because, even if its performance in terms of thermal resistance is slightly lower compared to the best performing option, the use of this material is coherent with the overall concept used for the prototype configuration.

The prototype is thus largely made of wood or wood-based materials (the structural frame is made of local wood).

The selected insulation material is based on wood fibres, and all of them are certified with the European quality mark “Natureplus” [3.33] and “FSC” certification [3.34] [3.38] [3.39], which guarantee environmentally-friendly production, protection of limited natural resources and suitability of application.

Moreover, from an LCA (life cycle assessment) perspective, several studies have shown that buildings with wooden structures require less energy and emit less CO<sub>2</sub> during their life cycle, than buildings with other types of structures [3.43] [3.45]. For example, in a Canadian office building, the embodied energy in a steel structure is 1.61 times greater than that in a concrete structure, which in turn is 1.27 times greater than that of a wooden structure [3.45]. Also in Northern European countries various life cycle studies have been carried out that indicate the advantages of wooden structures [3.46].

### **Prototype thermal characteristics**

In order to understand the influence of the presence of PV on the building envelope, the value of the thermal transmittance of the prototype is calculated in accordance with the UNI EN ISO 6946 [3.1] considering two situations: the building component with and without the PV system.

The International Standard UNI EN ISO 6946 provides in fact a simplified calculation method to assess the value of thermal transmittance and thermal resistance of building components.

The calculation is based on combining the individual thermal resistance of each thermally homogeneous layer to obtain the total thermal resistance of the component including the effect of surface resistances.

The air gap included in the prototype is treated in accordance with the Standard definitions as a well-ventilated air layer: the total thermal



transmittance is thus obtained by disregarding the thermal resistance of the air layer and all other layers between the air layer and external environment, and including an external surface resistance corresponding to still air, which is calculated in accordance to Annex A.

Table 3.3 summarizes the values of thermal conductivity which were used for each layer.

$\lambda$ : Coefficient of thermal conductivity of each layer (W/mK)							
1	2	3	4	5	6	7	8
0,352	0,042	0,22	0,13	0,042	0,13	0,043	0,2

Table 3.3: Coefficient of thermal conductivity of each layer (W/mK), referred to numbered items of Figure 3.27.

Following the calculation schema of the standard (as described in the next paragraph) the results show that the presence of PV do not affect in a significant way the total thermal resistance of the component: the thermal transmittance of the component with the integrated PV system (which is 0.188 W/sqm K) is slightly lower than the one without it (which is 0.191 W/sqm K) (Figure 3.21).

Therefore, according to this calculation schema, the PV system does not affect the building envelope performance in a negative way.

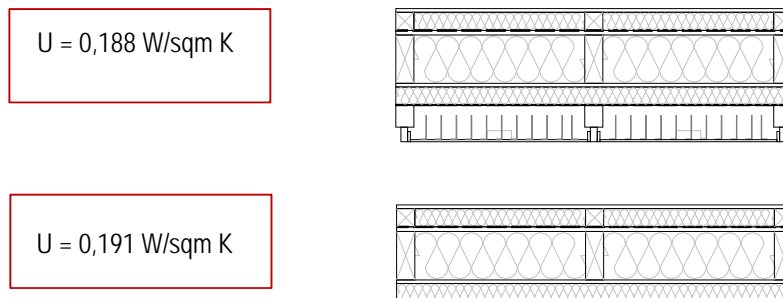


Figure 3.21: the U-value (i.e. thermal transmittance) calculated considering the prototype with and without PV modules.

### Prototype thermal transmittance - calculation method-

This paragraph describes the calculation method, as foreseen by the UNI EN ISO 6946 [3.1], for the evaluation of the prototype thermal transmittance.

The first step foresees the calculation of the thermal resistance of the homogeneous layers resulting from the thermal conductivity values which are taken from generic values given by the UNI EN ISO 10456:2008 [3.30] (for layers 1, 2b, 3, 4, 5b, 6, 7b and 8) and from the manufacturer datasheets, worsened for an amount of 10% as suggested by the standard (for layers 2a, 5a and 7a).

<b>R<sub>i</sub>: resistance value of each homogeneous layer (sqm K/W)</b>											
L	1	2a	2b	3	4	5a	5b	6	7a	7b	8
s	0.012	0.06	0.06	0.0003	0.015	0.16	0.16	0.012	0.06	0.06	0.0003
λ	0.352	0.042	0.13	0.22	0.13	0.042	0.13	0.13	0.043	0.13	0.2
R <sub>i</sub>	0.035	1.428	0.461	0.001	0.115	3.809	1.230	0.092	1.395	0.461	0.001

Table 3.4: L is the reference number of each layer referred to Figure 3.25, s is the thickness (m), λ is the thermal conductivity (W/m K), R<sub>i</sub> is the resistance of each homogeneous layer (sqm K/W)

### Surface resistances

In the second step, the surface resistances are calculated according to the appendix A of the standard, as illustrated in Table 3.5.

<b>R<sub>s</sub>: Surface resistances</b>			
h <sub>ci</sub>	Convection coefficient-inside	W/(m <sup>2</sup> )K	2.5
h <sub>ce</sub>	Convection coefficient-outside	W/(m <sup>2</sup> )K	2.5
h <sub>ri</sub>	Radiative coefficient -inside	W/(m <sup>2</sup> )K	5.04
h <sub>re</sub>	Radiative coefficient -outside	W/(m <sup>2</sup> )K	3.28
ε <sub>i</sub>	Surface emissivity-inside		0.8
ε <sub>e</sub>	Surface emissivity-outside		0.8
σ	Stefan-Boltzmann constant	W/(mq <sup>2</sup> K <sup>4</sup> )	5.67E-08
Heat flux	horizontal		
h <sub>ro i</sub>	Black body radiative coefficient-inside	W/(m <sup>2</sup> )K	6.3
h <sub>ro e</sub>	Black body radiative coefficient-outside	W/(m <sup>2</sup> )K	4.1
T <sub>i</sub>	Temperature-inside	°C	30
T <sub>e</sub>	Temperature-outside	°C	-10
<b>R<sub>si</sub></b>	<b>Surface resistance-inside</b>	<b>sqm*K/W</b>	<b>0.13</b>
<b>R<sub>se</sub></b>	<b>Surface resistance-outside</b>	<b>sqm*K/W</b>	<b>0.17</b>

Table 3.5: indoor and outdoor surface resistance calculation

### Total thermal resistance

As last step, the total thermal resistance is evaluated.

The total thermal resistance ( $R_T$ ) of the prototype, which consists of thermally homogeneous and thermally inhomogeneous layers parallel to the surface, is calculated as the arithmetic mean of the upper and lower limits of the resistance:

$$R_T = (R'_T + R''_T) / 2$$

where:

$R'_T$  is the upper limit of the total thermal resistance

$R''_T$  is the lower limit of the total thermal resistance

Calculation of the upper and lower limits are carried out by considering the component split into sections and layers, in such a way that the component is divided into parts,  $m_j$ , which are themselves thermally homogeneous. The prototype is considered divided into sections a, b, c, d and into layers 1, 2, 3, 4, 5, 6, 7, 8 (see Figure 3.23 and Figure 3.25)

The section  $m$  ( $m = a, b, c, d$ ) perpendicular to the surfaces of the component has a fractional area  $f_m$ . The layer  $j$  ( $j = 1, 2, \dots, 8$ ) parallel to the surfaces has a thickness  $d_j$ . The part  $m_j$  has a thermal conductivity  $l_{mj}$ , thickness  $d_j$ , fractional area  $f_m$  and thermal resistance  $R_{mj}$ .

The fractional area of a section is its proportion of the total area. Therefore,  $f_a + f_b + f_c + f_d = 1$  (see Table 3.6 and Table 3.7).

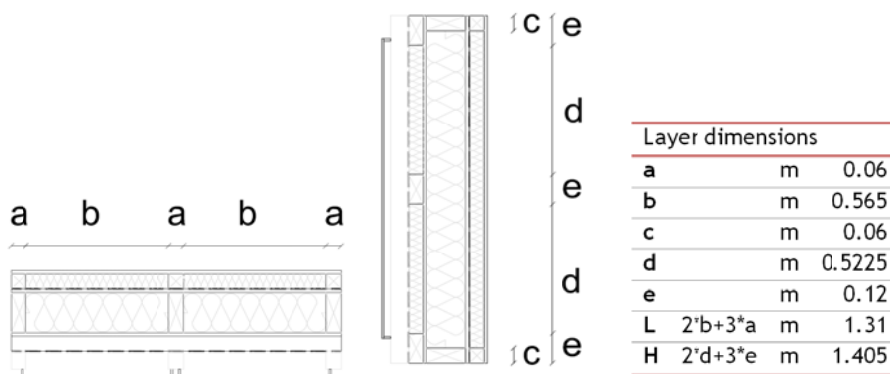


Figure 3.22: dimensions of each layer of the prototype

Upper limit of the total thermal resistance

The upper limit of the total thermal resistance,  $R'_T$ , is determined by assuming one-dimensional heat flow perpendicular to the surfaces of the component. It is given by the following expression, referred to sections a, b, c and d of Figure 3.23:

$$\frac{1}{R'_T} = \frac{f_a}{R_{Ta}} + \frac{f_b}{R_{Tb}} + \frac{f_c}{R_{Tc}} + \frac{f_d}{R_{Td}}$$

Where:

$R_{Ta}$ ,  $R_{Tb}$ ,  $R_{Tc}$ ,  $R_{Td}$ : are the total thermal resistances from environment to environment for each section;

$f_a$ ,  $f_b$ ,  $f_c$ ,  $f_d$ : are the fractional areas of each section.

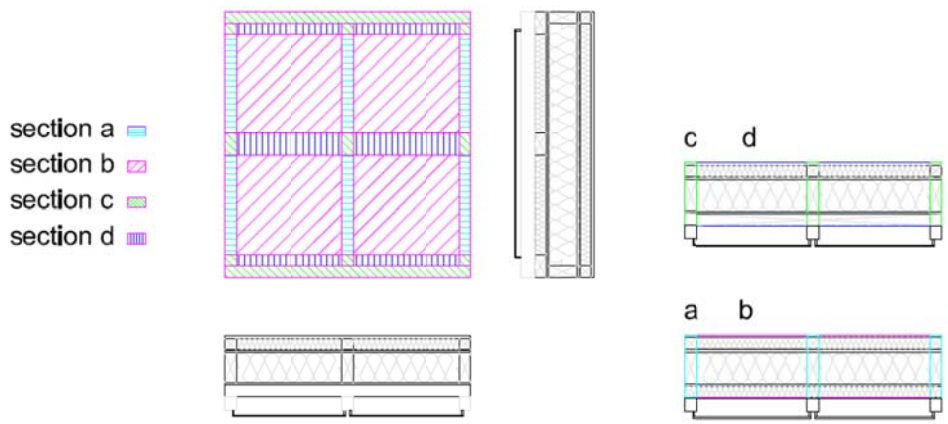


Figure 3.23: schema of the considered sections a, b, c and d

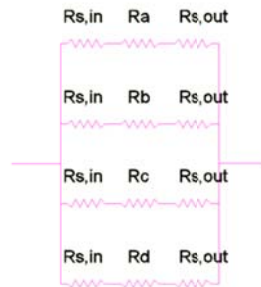


Figure 3.24: Schema of the considered resistances to calculate the upper limit of the total thermal resistance

<b>Upper limit of the total thermal resistance, <math>R'_T</math></b>			
Atot	total wall area	mq	1,84055
f	$(f_a+f_b+f_c+f_c+f_c)*f$		
Aa	area of section a	mq	0,1881
Ab	area of section b	mq	1,18085
Ac	area of section c	mq	0,2004
Ad	area of section d	mq	0,2712
$f_a$	fractional area of section a	-	0,102198
$f_b$	fractional area of section b	-	0,641575
$f_c$	fractional area of section c	-	0,10888
$f_d$	fractional area of section d	-	0,147347
$R_{Ta}$	total thermal resistance of section a	mq*K/W	3,65
$R_{Tb}$	total thermal resistance of section b	mq*K/W	7,19
$R_{Tc}$	total thermal resistance of section c	mq*K/W	2,71
$R_{Td}$	total thermal resistance of section d	mq*K/W	6,26
<b><math>R'_T</math></b>	<b>Upper limit of the total thermal resistance</b>	<b>mq*K/W</b>	<b>5,53</b>

Table 3.6: Calculation of the upper limit of the total thermal resistance

### Lower limit of the total thermal resistance

The lower limit of the total thermal resistance,  $R''_T$ , is determined by assuming That all planes parallel to the surfaces of the component are isothermal surfaces.

Calculating an equivalent thermal resistance,  $R_j$ , for each thermally inhomogeneous layer given by this expression:

$$\frac{1}{R_j} = \frac{f_a}{R_{aj}} + \frac{f_b}{R_{bj}} + \frac{f_c}{R_{cj}} + \frac{f_d}{R_{dj}}$$

The lower limit is then determined by the following expression, referred to the layers shown in Figure 3.25:

$$R''_T = R_{si} + R_1 + R_2 + R_3 + R_4 + R_5 + R_6 + R_7 + R_8 + R_{se}$$

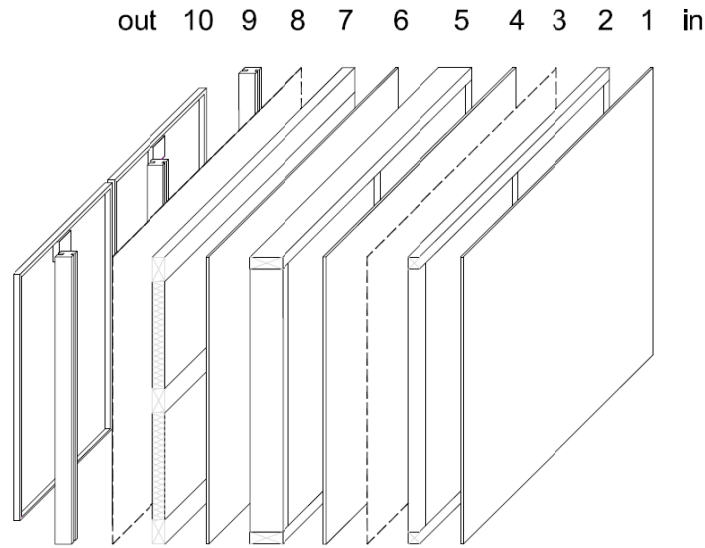


Figure 3.25: schema of the considered layers of the prototype

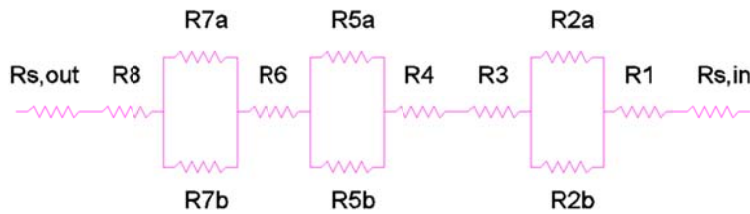


Figure 3.26: Schema of the considered resistances to calculate the lower limit of the total thermal resistance

Lower limit of the total thermal resistance, $R''_T$			
$R_1$	total thermal resistance of layer 1	$m^2K/W$	0,035511
$R_2$	total thermal resistance of layer 2	$m^2K/W$	0,99051
$R_3$	total thermal resistance of layer 3	$m^2K/W$	0,0015
$R_4$	total thermal resistance of layer 4	$m^2K/W$	0,115385
$R_5$	total thermal resistance of layer 5	$m^2K/W$	2,641359
$R_6$	total thermal resistance of layer 6	$m^2K/W$	0,092308
$R_7$	total thermal resistance of layer 7	$m^2K/W$	0,918951
$R_8$	total thermal resistance of layer 8	$m^2K/W$	0,0015
$R''_T$	somma delle 8 resistenze (da R1 a R8) in serie + Rsi + Rse	$W/m^2K$	5,11
<b><math>R''_T</math></b>	<b>Lower limit of the total thermal resistance</b>	<b><math>m^2K/W</math></b>	<b>5,11</b>

Table 3.7: Calculation of the lower limit of the total thermal resistance

### Resulting total thermal resistance

The resulting total thermal resistance of the whole prototype is:

$$U = 0.188 \text{ W}/(\text{sqm} \cdot \text{K})$$

And the corresponding total thermal resistance is

$$R_T = 5.32 (\text{sqm} \cdot \text{K})/\text{W}$$

The calculated thermal transmittance values can be considered a satisfying result in terms of building energy performance, and it is index of a well-insulated wall as its thermal transmittance is below, for an extent of 23%, the limit of 0.26 W/(sqm·K) required by the actual Italian law referring to the worst case scenario (“zona climatica F”) [5.1].

In fact, the concept that lead to the development of this BiPV prototype foresees the idea of a building component which is first of all “energy saving” and only afterwards “energy producing”. Energy saving is considered the first inescapable step toward an energy efficient BiPV system.

In addition, it is evaluated that the PV modules themselves do not affect in a significant way the value of thermal transmittance of the whole component, as calculated in the previous paragraphs according to the Standard UNI EN ISO 6946.

### 3.5 Prototype design

The final prototype design is the result of the theoretical study carried out as described in the previous paragraph.

The prototype [Figure 3.27] is conceived as a standardized modular unit with dimensions of 442 x 1310 x 1240 mm, characterized by a nominal power of 160Wp and with a calculated thermal transmittance value of 0,188 W/sqm K.

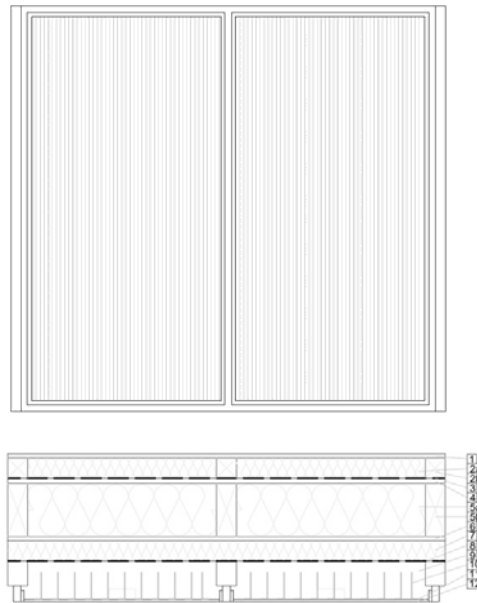


Figure 3.27: design of the frontal view and horizontal section of the prototype. The horizontal section is made of the following layers :

1. Gypsum fiber panels
- 2a. Wooden fiber thermal insulation
- 2b. Wooden frame
3. Vapor retarder
4. OSB
- 5a. Wooden fiber thermal insulation
- 5b. Wooden frame
6. OSB (Oriented Strand Board)
7. Thermal insulation
8. Waterproof barrier
9. Air gap
10. Metal fins
11. Thermoconductive glue
12. PV module (thin film technology)



### 3.6 Prototype application

The BiPV prototype of this thesis was developed within a wider research project entitled “Chi Quadrato: building construction of certified green buildings designed for training activities”, which aim was to design a prototypical elementary school of 200 sqm located in Condino (Province of Trento, North of Italy), entirely realized with prefabricated wood framed panels with high energy efficiency standard, developing innovative technological solutions, innovative processes (off-site construction) and promoting and enhancing the value of wood as a sustainable building material. The consortium “Chi Quadrato” is constituted by eight SME’s (small medium enterprises), coordinated by five research Institutions: Università IUAV di Venezia, Università degli Studi di Trento, CNR Ivalsa (National Research Council of Italy-Trees and Timber Institute-), Libera Università di Bolzano and Eurac. The partners of the consortium worked together following an integrated design process (IDP), i.e. a design process based on close multidisciplinary cooperation and iterative design loops.

The IDP includes the organization of several workshops during the entire design phase, in which all stakeholders involved in the project collaborate (architects, clients, solar energy consultants, specific contractors and manufacturers) to guarantee a more holistic approach to building design. These workshops were carried out for the project duration to clarify, after each design loop, architectural and technical target criteria and constraints.

At the beginning of the project, several hypothesis were considered for the PV integration, together with the architects and electricians. Figure 3.28 shows some of the considered preliminary hypothesis elaborated before the development of the BiPV wall prototype.

The BiPV wall prototype developed in this thesis is thus conceived as a “prototype in the prototype” (i.e. a BiPV wall prototype in a wooden prefabricated prototypal building).

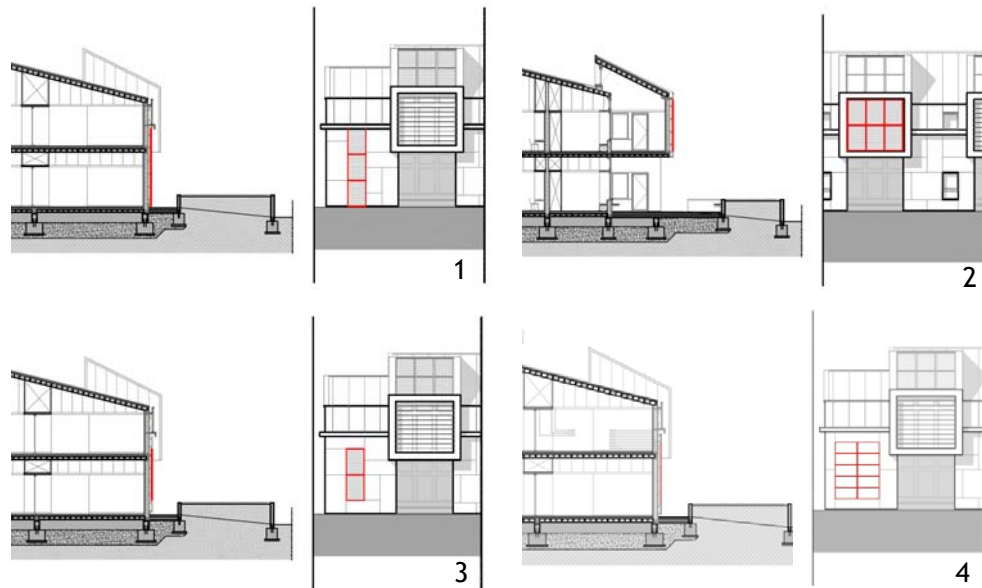


Figure 3.28: preliminary hypothesis for the BiPV wall prototype positioning, elaborated by the architects belonging to the “Chi Quadrato” Consortium at the beginning of the project (from the top left to the bottom right: solutions 1,2,3,4).

Among the considered hypothesis, as shown in Figure 3.28, the most suitable “place” for PV integration was selected using the IDP approach, together with architects, technicians and manufacturers, on the basis of two groups of criteria (according to the criteria identified by Wittkopf et al. [3.35]):

- Climatic and site characteristics
- Architectural characteristics

The first group of criteria considers: tilt, orientation and shading effect.

The first (tilt) is not applicable as an option as it is already fixed at  $90^\circ$ , being a façade application. In terms of orientation (azimuth) and shading, the South-West (azimuth= $+20$ ) façade is, by evidence, the one with the highest solar radiation potential considering the morphological configuration of the surrounding East and North-West mountains of the place (i.e. Condino, Province of Trento, Italy). All solutions of Figure 3.28 refer to that façade.

The second group of criteria considers: position, visibility from outside the building, accessibility, function and aesthetics.

According to these criteria, option number 2 was selected as the most suitable, for the following reasons:

- In option 4 the PV modules are in a position which, for some period during the day, is shadowed by an adjacent projecting building part (as shown in the section drawing of Figure 3.28)
- Positioning the modules as foreseen in options 1 and 3, would give public accessibility to the PV system: the adjacent ground is a public space where also children of the school are allowed to walk through. This could represent a problem in terms both of safety and also from aesthetic perception [as shown in Figure 3.29]
- In option 2 the PV modules are in a position easily accessible for technicians but not for public, visible to the public at a distance of at least 3 meters and in architectural coherence with the rest of the building [see Figure 3.30].



Figure 3.29: Visibility: module aesthetical perception vs observer position. The first picture is taken at a distance of 3 meters and the modules surface appears as an homogeneous pattern; the other picture is taken at a distance of 50 cm: the pattern appears marked by vertical lines, which are the cell connections



Figure 3.30: Rendering of the elementary school that was designed as a prototypal building within the project “Chi Quadrato”, including the BiPV prototype on the left. [re-arrangement L. Maturi from rendering Studio Arch. Frate]

Figure 3.30 shows a preliminary rendering of the elementary school to pre-evaluate the visual impact and the architectural coherence of the BiPV prototype with the whole architecture composition.

This rendering and the preliminary positioning hypothesis of Figure 3.28, were elaborated in the first phase of the project, when the design of the BiPV wall prototype (as described in paragraph 3.5) was not defined yet.

The BiPV wall prototype was in fact developed as a parallel task within the whole project.

The final design completed with architectural details, which was elaborated after the “BiPV wall prototype” development as described in this chapter, is shown in Figure 3.31.



Figure 3.31: architectural drawings and details of the BiPV wall prototype integrated in the elementary school design.

## References

- [3.1] UNI EN ISO 6946:2007, Building component and building elements - thermal resistance and thermal transmittance - calculation method
- [3.2] MC.Munari Probst, 2008. Architectural Integration and Design of Solar Thermal Systems. École Polytechnique Fédérale de Lausanne, doctoral thesis n. 4258
- [3.3] K. Farkas, 2011. The Perception of Formal and Symbolic Aesthetics of Photovoltaics. Proceedings of ISES Solar World Congress 2011, ISBN 978 39814659 0 7
- [3.4] M. Wall et al., 2008. IEA Task 41-Solar Energy and Architecture-Annex Plan. (available at: <http://members.iea-shc.org/publications/task.aspx?Task=41>)
- [3.5] MC Munari Probst, C Roecker et al., 2012. Report T.41.A.2: IEA SHC Task 41 Solar energy and Architecture. Solar energy systems in architecture - Integration criteria and guidelines. (available at: <http://members.iea-shc.org/publications/task.aspx?Task=41>)
- [3.6] Report T.41.A.3, in press: Designing photovoltaic systems for architectural integration -Criteria and guidelines for product and system developers, 2013.
- [3.7] K. Farkas, M. Horvat et al., 2012. Report T.41.A.1: Building Integration of Solar Thermal and Photovoltaics - Barriers, Needs and Strategies. (available at: <http://members.iea-shc.org/publications/task.aspx?Task=41>)
- [3.8] R. Gottschalg et al., 2003. Experimental study of variations of the solar spectrum of relevance to thin film solar cells. Solar Energy Materials & Solar Cells 79, 527-537
- [3.9] Energy-efficient buildings ppp - Multi-annual roadmap and longer term strategy-, prepared by the Ad-hoc Industrial Advisory Group, European Commission
- [3.10] J.J. Bloem, 2008. Evaluation of a PV-integrated building application in a well-controlled outdoor test environment. Building and Environment 43, 205-216
- [3.11] T. Schoen et al., 2001. Task 7 of the IEA PV power systems program - achievements and outlook, Proceedings of the 17<sup>th</sup> European Photovoltaic Solar Conference.

- [3.12] I. Bergmann, W. Weiss, 2002. Fassadenintegration von thermischen Sonnenkollektoren ohne Hinterlüftung. AEE Intec, Arbeitsgemeinschaft ERNEUERBARE ENERGIE, Institut für Nachhaltige Technologien
- [3.13] P. Funtan et al., 2009. MULTIELEMENT project-PV Elements in Building Services Engineering, (<http://www.pv-multielement.de/>)
- [3.14] J.K. Tonui & Y. Tripanagnostopoulos, 2008. Performance improvement of PV/T solar collectors with natural air flow operation. *Solar Energy* 82(1) 1-12
- [3.15] T.T. Chow, 2010. A review on photovoltaic/thermal hybrid solar technology, *Applied Energy*, 87(2) 365-379
- [3.16] Y. Tripanagnostopoulos et al., 2002. Hybrid photovoltaic/thermal solar systems, *Solar Energy* 72(3) 217-234
- [3.17] B. Norton et al., 2011. Enhancing the performance of building integrated photovoltaics, *Solar Energy* 85(8) 1629-1664
- [3.18] P. Batagiannis, C. Gibbons, 2001. Thermal assessment of silicon-based composite materials used in photovoltaics, Conference proceedings of Renewable Energy in Maritime Island Climates, Belfast, 151-157
- [3.19] B.J. Brinkworth & M. Sandberg, 2006. Design procedure for cooling ducts to minimise efficiency loss due to temperature rise in PV arrays, *Solar Energy* 80(1) 89-103
- [3.20] B.J. Brinkworth, 2006. Optimum depth for PV cooling ducts, *Solar Energy* 80, 1131-1134
- [3.21] Brinkworth, B.J. et al, 2000. A validated model of naturally ventilated PV cladding. *Solar Energy* 69, 67-81
- [3.22] Ji Jie et al., 2002. The annual analysis of the power output and heat gain of a PV-wall with different integration mode in Hong Kong, *Solar Energy Materials and Solar Cells*, Vol 71 Issue 4 435-448
- [3.23] H. Yang et al., 2001. Building-integrated photovoltaics: effect on the cooling load component of building facades, *Building Serv Eng Res Technol* 22 (3), 157-165
- [3.24] B. van Kampen, 2008. Actual Temperatures of Building Integrated PV Modules. Study in the framework of the EU IP Performance project, September 2008 (available at: [www.pv-performance.org](http://www.pv-performance.org))

- [3.25] L. Fanni et al., 2011. Maximum production conditions of a c-Si module in three different Italian locations. Proceedings of the 26th European Photovoltaic Solar Energy Conference and Exhibition. 3446 - 3449
- [3.26] Y. A. Cengel, 2006. Heat and Mass Transfer -A Practical Approach- 517-518
- [3.27] L. Maturi, R. Lollini, P. Baldracchi, W. Sparber, 2011. Building skin as electricity source: the prototype of a wooden BiPV façade component. Proceedings of the 26<sup>th</sup> European Photovoltaic Solar Energy Conference and Exhibition. 3991 - 3999
- [3.28] N. Friling et al., 2009. Modelling the heat dynamics of building integrated and ventilated photovoltaic modules. Energy and Buildings 41 (10), 1051-1057
- [3.29] L. Maturi et al., 2010. Analysis and monitoring results of a BiPV system in Northern Italy. Proceedings of the 25th European Photovoltaic Solar Energy Conference and Exhibition, 5131-5134
- [3.30] UNI EN ISO 10456:2008. Materiali e prodotti per edilizia - Proprietà igrometriche - Valori tabulati di progetto e procedimenti per la determinazione dei valori termici dichiarati e di progetto.
- [3.31] Flat-Plate Solar Array Project Final Report, 1986. Volume VI: Engineering Sciences and Reliability, JPL Publication 86-31.
- [3.32] B. Weller et al., 2010. Detail Practice: Photovoltaics, ed. Detail, ISBN 978-3-0346-0369-0.
- [3.33] [www.natureplus.org](http://www.natureplus.org)
- [3.34] [www.fsc.org](http://www.fsc.org)
- [3.35] S. Wittkopf et al., 2011. Testing a design methodology for building integration of photovoltaics (PV) using a PV demonstration site in Singapore. Architectural Science review 54, 192-205.
- [3.36] Directive 2010/31/EU of the European Parliament and of the Council of 19 May 2010 on the Energy Performance of Buildings (EPBD)
- [3.37] RES Directive 2009/28/CE the European Parliament and of the Council of 23 April 2009 on renewable energy sources

- [3.38] Graeme Auld et al., 2008. Certification Schemes and the Impacts on Forests and Forestry, Annual Review of Environment and Resources. Vol. 33: 187-211. DOI: 10.1146
- [3.39] V.A. Sample, 2003. Certification on Public and University Lands: Evaluations of FSC and SFI by the Forest Managers. Journal of Forestry, Volume 101 (8), 21-25(5)
- [3.40] G. Makrides et al., 2009. Temperature behaviour of different photovoltaic systems installed in Cyprus and Germany. Solar Energy Materials and Solar Cells 93, 1095-1099.
- [3.41] E. Skoplaki, J.A. Palyvos, 2009. On the temperature dependence of photovoltaic module electrical performance: A review of efficiency/power correlations. Solar Energy 83, 614-624.
- [3.42] P. Trinuruk et al., 2009. Estimating operating cell temperature of BIPV modules in Thailand. Renewable Energy 34, 2515-2523.
- [3.43] A. Buchanan A, B. Levine, 1999. Wood-based building materials and atmospheric carbon emissions. Environmental Science and Policy 2, 427-37.
- [3.44] L. Gustavsson et al, 2006. Carbon dioxide balance of wood substitution: comparing concrete- and wood-framed buildings. Mitigation and Adaptation. Strateg for Glob Change 11, 667-91.
- [3.45] R.J. Cole, P.C. Kernan, 1996. Life-cycle energy use in office buildings. Building and Environment 31(4), 307-17.
- [3.46] A.K. Petersen, B. Solberg, 2005. Environmental and economic impacts of substitution between wood products and alternative materials: a review of micro-level analyses from Norway and Sweden. Forest Policy and Economics 7, 249-59.





## CHAPTER 4

# Experimental campaign

### *Abstract*

This chapter describes the experimental campaign performed on a sample of the designed BiPV wooden wall. The tests are organized in three phases with the aim to explore the overall energy performance of the BiPV prototype (both “Bi”, i.e. building and “PV”, i.e. photovoltaic characteristics).

The first part of the chapter presents the two laboratories where the tests were carried out, including an overview on the measurements sensors, as well as a description of the tested specimen, which was built thanks to an industrial collaboration with a network of enterprises.

The second part of the chapter deals with the three experimental phases, explaining the aim, the experimental setup and the obtained results of each single phase.



## 4.1 Introduction

The double “core” of BiPV systems (Bi+PV), requires the need to use different facilities with different features to test together their “passive” (e.g. thermal transmission properties) and “active”(e.g. electrical production) performance and to understand the interaction between the active and passive layers.

A new experimental approach, based on three phases with the combination of different test facilities (i.e. INTENT lab and SoLaRE-PV lab), and original experimental set-ups, were defined and applied to properly test the BiPV prototype.

The experimental campaign is divided into three phases which aim at exploring the overall energy performance of the BiPV prototype. Since the energy behaviour of a BiPV system is defined by the synergy between the thermal “Bi” side (i.e. the building) and the energy “PV” side (i.e. the photovoltaic system), both aspects are considered in this experimental campaign.

The organization of the tests in three phases is essential for the evaluation of the two aspects: in the first two phases each feature is treated separately in detail, while the last phase helps to merge both aspects and their interaction together so to come out with an overall overview of the energy behaviour.

The first phase focuses on the characteristics related to the “Bi” side, and in particular on the thermal characterization of the prototype with the measurement of its thermal transmittance; the second phase deals with the “PV” side, and in particular with the electrical characterization of the modules through the measurements of the I-V characteristic curve at different conditions. The goal of the last phase is to merge together the “Bi” and the “PV” sides, and it focuses on the thermal-energy characterization of the integrated PV modules.

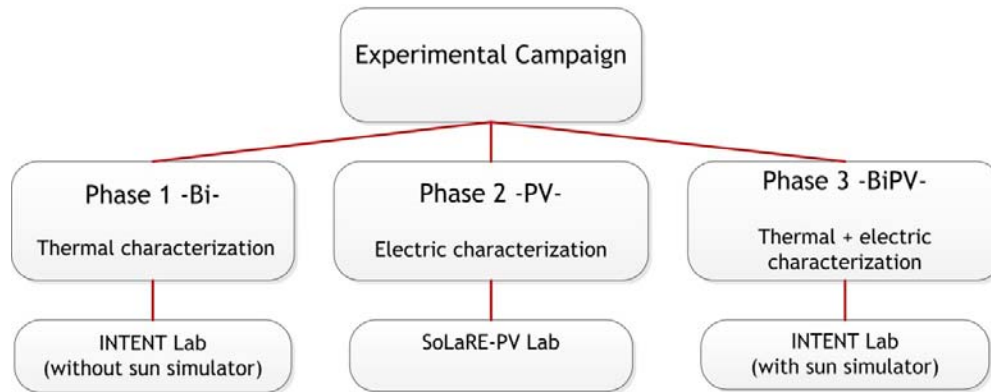


Figure 4.1: The diagram shows the organization of the experimental campaign, which is divided into three phases

The double “core” of BiPV systems entails the need to use different facilities with different features to test together “passive” (e.g. thermal transmission properties) and “active”(e.g. electrical production) performances and to understand the energy interaction between the active and passive layers. The tests carried out in this experimental campaign are performed in two laboratories at the Institute for Renewable Energy of Eurac: INTENT Lab and SoLaRE-PV Lab [1.9]. The first laboratory is a test facility for building systems that allows the performance analysis of passive and active building envelope systems, while the second one is an indoor test facility for PV module characterisation according to relative IEC standards. The features of the two test facilities are described in the next paragraphs.

## 4.2 INTENT Lab

INTENT (INTEgrated ENergy walls Test facility) is a laboratory that can evaluate, either in dynamic or static mode, the thermal and energy performance of building envelope systems, such as walls and floors that integrate active solar systems for energy production or radiant circuits for heating/cooling.

The laboratory includes:

- a calorimeter, which has been designed and planned on the basis of the International standards UNI EN ISO 8990 [3.1] and UNI EN ISO 12567-1 [4.2] with some technical changes. The calorimeter is composed by a cold chamber, a metering box and a guard chamber (see Figure 4.2), which simulate respectively the outdoor and indoor conditions by controlling temperature, humidity and air velocity;
- a steady-state sun simulator, that varies in a range of irradiance from 400 W/m<sup>2</sup> to 1000 W/m<sup>2</sup>, class BBB as reported in the standard IEC 60904-9 [4.3]: spectral match, spatial uniformity, temporal stability, referred to a maximum irradiated surface of 1.5m x 2.0m;
- an hydraulic measurement circuit to assess the performance of possible thermal active systems integrated in the envelope;
- a detailed monitoring system made of sensors and data acquisition instruments that measure significant physical parameters with the aim of determining the characteristics of the test sample.

During the tests, the prototype is inserted into a frame surrounded by thermal insulation, located between the cold and a hot box which is constituted of a guard chambers.

The solar simulator reproduces the irradiation conditions on the external surface of the test sample. The glazed panel at the bottom of the cold-box allows us to keep the desired climatic conditions in the cold chamber and at the same time guarantees the needed transparency for the irradiation of the sample.

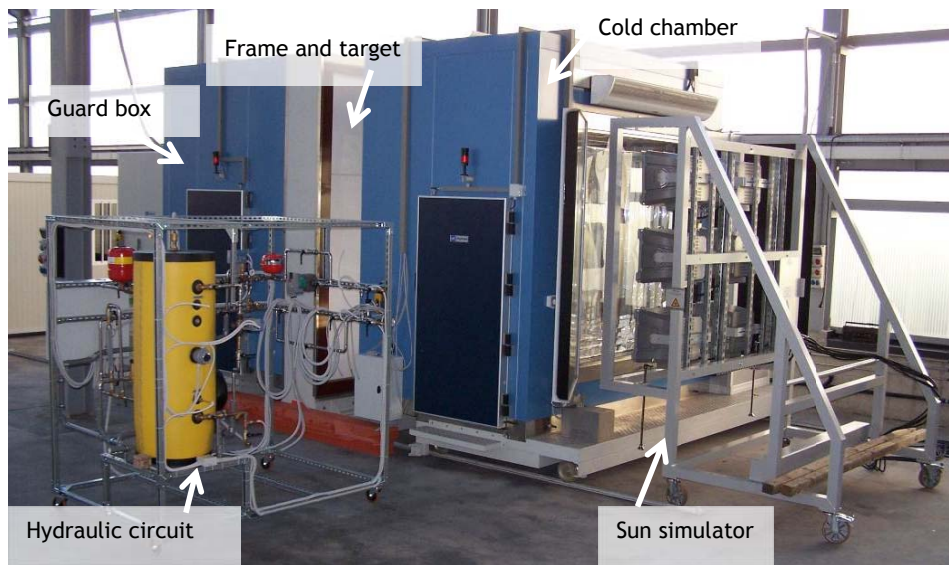


Figure 4.2: INTENT Lab at Eurac: the calorimeter with the sun simulator and the hydraulic circuit

#### Technical characteristics of the calorimeter

Dimensions (H, L, W)	4000 mm x 6380 mm x 4300 mm
Cold Chamber	T= $-20 \div 40^{\circ}\text{C}$ , V= $0.1 \div 5$ m/s; RH= $40 \div 80\%$
Metering Chamber	T= $18 \div 40^{\circ}\text{C}$ , V< 0.3 m/s; RH< 15%
Characteristics of the specimen to test	max dim.: 2000 mm x 1500 mm max thickness: 500 mm
Monitoring and data acquisition systems	Temperature (T), air velocity (V), humidity (RH) measurements
Max temperature gradient	$0.2^{\circ}\text{C}/\text{min}$

Table 4.1: Technical characteristics of the calorimeter of INTENT Lab

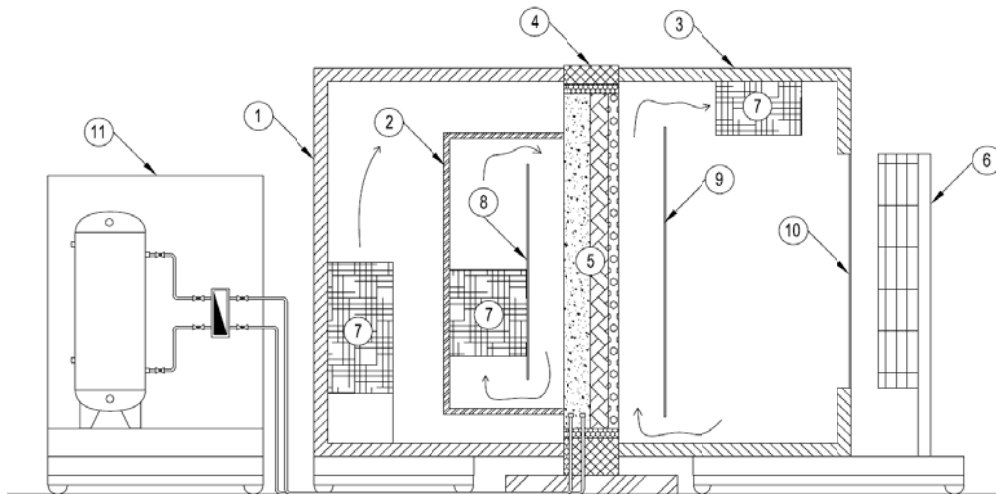


Figure 4.3: general schema of INTENT lab, which is made of.

Numbers of Figure 4.3 refer to: (1) Guard chamber (3,36x2,23x3,48 m LxTxH); (2) Metering Chamber (2,00x1,00x2,50 m LxTxH); (3) Cold Chamber (3,36x2,09x3,48 m LxTxH); (4) Fixed sample frame; (5) Wall samples; (6) Sun simulator; (7) Air conditioning devices; (8) Opaque panel to control air flux; (9) Transparent panel to control air flux; (10) Tempered glass; (11) Hydraulic circuit.

### 4.2.1 Measurement sensors

The temperature values are acquired with 70 surface thermocouples (Type T) and 40 air thermocouples (Type T). The metering box is equipped with an heating device. The guard and the cold chambers have air conditioning systems. The ambient temperature within the three climatic chambers (guard, metering and cold), is controlled using PT100 temperature sensors distributed within them. The air velocity can either be mechanically regulated by varying the dimensions of the channels in which the air is conveyed or automatically by regulating the speed of the installed fans. The air velocity is measured by two fixed anemometer (velocity transmitters EE75, uncertainty of measurement: 0.02m/s, accuracy in air at 25°C at 45% RH and 1013hPa:  $\pm 0.03$ m/s from 0.06 to 2 m/s; uncertainty of factory calibration:  $\pm 1\%$  of measuring value, temperature dependence electronics type:  $-0.005\%$  of measuring value/°C, dependence of angle of inflow  $<3\%$  for  $\alpha < 20^\circ$ , dependence of direction of inflow:  $<3\%$ , calibrated respectively at 1.5-9.5 m/s and 0.5-1.9 m/s) and one moveable hot-wire anemometer (air velocity hand-probe 0-20 m/s FV A935-TH5K2; relative measurement uncertainty: 5%). The moveable anemometer allows us to check the air velocity field within the air stream channels.

The irradiance is measured with a pyranometer placed on the same plane of the PV modules (Kipp&Zonen CMP 21, inaccuracy:  $\pm 0.05\%$ , estimated total instrument calibration uncertainty:  $\pm 1.5\%$ , sensivity: 9.29  $\mu\text{V}/\text{W}/\text{sqm}$  at normal incidence on horizontal pyranometer). All measured values are continuously controlled and acquired, with 1 minute interval. In addition to this instrumentation which is integrated into the fixed experimental station, other portable measuring instruments were used for the experimental campaign of this thesis, and they are described in the next chapters.



### 4.3 SoLaRE-PV Lab

SoLaRE-PV (South Tyrol Laboratory for Renewable Energy-PV) is a laboratory for the assessment of the characteristics and performance of photovoltaic modules based on different technologies. The laboratory includes:

- one solar simulator with a range of irradiance from 100 W/m<sup>2</sup> to 1200 W/m<sup>2</sup>, classified as “AAA” class according to the international standard IEC 60904-9 [4.3] (i.e. Non-uniformity of irradiance  $\leq 1\%$ , Pulse instability  $\leq 1\%$ , Spectral irradiance distribution  $\leq \pm 12.5\%$ ) with 10 ms as maximum usable duration of the pulse;
- one climatic chamber for the execution of thermal and humidity accelerated cycles;
- a detailed monitoring system that includes sensors and acquisition tools to measure the physical parameters that characterise the DUT (device under test).

The PASAN SunSim 3b solar simulator [Figure 4.4] is equipped with 4 Xenon flash tubes to generate a pulsed, calibrated light. The light travels through a black tunnel and illuminates the module, which is positioned at a 8 meters distance on an uniformly illuminated 3x3 meters surface. Different irradiance levels can be reproduced by attenuating the light with special masks (100, 200, 400, 700 W/m<sup>2</sup>) placed in front of the lamps. A tracer records the electrical response of the module measuring up to 4000 points of the I-V curve, along with other electrical parameters.

The Angelantoni PV4500 climatic chamber [Figure 4.4] is equipped with a heating, cooling, humidification and dehumidification system for the complete control of temperature and humidity conditions. The tests can be performed according to international standards IEC 61215 (crystalline silicon modules) and IEC 61646 (thin film modules), and simulate the environmental conditions under which a module is normally exposed to during its life cycle, accelerating the process of natural degradation. For the purpose of this thesis, the climatic chamber was used to decrease the modules temperature at the desired levels to perform the  $P_{mppt}$  matrix.



Figure 4.4: PV-SoLaRE Lab at Eurac: the sun simulator and the climatic chamber

<b>Technical characteristics of the climatic chamber</b>	
Internal dimensions (L, W, H)	1300 mm x 1520 mm x 2200 mm
Temperature and r.humidity range	T= -50÷90 °C; RH= 20÷95%
Max capacity	10 modules
Max temperature gradient	1.7 °C/min (1.0 °C/min from 0 °C to -40 °C)

Table 4.2: Technical characteristics of the climatic chamber of SoLaRE-PV Lab

### 4.3.1 Measurement sensors

In the climatic chamber, the ambient and the module temperature values are acquired with seven Pt100.

In the solar simulator, the ambient temperature values are acquired with one Pt1000 and the module temperature with one Pt100. The irradiance is measured with two monocrystalline silicon reference cells.

The temperature values are continuously controlled and acquired, with 1 minute interval.

#### 4.4 The use of INTENT and SoLaRE-PV Labs (phase 2&3)

As mentioned in the introduction of this paragraph, the double “core” of BiPV systems (Bi+PV), requires the need to use different facilities with different features to test together their “passive” (e.g. thermal transmission properties) and “active”(e.g. electrical production) performance and to understand the interaction between the active and passive layers.

The coupled use of INTENT and SoLaRE-PV Labs provides a great opportunity to focus on the building thermal performance and on the PV energy output at the same time.

The experimental results obtained as an output in INTENT Lab are used, for this experimental campaign, as an input for the test performed in SoLaRE-PV Lab.

The concept for the test phases 2&3 is thus to use separately the two labs merging then together the results to characterize the BiPV component as a whole.

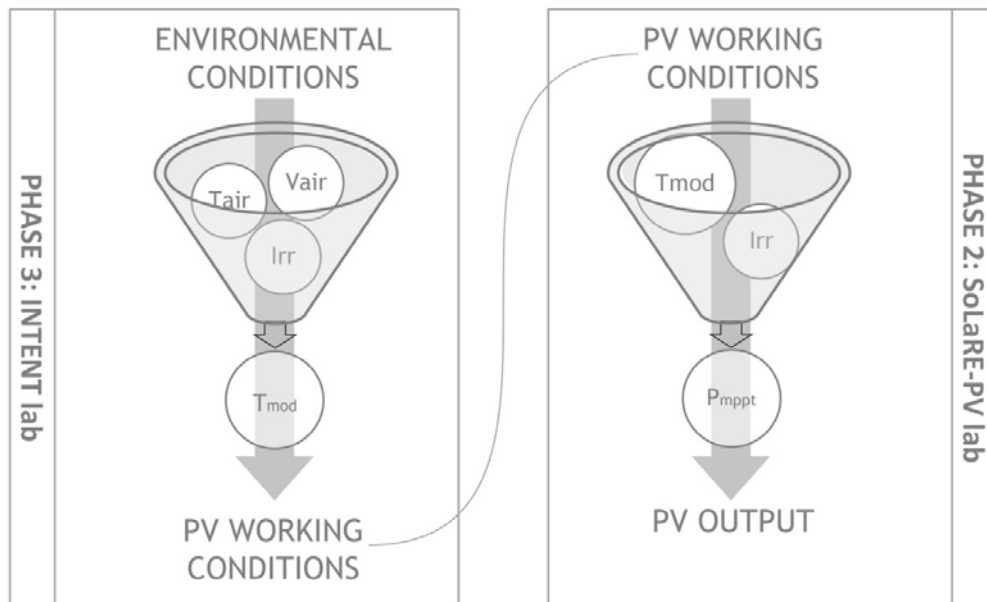


Figure 4.5: The diagram shows the concept behind the organization of the experimental campaign related to phase 2 and 3.

## 4.5 The specimen

### 4.5.1 Specimen construction drawing

The specimen is a modular unit with dimensions of 442 x 1400 x 1310 mm, with two PV modules integrated in a wooden structure (see Figure 3.27). One of the two PV modules has eleven fins (as described in the previous chapter) attached on the back (as shown in Figure 3.27 and Figure 4.7).

This configuration allows us to get measurements of temperature in both PV configurations (with and without fins) and thus permits the data comparability between the two modules which works in identical controlled conditions.

The fins are attached on the back side of the module by means of a thermo conductive adhesive layer (as described in the previous chapter).

The vertical PV mounting structure, without obstacles in the air gap, which has a depth of 10 cm, allows the triggering of natural ventilation. The same dimension of 10 cm is kept for the inlet and outlet gaps.

The detailed specifications of the specimen can be found in the executive design drawing in the annex section.

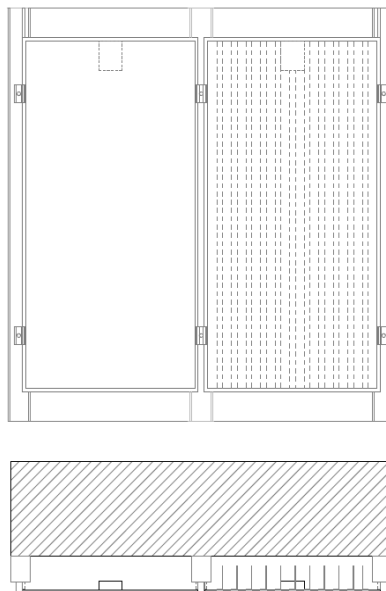


Figure 4.6: frontal view and horizontal section of the specimen (see annex A for further details)

### 4.5.2 Specimen construction: the industrial collaboration

The specimen was built by a network of enterprises sited in province of Trento called “Chi Quadrato”, that is a consortium gathered together through a local project entitled “CHI QUADRATO - costruire strutture in bioedilizia certificate per attività formative” (“Chi Quadrato: construction building of certified green buildings designed for training activities”), co-financed from the Autonomous Province of Trento in the framework of the Program FESR 2007-2013 Obiettivo 2 (Bando 1/2008 - “Promozione di progetti di ricerca applicata inerenti il Distretto Tecnologico Energia ed Ambiente”).

General aim of the project was to design a prototypical elementary school of 200 m<sup>2</sup> entirely realized with prefabricated wood framed panels with high energy efficiency standard, developing innovative technological solutions and promoting and enhancing the value of wood as a sustainable building material. The BiPV wall prototype developed in this thesis is part of this project and it is conceived as a “prototype in the prototype”.

In particular the specimen was built by two enterprises which work in the field of wooden sustainable buildings (Legno Più Case s.p.a.) and in the electricity sector (G&G Impianti Elettrici s.r.l) belonging to Chi Quadrato consortium.



Figure 4.7: The specimen built by two enterprises belonging to the network Chi-Quadrato. The picture on the left shows the modular specimen; The other picture shows one of the two PV modules which has eleven fins attached on the back side.

## 4.6 Phase 1: “Bi” characterization

### 4.6.1 Aim of the test

The first test phase was carried out to measure the steady-state thermal transmission properties of the prototype and to assess its global thermal transmittance in accordance with the UNI EN ISO 8990 [3.1] and UNI EN ISO 12567-1 [4.2]. The standard UNI EN ISO 8990 regards the determination of steady-state thermal transmission properties in calibrated and guarded hot box, and shows the heat fluxes through all parts of the apparatus. For the guarded hot box, an overview of the heat fluxes is given by Figure 4.8: the metering chamber is surrounded by the guard chamber with controlled conditions to minimize the lateral heat flux in the specimen ( $\Phi_2$ ) and the heat flux through the metering chamber envelope ( $\Phi_3$ ). Ideally, when the specimen is homogenous, the temperatures are uniform both internally and externally to the metering box, as well as when the hot side temperatures and the surface heat transfer coefficients are uniform, a thermal balance for the air (both internally and externally to the metering box), would imply a balance on the specimen surface and the other way round, e.g.  $\Phi_2 = \Phi_3 = 0$ . The total heat flux through the specimen is the same as the one provided in the metering box ( $\Phi_p$ ).  $\Phi_p$  is the sum of the thermal power provided by the fans and by the heater, which is made of five electrical resistances: 4 x 120W “on-off” resistances and 1 x 100W “continuously-variable” resistance.

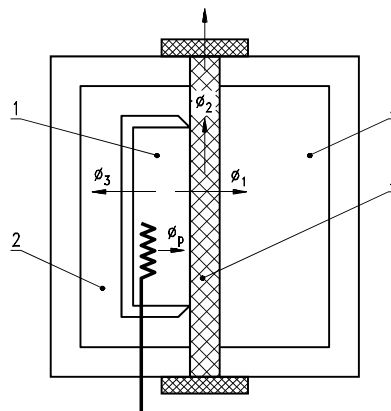


Figure 4.8: guarded hot box as foreseen by the UNI EN ISO 8990 [3.1], where: 1 is the metering box, 2 is the guarded box, 3 is the cold chamber and 4 is the specimen.

According to the standard UNI EN ISO 12567-1 [4.2], the determination of the thermal transmittance involves two stages. Firstly, measurements are made on two calibration panels with known thermal properties, from which the surface coefficient of the heat transfer (radiative and convective components) on both sides of the calibration panel with surface emissivity on average similar to those of the specimen to be tested and the thermal resistance of the surround panel are determined. Secondly, measurements are made with the specimen and the hot-box apparatus is used with the same fan settings on the cold side as during the calibration procedure [4.2].

The principal heat fluxes through the surrounding panel, which provides thermal insulation around the specimen, and through the test specimen are shown in Figure 4.9:  $\Phi_{\text{sur}}$  is heat transfer through the surround panel,  $\Phi_{\text{cal}}$  is the heat transfer through the calibration panel,  $\Phi_{\text{edge}}$  is the boundary edge heat transfer.  $\Phi_{\text{edge}}$  is equal to zero for the considered BiPV specimen.

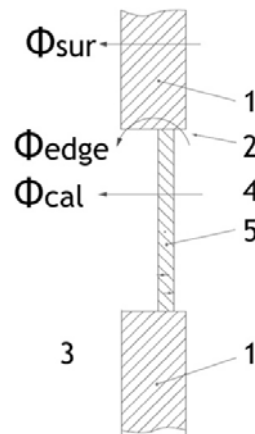


Figure 4.9: calibration and surrounding panel in the frame of the guarded hot-box as foreseen by the UNI EN ISO 12567 [4.2], where: 1 is the surround panel, 2 is the boundary effect, 3 is the cold side, 4 is the warm side, 5 is the calibration panel.

## 4.6.2 Experimental setup

INTENT lab apparatus is used for this test phase without the use of the solar simulator, as required by the standard. The specimen is placed in the calorimeter of INTENT Lab and is surrounded by four pre-shaped blocks of expanded polystyrene EPS (thickness=44.3cm, density=30 kg/cm).

Steady state conditions are reached and kept for three hours in the calorimeter, with a  $\Delta T$  of approximately 40°C between the hot and the cold chambers: the cold chamber is set to -10°C, the hot one to 30°C.

77 thermocouples type T are used during the test and in particular: 25 surface thermocouples on the specimen, 18 surface thermocouples on the baffle panels, 16 surface thermocouples on the surrounding panel.

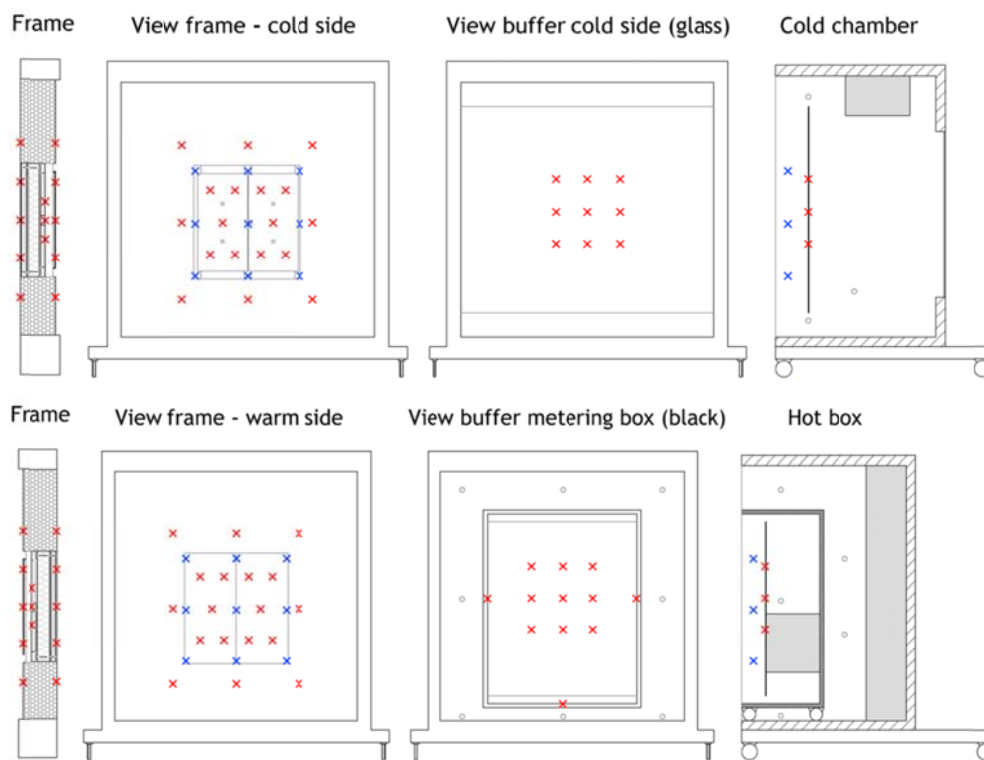


Figure 4.10: drawing of the calorimeter with the specimen during test of phase 1.

The temperature sensors are shown as follows:

x = surface thermocouple

x = air thermocouple

x = surface thermocouple on the wall behind the PV modules

o = air thermocouple of the chambers

A clearer drawing can be found in the annex section.



### 4.6.3 Results

The thermal transmittance measured by the hot box method according to UNI EN ISO 12567 [4.2], results to be **0.204 W/(m<sup>2</sup>K)**. The discrepancy between the measured and calculated values (which is 0.188 W/(m<sup>2</sup>K), as reported in the previous chapter) lies within the 8.5% measurements error.

Specimen measurement results			
Cold temperatures - measured			
$\theta_{ce}$	Air	°C	-9.97
$\theta_{se,b}$	Baffle	°C	-10.38
$\theta_{se,p}$	Reveal temperature	°C	---
$\theta_{se,sur}$	Surround panel temperature	°C	-10.19
Warm temperatures - measured			
$\theta_{ci}$	Air	°C	29.97
$\theta_{si,b}$	Baffle	°C	29.95
$\theta_{si,sur}$	Surround panel temperature	°C	29.71
$\Phi_{in}$	Input power in hot box	W	23.80
$V_i$	Air flow warm, down	m/s	0.16
$V_e$	Air flow cold, up	m/s	0.13

Table 4.3: Measured values registered during the test, required by the UNI EN ISO12567-1 [4.2] for the assessment of the thermal transmittance.

Thermal transmittance calculation			
$\theta_{me,sur}$	Mean temp. of surround panel	°C	
$R_{sur}$	Surround panel thermal resistance	m <sup>2</sup> K/W	12.63
$\lambda_{sur}$	Conductivity of surround panel	W/(mK)	0.04
$\psi_{edge}$	for w=20 mm / d=150 mm	W/(mK)	0.00
$\Delta\theta_{s,sur}$	Temp. Difference of surround panel	K	39.89
$\Delta\theta_c$	Air temperature difference	K	39.94
$\Phi_{in}$	Input power to hot box	W	23.80
$\Phi_{sur}$	surround panel heat flow	W	8.78
$\Phi_{edge}$	Edge zone heat flow	W	0.00
$q_{sp}$	Heat flow density of specimen	W/m <sup>2</sup>	8.16
$F_{ci}$	Convective fraction - warmside	-	0.52
$F_{ce}$	Convective fraction - coldside	-	0.81
$R_{s,t}$	Total superficial thermal resistance	m <sup>2</sup> K/W	0.15
$\theta_{ri}$	Radiant temperature - warmside	°C	29.95
$\theta_{re}$	Radiant temperature - coldside	°C	-10.38
$\theta_{ni}$	environmental temp. - warmside	°C	29.96
$\theta_{ne}$	environmental temp. - coldside	°C	-10.05
$\Delta\theta_n$	environmental temp. difference	K	40.01
$U_m$	Measured thermal transmittance	W/(m <sup>2</sup> K)	0.204
$\Delta u_m$	Uncertainty of the measurement	W/(m <sup>2</sup> K)	± 0.08

Table 4.4: this table summarizes the main average values measured during the steady conditions used for the thermal transmittance calculation according to the UNI EN ISO12567-1 [4.2]

## 4.7 Phase 2: “PV” characterization

### 4.7.1 Aim of the test

The second test phase was carried out to measure the PV-related characteristics of the CIGS modules (I-V characteristic curve,  $V_{oc}$ ,  $I_{sc}$ ,  $P_{mppt}$  values at different conditions) and in particular to plot a “ $P_{mppt}$  matrix” which provides the  $P_{mppt}$  value at each condition of irradiance and temperature. From the matrix it is possible to evaluate the value of the temperature coefficient  $\gamma$  at different irradiance values (AM 1.5) according to the International Standard IEC 61646 [4.4] and IEC 60891 [4.5]. The two standards contain the apparatus description and the procedures to determine the temperature coefficients of current ( $\alpha$ ), voltage ( $\beta$ ) and peak power ( $\gamma$ ) from module measurements referred to one Irradiance value.

The procedure specified in the standard requires to [4.5]:

- a) Heat or cool the module to the temperature of interest until its temperature is uniform within  $\pm 2$  °C. Once the module temperature has stabilized, set the irradiance to the desired level, using the reference device (IEC 60904-2).
- b) Record the current-voltage characteristic and temperature of the specimen and take the values of  $I_{sc}$ ,  $V_{oc}$  and  $P_{max}$ .
- c) Change the module temperature in steps of approximately 5 °C over a range of interest of at least 30 °C and repeat steps a) and b).

This procedure is repeated for 11 Irradiance values (from 100W/sqm to 1100W/sqm) over a range of 70°C (from 5°C to 75°C) in order to build the “ $P_{mppt}$  matrix” of the CIGS module.

### 4.7.2 Experimental setup

The apparatus used to control and measure the test conditions meets the requirements foreseen by the IEC 61646 [4.4], and includes:

- a radiant source which is a solar simulator, class AAA in accordance with IEC 60904-9 [4.3];
- a PV reference device with a known short-circuit current versus irradiance characteristic determined by calibrating against an absolute radiometer in accordance with IEC 60904-2;
- equipment necessary to control the temperature of the test specimen over the range of interest. For this purpose, two different devices are used: a thermal blanket placed on the back side of the module to heat it up and the climatic chamber (see paragraph 4.3) to cool it down. With regard to the latter, in order to guarantee the temperature stability after the refrigeration in the climatic chamber, a thermal insulation together with an high thermal inertia material were applied to the back side of the module;
- a suitable mount for supporting the test specimen and the reference device in the same plane normal to the radiant beam;
- an electronic load to measure the I-V curve in accordance with IEC 60904-1.

### 4.7.3 PV module preconditioning

Thin-film module technologies are known for their metastability and thus it is recommended [4.4] to stabilize their electrical characteristics before each measurement. In particular, CIGS modules are subject to light-induced change of the module efficiency and, as a consequence, an appropriate preconditioning treatment needs to be applied to ensure that the performance measurements are representative of those expected in normal operation.

The CIGS modules are in fact affected by “dark ageing” phenomenon, which means that if they are stored in the dark, fill factor and  $V_{oc}$  decrease considerably (especially at high temperatures), while  $I_{sc}$  is affected only to a minor extent (reflecting changes of the spectral quantum efficiency) [4.7].

This phenomenon is reversible by light-soaking (LS), although the recovery is not always complete. In general, the improvement is greater for poorer performing devices, but even high efficiency modules can show significant gains. Light soaking in general can strongly influence the performance, even within very short time intervals (from seconds to hours). On the other hand, Kenny et al. [4.6] have shown that these module technologies may degrade with light exposure. It is difficult to predict how a given CI(G)S material will behave and each device is somehow unique. The behaviour is, in general, very dependent on the deposition and exact material composition: the material's actual composition or stoichiometry, the deposition temperature and thickness of the CdS buffer layer, the presence of gallium or sulphur in the quaternary (Cu(In,Ga)Se<sub>2</sub>) and the different deposition processes can all influence the meta-stable state [4.7].

However, in general, these modules exhibit a short-term meta-stable behaviour modulated by light but for long-term light exposure, CIS/CIGS devices appear to be very stable [4.8]. Moreover, [4.6] shows that the IEC 61646 stabilization procedure could be considered a valid one for CIS and CIGS modules as long as the measurement is made immediately following the LS in order to minimize the relaxation effect of dark storage. The CIGS modules are thus pre-conditioned, as required by the International Standard IEC 61646 [4.4] through controlled Light-Soaking by means of simulated solar irradiation, and measured immediately after.

### **Apparatus used for preconditioning**

INTENT lab is used as apparatus for the module preconditioning, since it complies with the standard IEC 61646 requirements and includes:

- a class BBB solar simulator in accordance with the IEC 60904-9, which is the sun simulator part of INTENT lab;
- a suitable reference device (Kipp&Zonen CMP 21, as described in paragraph 4.2), for monitoring the irradiation;
- means to mount the modules (the frame in Figure 4.2), co-planar with the reference device.

- means for measuring the temperature of the modules to an accuracy of  $\pm 1$  °C (three thermocouples Type T placed on the back side of each module)
- a resistor sized such that at STC (standard test condition) the modules will operate near their maximum power point (resistance of 33 ohm).

### Procedure for preconditioning

The procedure described in the IEC 61646 [4.4] foresees a series of light soaking periods at 600-1000 W/m<sup>2</sup> and 40-60°C module temperature with modules connected to the resistor, until the maximum power value stabilizes. Stabilization occurs when measurements from two consecutive periods of at least 43 kWh/m<sup>2</sup> each integrated over periods when the temperature is between 40 °C and 60 °C, meet the following criteria:  $(P_{max} - P_{min})/P_{average} < 2\%$ . The stabilization for the two CIGS modules connected in series, occurred after three light soaking periods (LS1: Irradiation = 650W/m<sup>2</sup>, T<sub>mod</sub> = 45°C-48°C, Energy = 46.150 kWh/m<sup>2</sup>; LS2: Irradiation = 650W/m<sup>2</sup>, T<sub>mod</sub> = 45°C-48°C, Energy = 46.475 kWh/m<sup>2</sup>; LS3: Irradiation = 600W/m<sup>2</sup>, T<sub>mod</sub> = 40°C-45°C, Energy = 51.600 kWh/m<sup>2</sup>). All intermediate maximum power measurements were performed at module temperature of 30.5°C reproduced within  $\pm 2$  °C.

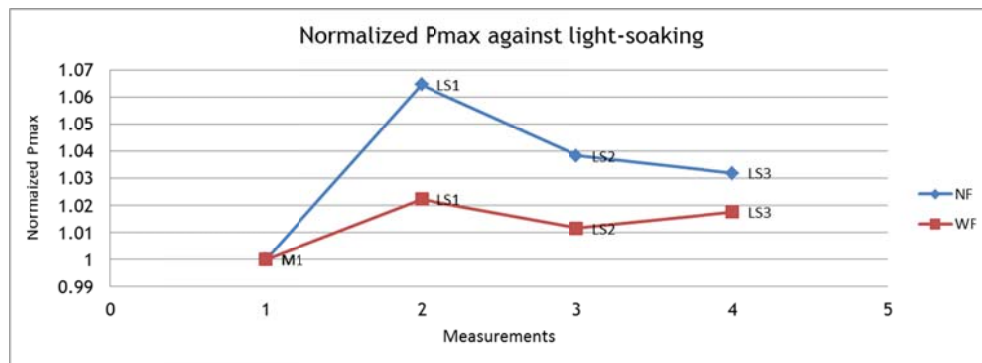


Figure 4.11: Normalized Pmax (i.e. normalized to the value of Pmax at M1, before light soaking) against light-soaking cycles referred to the no-fins CIGS module (NF) and the CIGS module with fins (WF).

The measurements of I-V characteristic curves were made immediately following the light soaking in order to minimise the effects related to the sensitivity of these devices to short term dark ageing effects.

## 4.7.4 Results

### P<sub>mppt</sub> matrices

The values of  $P_{mppt}$  is measured at different conditions of temperature and Irradiation with a step respectively of  $5^{\circ}\text{C}$  and  $100\text{ W/sqm}$ . Measurements are performed for both modules, with and without fins. The module without fins (NF) will be used as reference module for the discussion in next chapters. The matrix for the module without fins is assembled in two following stages, due to a practical convenience of heating the module up with the heating blanket in stage 1 and cooling the module down with the climatic chamber in stage 2: in the first stage, the I-V curve measurements are taken at each irradiance value (steps of  $100\text{W/sqm}$ , from  $100\text{W/sqm}$  to  $1100\text{W/sqm}$ ) starting from a temperature of  $25^{\circ}\text{C}\pm 2^{\circ}\text{C}$  to a temperature of  $75^{\circ}\text{C}\pm 2^{\circ}\text{C}$  with a step of approximately  $5^{\circ}\text{C}$ . In the second stage the I-V curve measurements are taken at some irradiance values ( $100\text{-}200\text{-}400\text{-}700\text{-}800\text{-}1000\text{W/smq}$ : the remaining irradiance values were not measured because of the difficulty to keep stable temperatures for a longer period required to flash for all irradiances values) from a temperature of  $5^{\circ}\text{C}\pm 2^{\circ}\text{C}$  to a temperature of  $20^{\circ}\text{C}\pm 2^{\circ}\text{C}$  with a step of approximately  $5^{\circ}\text{C}$ . The matrix for the module with fins is performed through measurements taken at each irradiance value (steps of  $100\text{W/sqm}$ , from  $100\text{W/sqm}$  to  $1100\text{W/sqm}$ ) starting at  $25^{\circ}\text{C}\pm 2^{\circ}\text{C}$  to  $75^{\circ}\text{C}\pm 2^{\circ}\text{C}$  with a step of approximately  $5^{\circ}\text{C}$ . Measurements for temperatures below  $25^{\circ}\text{C}$  were not performed, considering that this module is not taken as a reference for the following chapters.

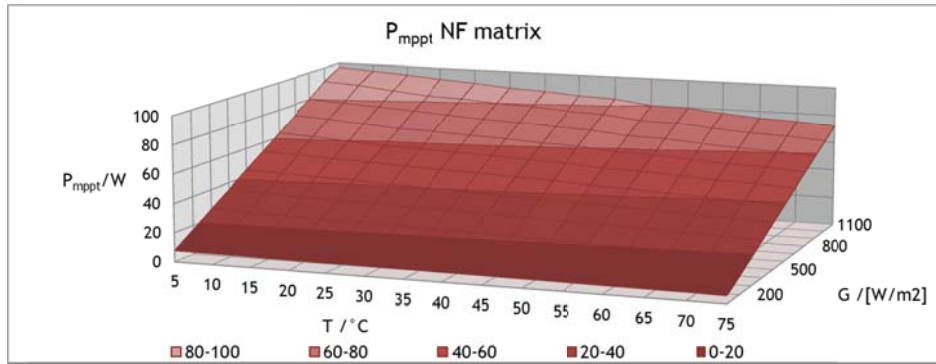


Figure 4.12: Surface that interpolate the measured maximum power point values of the module without fins (NF) at different temperature and Irradiance conditions. The values in the graph from 5 °C to 20 °C for Irradiances of 1100, 900, 600, 500, 300 W/sqm, are interpolated values since they have not been measured.

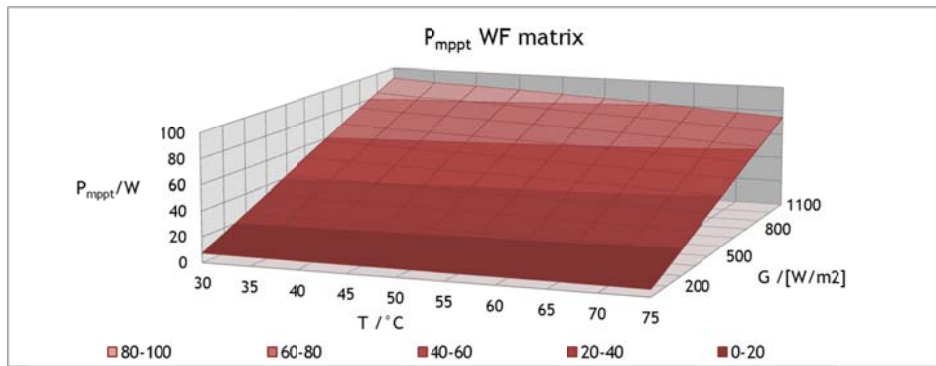


Figure 4.13: Measured maximum power point values of the module with fins (WF) at different temperature and Irradiance conditions.

During the last measurements (i.e. measurements at  $T_{mod}=75^{\circ}\text{C}$ ) of the WF  $P_{mppt}$  matrix, some cracks on the glass of the WF module appeared. This was caused by the thermal stress especially at  $75^{\circ}\text{C}$  and the different thermal expansion coefficient among the aluminium fins, the thermally conductive epoxy adhesive and the glass (thermal expansion coefficient of the aluminium is around three times the glass one).

As a consequence, the power output of the WF module slightly decreases after the second phase measurements.

Thus, only the NF module is used as reference module for the following test phases.

Equation 4.1 is the function that approximates, using the least error squares method and considering  $P_{mppt}$  linear to both irradiance and temperature, the

measured maximum power point values of the NF module, depending on Irradiance and module temperature.

$$P_{\text{mppt,NF}} = 0.0818 \cdot \text{Irr} - 0.1085 \cdot T_{\text{mod}} \quad [\text{W}]$$

Equation 4.1

### Temperature coefficient measurements

For each Irradiance value, the relative temperature coefficient is assessed from the measurements presented in the previous paragraph for both CIGS modules. According to the Standard IEC 61646 [4.4], values of Pmppt as functions of the device temperature is plotted and a least-squares-fit curve through each set of data is constructed. From the slopes of the least squares fit, straight lines for Pmppt are drawn and the temperature coefficient of Pmppt ( $\gamma$ ) is calculated (see Figure 4.14 as an example).

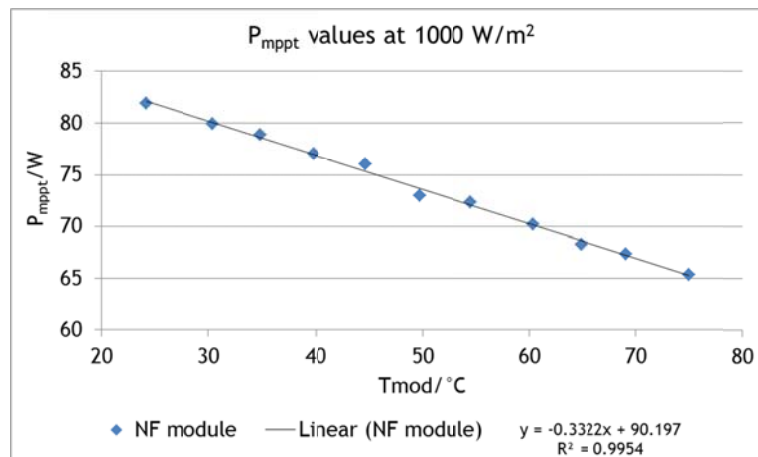


Figure 4.14: Pmppt values of the module no fins at 1000W/sqm (AM 1.5) as function of the device temperature (over a range of 50 °C) with a least-squares-fit curve through the set of data.

The power temperature coefficients are measured at each irradiance value for both the modules (with and without fins) over a temperature range, respectively, of 45 °C (30 °C-75 °C) and 50 °C (25 °C-75 °C), and the plots for each condition are inserted in the annex section.



In addition, the relative power temperature coefficients expressed as percentages are determined for each irradiance value by dividing the calculated  $\gamma$  by the value of peak power at 25 °C (see Table 4.5).

The measured temperature coefficients refer to AM 1.5.

---

**NF module**


---

G/[W/sqm]	$\gamma$ / [W/°C]	measured $P_{mppt}$ at 25 °C/[W]	$\gamma_{rel}$ / [%/°C]
1100	-0.36	89.81	-0.40
1000	-0.33	81.93	-0.41
900	-0.30	73.88	-0.41
800	-0.27	65.73	-0.42
700	-0.24	57.43	-0.43
600	-0.21	49.12	-0.43
500	-0.18	40.75	-0.44
400	-0.14	32.16	-0.45
300	-0.11	23.77	-0.46
200	-0.07	15.35	-0.47
100	-0.04	7.12	-0.50

---

Table 4.5: no fins module: power temperature coefficients ( $\gamma$ ) and relative power temperature coefficients ( $\gamma_{rel}$ ), calculated for each irradiance value (AM 1.5) from the measured  $P_{mppt}$  values at different temperatures over a range of 50 °C (25 °C-75 °C)

---

**WF module**


---

G/[W/sqm]	$\gamma$ / [W/°C]	calculated $P_{mppt}$ at 25 °C/[W]	$\gamma_{rel}$ / [%/°C]
1100	-0.37	93.65	-0.40
1000	-0.34	85.44	-0.40
900	-0.31	77.10	-0.40
800	-0.28	68.63	-0.40
700	-0.25	60.15	-0.41
600	-0.21	51.48	-0.42
500	-0.18	42.78	-0.42
400	-0.15	33.92	-0.43
300	-0.11	25.12	-0.44
200	-0.07	16.26	-0.45
100	-0.04	7.64	-0.47

---

Table 4.6: with fins module: power temperature coefficients ( $\gamma$ ) and relative power temperature coefficients ( $\gamma_{rel}$ ), calculated for each irradiance value (AM 1.5) from the measured  $P_{mppt}$  values at different temperatures over a range of 45 °C (30 °C-75 °C)

Finally, the values of the relative temperature coefficient of  $P_{mppt}$  ( $\gamma_{rel}$ ) for the two modules are plotted for each irradiance (Figure 4.15).

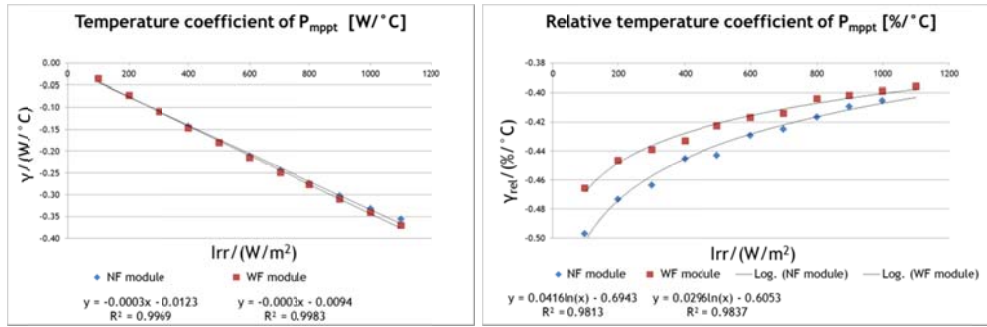


Figure 4.15:  $\gamma$  and  $\gamma_{rel}$  of the NF and WF modules are plotted for each irradiance value (AM 1.5) from the measured  $P_{mppt}$  values at different temperatures over a range of: 50 °C (25 °C-75 °C) for the NF module and 45 °C (30 °C-75 °C) for the WF module.

As shown in Figure 4.15, the relative temperature coefficient of  $P_{mppt}$  against Irradiance, for both modules, has a logarithmic regression trend, which is in accordance with [4.9], where a crystalline silicon module is tested.

The resulting dependency of the temperature coefficient  $\gamma$  on irradiance for the NF module, which is taken as a reference for the following chapters, is expressed by the following equation:

$$\gamma = -0.0003 \cdot Irr - 0.0123 \quad (R^2=0.998) \quad [W/^{\circ}C]$$

Equation 4.2

## 4.8 Phase 3: “PV in Bi” characterization

### 4.8.1 Aim of the test

Main aims of the third phase are to measure the temperature distribution of the two modules (NF and WF) integrated in the wooden wall as well as to evaluate the averaged  $\Delta T_{NF-WF}$  (i.e. average temperature difference between the two modules) operating in different environmental conditions (i.e. air temperature and irradiance). The mathematical equations which approximate the measured data are then assessed through the experimental results in order to:

- understand the dependency of the working module temperatures on the environmental conditions (i.e. air temperature and irradiance), and thus to evaluate the effectiveness of the proposed BiPV configuration;
- understand the dependency of the  $\Delta T_{NF-WF}$  between the two modules on the environmental conditions (i.e. air temperature and irradiance), and thus to evaluate the contribution provided by the fins to decrease the module temperature in each condition of irradiance and air temperature.

The modules temperature distribution and  $\Delta T_{NF-WF}$  between the two modules are measured for irradiance and air temperature conditions over an irradiance range of 600 W/sqm in steps of 200W/sqm and over a temperature range of 40°C in steps of 10°C.

### 4.8.2 Experimental setup

Measurements of this experimental phase are carried out in INTENT lab. In this third phase, unlike the phase 1, also the steady state sun simulator is used (see paragraph 4.2 for the lab description). In addition, in order to guarantee the correct functioning of the two modules close to their maximum power point value, a “stand-alone system” with an mppt tracer is set up. The stand-alone system includes:

- a maximum power point tracking solar charge controller (max. PV input voltage of 150 VDC, rated load current 10A, max. PV input power of 260W, system voltage 12 / 24VDC);
- four loads (two DC lamps of 60 W and two DC lamps of 40 W) to dissipate the produced energy depending on the working condition;
- two AGM batteries 12V-26Ah connected in series;
- cables (4mm<sup>2</sup>) to connect the system;
- an electric panel with safety devices and switches.

To size the solar charge controller considering the test conditions, the measured values of  $I_{sc}$  and  $V_{oc}$  of the two modules connected in series are verified according to the device requirements (max. PV input voltage of 150 VDC, rated load current 10A, max. PV input power of 260W).

<b>Isc [A], two modules in series</b>											
	1100	1000	900	800	700	600	500	400	300	200	100
5	2.91*	2.70	2.39*	2.17	1.89	1.60*	1.33*	1.08	0.80*	0.54	0.27
10	2.91*	2.70	2.39*	2.16	1.89	1.60*	1.34*	1.08	0.80*	0.54	0.27
15	2.92*	2.66	2.39*	2.14	1.87	1.60*	1.34*	1.07	0.80*	0.54	0.27
20	2.92*	2.66	2.40*	2.13	1.87	1.60*	1.34*	1.07	0.80*	0.54	0.27
25	2.92	2.66	2.40	2.14	1.87	1.60	1.34	1.07	0.81	0.54	0.27
30	2.93	2.67	2.40	2.14	1.87	1.61	1.34	1.07	0.81	0.54	0.27
35	2.93	2.67	2.41	2.14	1.87	1.61	1.35	1.07	0.81	0.54	0.27
40	2.93	2.67	2.41	2.14	1.88	1.61	1.35	1.07	0.81	0.54	0.27
45	2.93	2.67	2.41	2.14	1.88	1.61	1.35	1.08	0.81	0.54	0.27
50	2.94	2.68	2.41	2.15	1.88	1.61	1.35	1.08	0.81	0.54	0.27
55	2.94	2.68	2.41	2.15	1.88	1.62	1.35	1.08	0.81	0.54	0.27
60	2.94	2.68	2.42	2.15	1.88	1.62	1.35	1.08	0.81	0.54	0.27
65	2.95	2.69	2.42	2.16	1.89	1.62	1.35	1.08	0.81	0.54	0.27
70	2.95	2.69	2.42	2.16	1.89	1.62	1.36	1.08	0.81	0.54	0.27
75	2.96	2.69	2.43	2.16	1.89	1.63	1.36	1.09	0.82	0.54	0.27

\*calculated value (extrapolation)

Table 4.7: Isc values of the two modules connected in series for different conditions. The values are taken from the measurements of the NF module.

<b>Voc [V], two modules in series</b>											
	1100	1000	900	800	700	600	500	400	300	200	100
5	93.68*	93.33	92.98*	92.09	91.27	91.18*	90.34*	88.31	87.93*	84.62	80.81
10	92.39*	91.94	91.64*	90.71	89.98	89.78*	88.91*	87.07	86.44*	83.33	79.54
15	91.10*	90.52	90.31*	89.35	88.65	88.38*	87.49*	85.72	84.96*	82.06	78.28
20	89.81*	88.56	88.97*	87.41	86.73	86.98*	86.07*	83.79	83.48*	80.09	76.32
25	88.27	87.91	87.36	86.73	86.08	85.23	84.24	83.09	81.51	79.39	75.58
30	87.13	86.77	86.25	85.65	85.02	84.22	83.27	82.16	80.61	78.51	74.79
35	86.24	85.78	85.22	84.56	83.86	83.00	82.02	80.86	79.30	77.11	73.07
40	84.78	84.30	83.73	83.03	82.33	81.47	80.46	79.21	77.60	75.43	71.56
45	83.99	83.45	82.78	82.07	81.33	80.40	79.34	78.10	76.44	74.19	70.26
50	81.43	80.96	80.38	79.73	79.07	78.18	77.16	75.96	74.32	72.08	68.08
55	81.09	80.51	79.85	79.12	78.35	77.39	76.30	74.99	73.27	70.86	66.80
60	79.34	78.77	78.10	77.36	76.49	75.55	74.66	73.37	71.63	69.24	65.11
65	77.92	77.34	76.69	75.95	75.20	74.22	73.11	71.77	70.02	67.58	63.42
70	77.18	76.55	75.80	75.02	74.21	73.17	72.03	70.64	68.79	66.33	62.03
75	75.67	74.96	74.27	73.42	72.56	71.50	70.19	68.81	66.94	64.37	60.07

\*calculated value (extrapolation)

Table 4.8: Voc values of the two modules connected in series for different conditions. The values are calculated multiplying by two the measurements of the NF module.

Considering Table 4.7 and Table 4.8, the maximum PV output current is 2.96 A, and the maximum PV output voltage is 93.68 V. The two values lie below the requirements foreseen by solar charge controller and they are thus verified.

Other devices are used during the third phase experiments, and in particular:

- a current probe and a tester to double check the correct working conditions at mppt of the two modules during the experiment

- a peak power measuring device with I-V-curve tracer (PVPM 1000C), to double check the I-V curve of each module at some conditions (e.g. see Figure 4.19), with the following characteristics: Peak power measurement:  $\pm 5\%$ , duration of single measurement: 2s, reference cell Phox sensor with integrated Pt1000 sensor (Solar Radiation Sensor SOZ-03, calibrated on the 17.04.2012, calibration value: 96,0 mv at 1000W/sqm)
- an additional hot wire anemometer (air velocity handprobe 0-20 m/s FV A935-TH5K2; relative measurement uncertainty: 5%) to measure the air velocity speed in different points .



Figure 4.16: test devices used during experiments of phase 3: a current probe with a tester, a peak power measuring device with I-V-curve tracer and a stand-alone system with mppt tracer connected to the two modules. The image on the right shows the experimental setup connected to the specimen placed in the INTENT calorimeter.

The BiPV specimen is placed in INTENT calorimeter (see Figure 4.17) and the two PV modules (NF and WF) are connected in series to the stand alone system placed close to the calorimeter. The temperature distribution of the two modules is measured with twelve surface thermocouples (type T) placed on the back side of each module (see Figure 4.17). Moreover, to identify the boundary conditions of the heat transfer problem, the following data are acquired:

- the irradiation of the modules, measured with a pyranometer (as described in paragraph 4.2) placed vertically next to the modules (see Figure 4.17);
- the cold chamber air velocity, measured with a hot-wire anemometer placed at the top of the cold chamber next to the target to get the vertical value of the air velocity (see Figure 4.17);
- the cold chamber air temperature, measured with eight air thermocouples (Type T) placed next to the target (Figure 4.17);
- the surface wall temperature behind the two modules, measured with eight surface thermocouples (Type T) (see Figure 4.17);
- the air temperature in the middle of the air gap between the modules and the wall (see Figure 4.17), measured with four air thermocouples (Type T);

- the air velocity (vertical direction) in the gap between the NF module and the wall, measured with a hot-wire anemometer (see Figure 4.17).

The tests are repeated for twenty environmental conditions: varying the irradiance over a range of 600 W/sqm in steps of 200W/sqm (400W/sqm-1000W/sqm) and varying the ambient air temperature (i.e. the air temperature of the calorimeter cold chamber) over a range of 40°C in steps of 10°C (0°C-40°C). For each condition, the cold chamber air velocity (which represent the “outdoor” air velocity tangent to the PV modules and which is measured close to the target as shown in Figure 4.17) is kept constant with a value of 2m/s.

Each condition (which is a combination of air temperature and irradiance) is kept for at least two hours after reaching the steady-stead conditions.

During each test condition, the two modules operate in the same environmental conditions to ensure the comparability of the data.

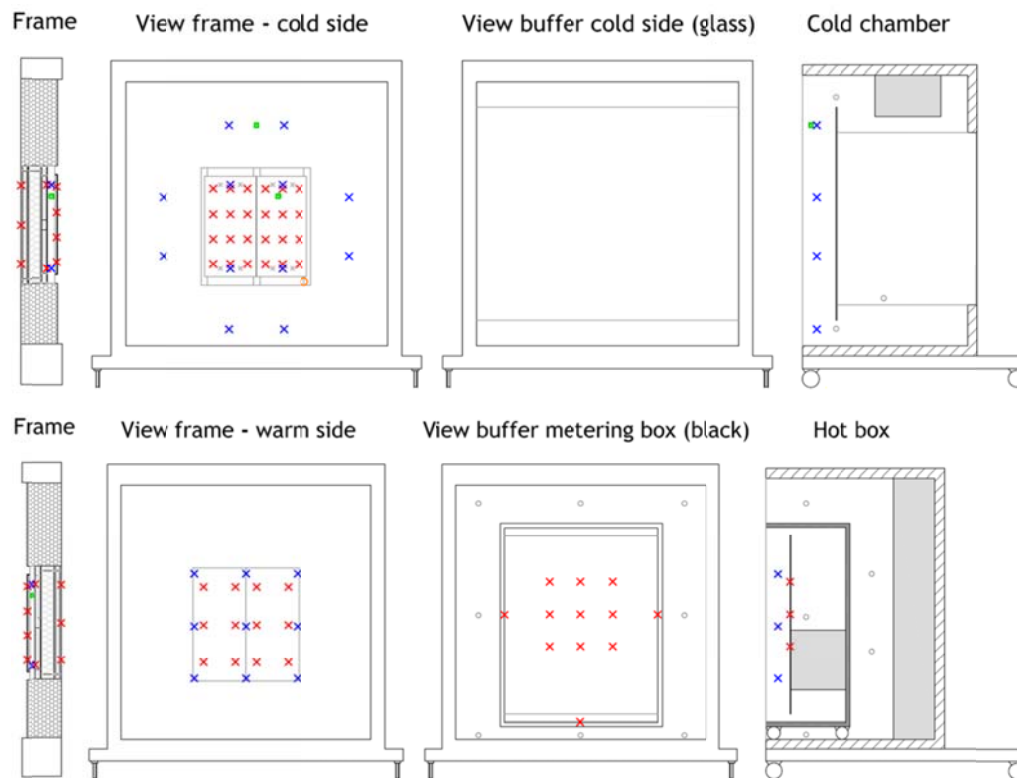


Figure 4.17: Positioning of the temperature, air velocity and irradiance sensors during the third phase of the experimental campaign (see the annex section for a more detailed drawing). The sensors are shown as follows:

**x** = surface thermocouple; **x** = air thermocouple; **x** = surface thermocouple on the wall behind the PV modules; **o** = air thermocouple of the chambers; **□** = hot wire anemometer; **o** = pyranometer

### 4.8.3 Results

The temperature distribution of each module is measured for each environmental condition with twelve thermocouples attached on the back side of each module.

Figure 4.18 shows the average temperature (i.e. the average of the values measured by the twelve thermocouples) of the two PV modules (NF and WF) and the resulting  $\Delta T_{NF-WF}$  at each environmental condition. During each test condition, the irradiance and air temperature values are kept in steady state conditions for at least two hours with a constancy over time, respectively, of  $\pm 2\%$  and  $\pm 0.2^\circ\text{C}$  (as shown in Figure 4.20). The air velocity in the cold chamber is kept at a constant value of  $2\text{m/s}$  ( $\pm 0,1\text{m/s}$  over time) in the vertical direction, as measured by the anemometer close to the PV modules surface (see Figure 4.17).

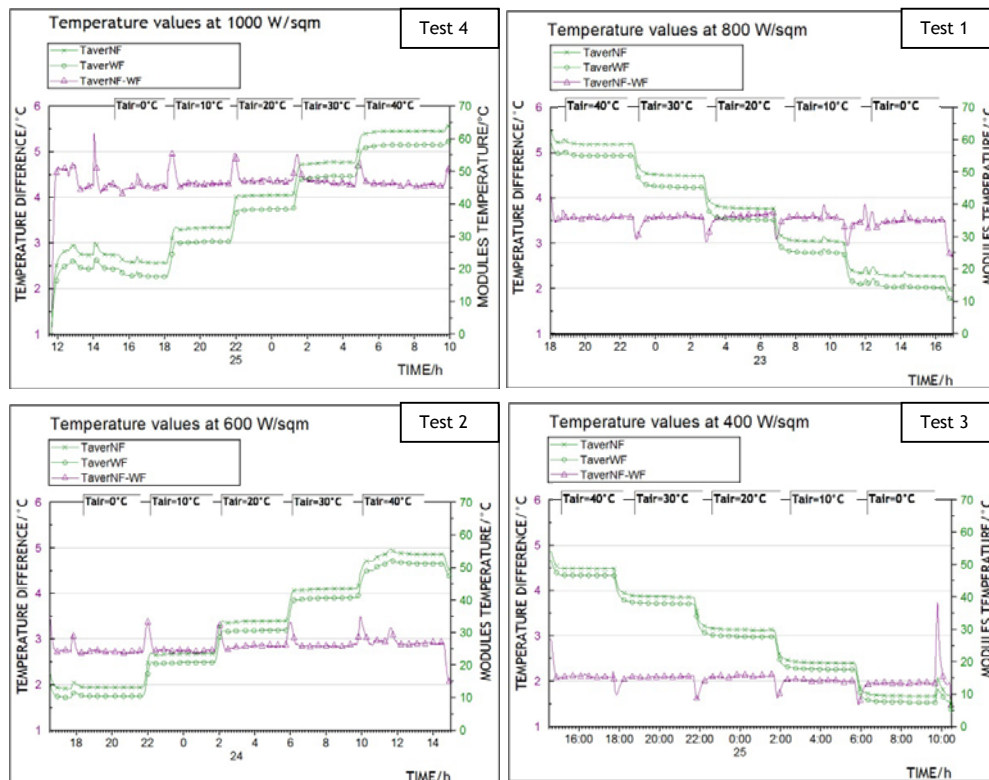


Figure 4.18: Measured average values of modules temperature (NF and WF) at twenty different set point conditions of air temperature and irradiance. The purple line shows the resulting temperature difference between the two modules.

The small peaks of “TaverNF-WF” (which is the average temperature difference between NF and WF modules) within some test conditions shown in Figure 4.18 (e.g. the three picks of Test 1, Tair of 40 °C) are due to temporary operation of the modules at Voc, since in those short periods the modules are disconnected and singularly measured with the peak power measuring device to double check the I-V curve of each module.

Figure 4.19 shows the I-V curves of the two modules measured during Test 1 (see the pick at Tair of 30 °C, Test 1, visible in Figure 4.18). The plot shows that WF module has a slightly worse performance (its current is lower), probably because of the crack in the glass mentioned in page 93. Anyway, the Pmppt value of the two modules is quite close (power difference of 2%), so that even if the two modules are connected in series to one single mppt tracer, it is clear that both modules are working close to their mppt.

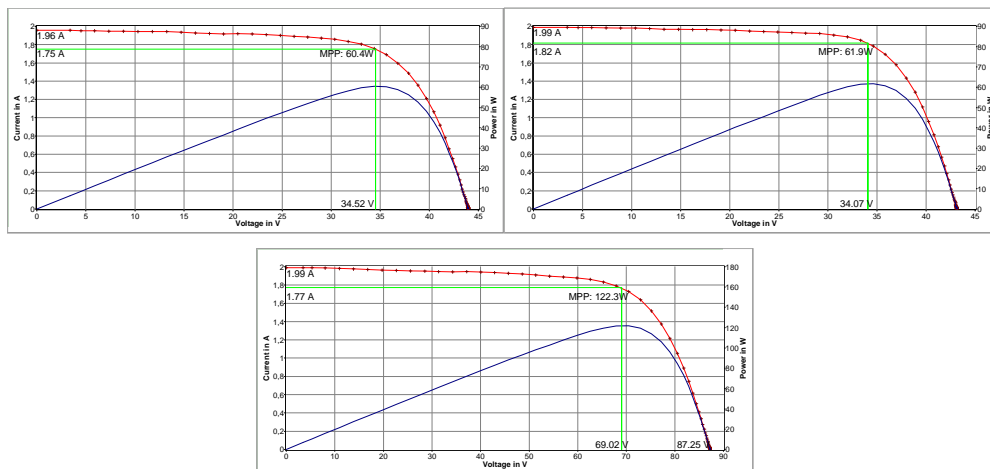


Figure 4.19: I-V characteristic curve of the WF module (above, on the left), the NF module (above, on the right) and of both modules connected in series (below) measured with a peak power measuring device with I-V-Curve tracer at an irradiance of 797W/sqm.

A filtering procedure is applied to keep only the significant data referred to the steady state conditions, eliminating the transient values between each test condition (see Figure 4.20).



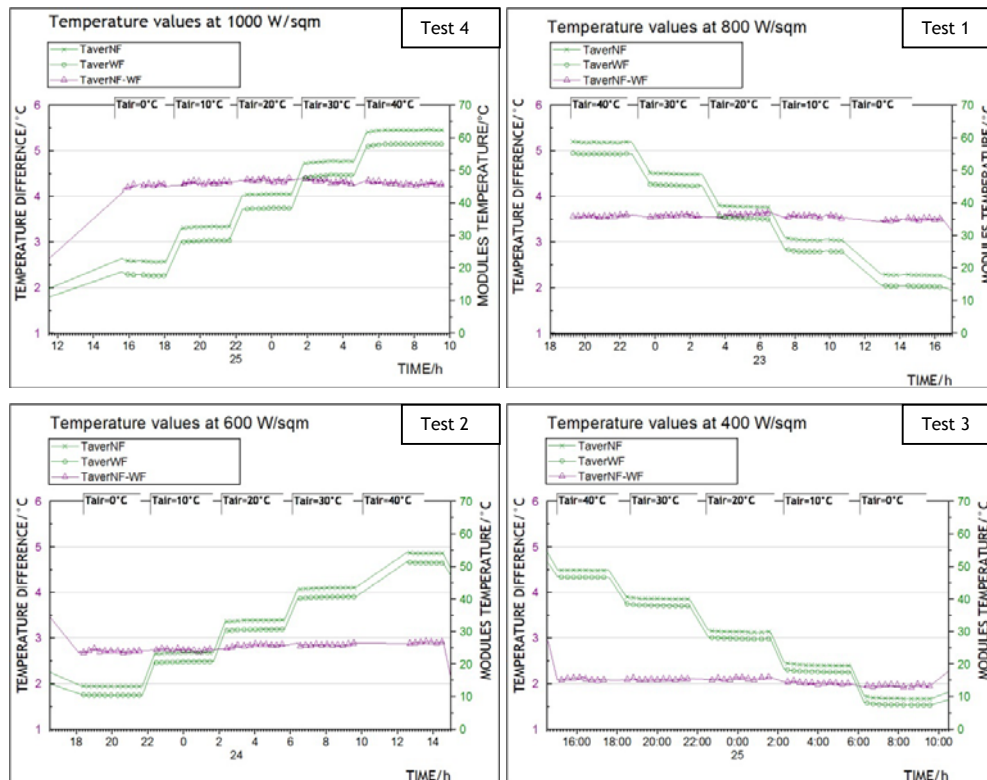


Figure 4.20: Measured average values of modules temperature (NF and WF) and resulting  $\Delta T$  between them at twenty different set point conditions of air temperature and irradiance, after applying the filtering procedure to eliminate transient points.

Figure 4.21 and Figure 4.22 show, respectively, the test boundary conditions measured in the cold chamber and in the air gap of the specimen (between the PV modules and the wooden wall), where: “Pyranometer” is the measured irradiance on the PV modules plane; “TaverAircold” is the average temperature of eight thermocouples in the calorimeter cold chamber (see Figure 4.17); “VelocityAirColdChamber” is the vertical component of the velocity tangent to the modules in the cold chamber (see Figure 4.17); “VelocityAirGap\_anemometer” is the measured air velocity in the middle of the air gap; “AirGap TNF” is the average temperature of two thermocouples in the air gap behind the NF module (see Figure 4.17); “AirGap TWF” is the average temperature of two thermocouples in the air gap behind the WF module (see Figure 4.17).

During the experiments, the air temperature of the hot chamber is kept constant at 20°C.

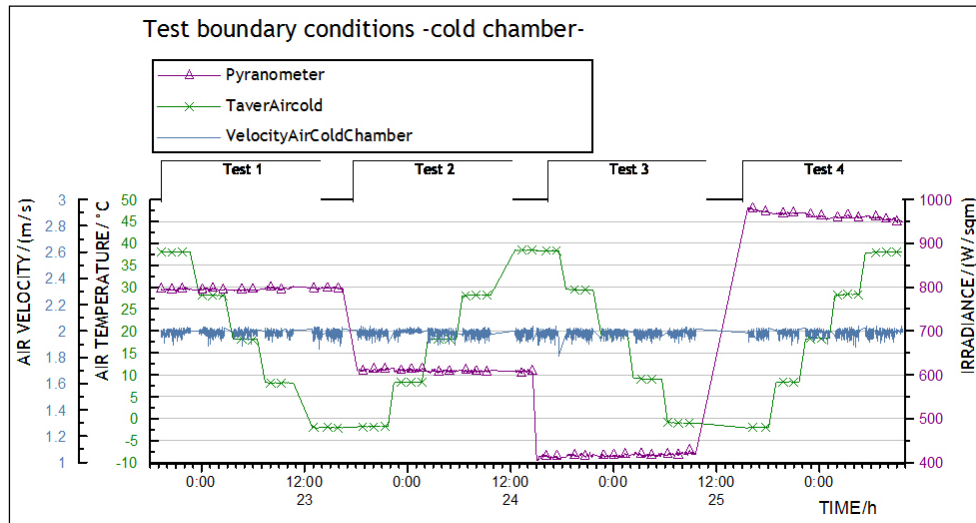


Figure 4.21: test boundary conditions of air velocity, air temperature and irradiance kept in the calorimeter cold chamber during the experiment.

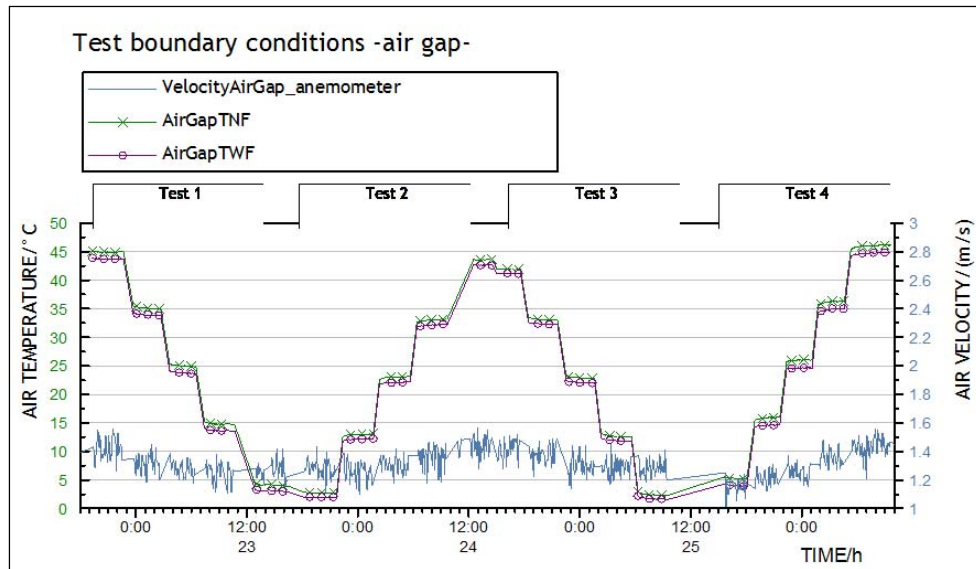


Figure 4.22: test boundary conditions of air temperature and air velocity measured in the air gap between the modules and the wooden wall during the experiment.

### Expression of $T_{NF}$ and $T_{WF}$ as function of $T_{air}$ and $I_{rr}$

After filtering the data as shown in Figure 4.20, the function which approximate the measured modules temperature values (NF module and WF module) depending on Irradiance and air temperature values is assessed using the least error squares method (Equation 4.3 and Equation 4.4).

Figure 4.23 shows the surface which approximate the measured average temperature values of the two modules depending on the cold chamber air temperature and the irradiance values, where: “T mod” is the average temperature of the NF module (on the left) and of the WF module (on the right); “Tair” is the average temperature of the air in the calorimeter cold chamber; “Irr” is the sun simulator irradiance on the modules plane.

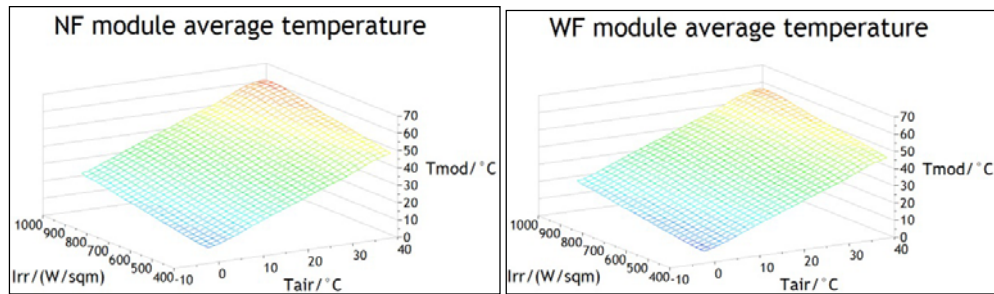


Figure 4.23: Approximated surface through the average T measured values of the two modules depending on Tair and Irradiance.

$$T_{NF} = 1.0122 \cdot T_{air} + 0.0250 \cdot Irr \quad [^{\circ}C]$$

Equation 4.3

$$T_{WF} = 1.0071 \cdot T_{air} + 0.0206 \cdot Irr \quad [^{\circ}C]$$

Equation 4.4

### NOCT model vs experimental data

The resulting Equation 4.3 can be compared with one of the most commonly used prediction model of the operating module temperature, e.g. the nominal operating cell temperature (NOCT) model [4.10] [4.11].

According to this model, the module operating temperature can be retrieved by Equation 4.5, as give below:

$$T_{mod} = T_{air} + Irr \cdot (NOCT - 20) / 800 \quad [^{\circ}C]$$

Equation 4.5

Where: Tmod, is the module temperature; Tair is the ambient temperature; Irr is the solar irradiation; NOCT is the Nominal Operating Cell Temperature

defined as the temperature reached by open circuited cells in a module under the conditions of: Irradiance on cell surface = 800 W/sqm; Air Temperature = 20°C; Wind Velocity = 1 m/s; Mounting = open back side.

For the considered CIGS module, which has an NOCT value of 47°C ±3°C (data from the datasheet), Equation 4.5 would be:

$$T_{\text{mod}} = T_{\text{air}} + 0.0338 * I_{\text{rr}} \quad [^{\circ}\text{C}]$$

Equation 4.6

The coefficients of the resulting Equation 4.6 differ from the coefficients of Equation 4.3 of 1% with regard the  $T_{\text{amb}}$  and between 17% and 33% (according to the NOCT value uncertainty given in the module datasheet:  $\text{NOCT} = 47^{\circ}\text{C} \pm 3^{\circ}\text{C}$ ) with regard the  $I_{\text{rr}}$ . Significant errors of predictions by this model are thus found with regard this application. In fact, the NOCT approach is based on the more common scenario where both sides of the PV module see the same ambient temperature and wind conditions. Instead, the two sides of the modules integrated in the prototype, are subjected to significantly different environmental conditions, as it is for most BiPV applications [4.10],[4.11],[4.13],[4.14]. Other studies [4.10] [4.11] confirm that significant errors of prediction by this model are found when the conditions of installation are different from the standard conditions as regards mounting configuration, loading and environmental conditions.

It is thus suggested not to rely on this model, even if it is a very handy and simple one, when dealing with these kind of BiPV applications, but to use more accurate techniques, such as:

- Expressions which include a parameter for BiPV situations depending on the level of integration and (ventilation) gap size, such as the one developed by Nordmann and Clavadetscher [4.15], or the one developed by Krauter [4.16];
- Expressions which include wind velocity as a parameter, such as [4.17],[4.18],[4.19],[4.20];
- A more complex, one-dimensional heat transfer model developed by Davis et al. [4.11], which includes forced and natural convection relations.

Other more complex models can be found in [4.14], which report several implicit equations for the evaluation of  $T_{mod}$ .

### Expression of $\Delta T_{NF-WF}$ as function of $T_{air}$ and $I_{rr}$

As last step, the function which approximate the measured  $\Delta T_{NF-WF}$  values (i.e.  $\Delta T$  between NF module and WF module) depending on Irradiance and air temperature values is assessed using the least error squares method (Equation 4.7). Figure 4.24 shows the  $\Delta T_{NF-WF}$  linear relation with air temperature and Irradiance, where:  $\Delta T$  is the temperature difference between the average temperature of NF module and of WF module; “ $T_{air}$ ” is the average temperature of the air in the calorimeter cold chamber; “Irradiance” is the sun simulator irradiance on the modules plane.

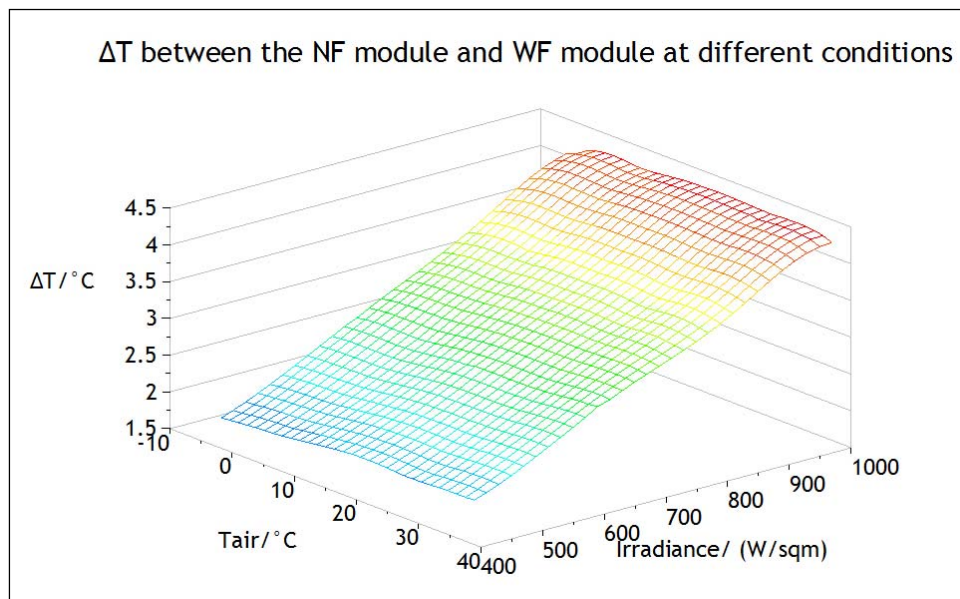


Figure 4.24: Approximated surface through the  $\Delta T$  measured data depending on  $T_{air}$  and Irradiance.

$$\Delta T_{NF-WF} = 0.0051 * T_{air} + 0.0044 * I_{rr} \quad [^{\circ}C]$$

Equation 4.7

RMS (root mean squared) of residuals= 0.0874202;  $R^2=0.989102$

Equation 4.7 refers to the measured conditions of:

- Irradiance ranging from 400W/sqm to 1000W/sqm

- Air temperature ranging from 0 to 40 °C
- Velocity of the air adjacent to the PV modules kept constant at 2m/s (as shown in Figure 4.21)
- Air gap velocity ranging between 1.1 m/s and 1.5m/s (as measured, see Figure 4.22)
- Irradiation referred to the spectrum AM 1.5

Regarding the last point, it has to be underlined that, since all measured data of irradiance refer to the spectrum AM 1.5, the spectral effects are not considered. However, this simplification is justified by the fact that the spectral effect for CIGS technology is negligible [4.12]. CIGS in fact is one of the materials which present the highest range of spectral response (as shown in Figure 4.25).

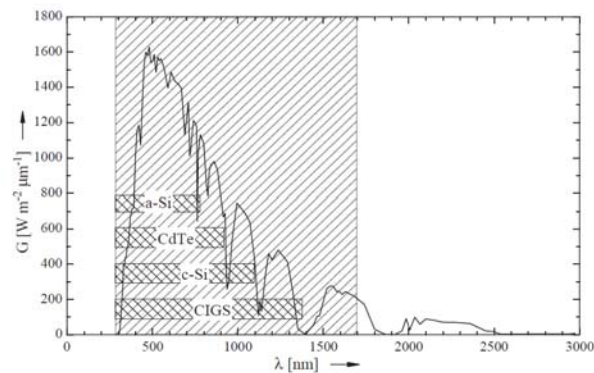


Figure 4.25: AM1.5 spectrum and corresponding spectral response of different solar cell materials. The spectral response of various materials is indicated by the boxes [4.12]

Figure 4.1 and Equation 4.7 show that the influence of  $T_{air}$  on  $\Delta T_{NF-WF}$  is much lower than the irradiance's one, considering the typical ambient conditions on the Earth ( $I_{rr}$  is typically an order of magnitude higher than  $T_{air}$ ).

For instance, a peak temperature of 50 °C would affect the value of  $\Delta T_{NF-WF}$  for an extent of 0.25 °C, while a peak irradiance of 1100W/sqm would affect the value of  $\Delta T_{NF-WF}$  for an extent of 4.8 °C, i.e. around 19 times the value due to  $T_{air}$ .

Considering the city of Aswan in Egypt as a limit example, the highest irradiance on a best oriented module (i.e. azimuth of 0° and tilt of 23°) is 1172 W/sqm and the corresponding  $T_{air}$  is 28.8 °C, happening on the 7<sup>th</sup> of March at

noon referring to the meteorological database of the commercial software PV-SOL.

In these peak conditions ( $I_{rr}=1172$  W/sqm and  $T_{air}=28.8^{\circ}\text{C}$ ), the resulting  $\Delta T_{NF-WF}$  would be  $5.3^{\circ}\text{C}$ . This number can be considered as a limit value of the maximum contribution that can be provided by the fins to decrease the module temperature in the considered conditions (as listed below the Equation 4.7).

## References

- [4.1] International Standard UNI EN ISO 8990, 1999. Thermal Insulation - Determination of steady-state thermal transmission properties - Calibrated and guarded hot box.
- [4.2] International Standard UNI EN ISO 12567, 2002. Thermal performance of windows and doors - Determination of thermal transmittance by hot box method.
- [4.3] International Standard IEC 60904-9, 2007. Photovoltaic devices -Part 9: Solar simulator performance requirements.
- [4.4] International Standard IEC 61646, 2008. Thin film terrestrial photovoltaic (PV) modules - Design qualification and type approval.
- [4.5] International Standard IEC 60891, 2009-12. Photovoltaic devices - Procedures for temperature and irradiance corrections to measured I-V characteristics.
- [4.6] Robert P. Kenny, Anatoli I. Chatzipanagi and Tony Sample, 2012. Preconditioning of thin-film PV module technologies for calibration. Progress in Photovoltaic: research and applications, DOI: 10.1002/pip.2234.
- [4.7] N. Taylor et al., April 2011. Guidelines for PV Power Measurement in Industry. Report of Performance FP6 Integrated Project.
- [4.8] M. Gostein & L. Dunn, 2011. Light Soaking Effects on Photovoltaic Modules: Overview and Literature Review. Proceedings of the 37th IEEE Photovoltaic Specialists Conference (PVSC), Seattle, Washington. 003126-003131.
- [4.9] D. L. King, J. A. Kratochvil and William E. Boyson, 1997. Temperature Coefficients for PV Modules and Arrays: Measurement, Methods, Difficulties and Results. Proceedings of the 26th IEEE Photovoltaic Specialists Conference, Anaheim, California, 1183-1186.
- [4.10] P. Trinuruk, C. Sorapipatana, D. Chenvidhya, 2009. Estimating operating cell temperature of BIPV modules in Thailand. Renewable Energy 34, 2515-2523.
- [4.11] M.W. Davis, B.P. Dougherty, A.H. Fanney, 2001. Prediction of Building integrated Photovoltaic Cell Temperatures. ASME Transactions the journal of Solar Energy Engineering, Vol. 123, No.2, 200-210.



- [4.12] R. Gottschalga et al., 2003. Experimental study of variations of the solar spectrum of relevance to thin film solar cells. *Solar Energy Materials & Solar Cells* 79, 527-537.
- [4.13] E. Skoplaki et al., 2008. A simple correlation for the operating temperature of photovoltaic modules of arbitrary mounting. *Solar Energy Materials & Solar Cells* 92, 1393-1402.
- [4.14] E. Skoplaki et al., 2008. Operating temperature of photovoltaic modules: a survey of pertinent correlations. *Renewable Energy* 34, 23-29.
- [4.15] T. Nordmann T, L. Clavadetscher, 2003. Understanding temperature effects on PV system performance. In *Proceedings of the third world conference on photovoltaic energy conversion*, Osaka, Japan. 2243-6.
- [4.16] S.C.W. Krauter, 2004. Development of an integrated solar home system. *Solar Energy Materials and Solar Cells* 82, 119-30.
- [4.17] R. Chenni et al., 2007. A detailed modelling method for photovoltaic cells. *Energy* 32, 1724-30.
- [4.18] V.V. Risser, M.K. Fuentes, 1983. Linear regression analysis of flat-plate photovoltaic system performance data. In: *Proceedings of the fifth E.C. photovoltaic solar energy conference*, Athens. 623-7.
- [4.19] D.L. King, 1997. Photovoltaic module and array performance characterization methods for all system operating conditions. In *Proceedings of the NREL/SNL photovoltaic program review meeting*, Lakewood, CO, 1-22.
- [4.20] J.M. Servant, 1985. Calculation of the cell temperature for photovoltaic modules from climatic data. In *Proceedings of the 9<sup>th</sup> biennial congress of ISES - Intersol 85*, Montreal, Canada, extended abstracts, p. 370.

## CHAPTER 5

### Test results and discussion

#### *Abstract*

In this chapter the results obtained from the whole experimental campaign are analysed and discussed.

The output of all test phases are linked together and general outcomes are provided regarding the “Bi” and the “PV” performance.

In order to evaluate the effectiveness of the proposed BiPV prototype configuration, in terms of PV performance related to the integration characteristics, the results measured for the BiPV wall prototype are compared with:

- monitored data of two BiPV systems (one façade and one roof integrated PV system) located in South Tyrol (North of Italy);
- monitored data of two ground mounted PV systems located in Bolzano (North of Italy).

Afterwards, the further improvement of the prototype PV performance due to fins application, is investigated: the expression of  $\Delta P_{NF-WF}$  (defined as the additional power produced by the PV module thanks to the influence of the fins that work as heat sinks) as a function of ambient temperature and irradiance is provided. These results are then extended to the behaviour of other PV technologies at outdoor conditions (mc-Si, a-Si, a-Si/a-Si, a-Si/ $\mu$ c-Si), using monitored data collected for one year period at the ABD PV plant of Bolzano (North of Italy).

Finally, the results are extended to one year time period considering two different locations in Italy (in the North and the South).



## 5.1 Introduction

In chapter 4, the results are presented in separate ways for each experimental phase, while chapter 5 aims at linking together the output of each part to generalize and further discuss the outcomes of the whole experimental campaign.

In particular, while phase 1 is strictly connected to the “building performance” and provides data which are independent by the other tests, phase 2 and 3 are strongly connected together and, as shown in chapter 4, the output of phase 3 is used as an input for phase 2.

The expression of “ $\Delta T_{NF-WF}$ ” (mean temperature difference between NF and WF modules) found in phase 3, is merged here together with the output of phase 2, which provides information on the dependence of the PV module performance on its operating temperature. Hence, an expression of “ $\Delta P_{NF-WF}$ ”, which is defined as the  $P_{mppt}$  difference between NF and WF modules, is derived. This expression of  $\Delta P_{NF-WF}$  as function of  $T_{air}$  (air temperature) and  $I_{rr}$  (Irradiance), allows us to generalize the results obtained in the experimental campaign to evaluate the influence of the fins on the back side of the module, considering different scenarios presented in the next paragraphs.

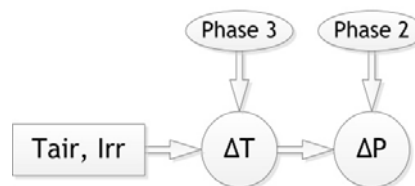


Figure 5.1: Schema linking the two test phases. Phase 3 reports the values of  $\Delta T$  (mean temperature difference between NF and WF modules) for each condition of ambient temperature ( $T_{air}$ ) and Irradiance ( $I_{rr}$ ). Values of  $\Delta P$  (i.e. additional power produced by the PV module thanks to the influence of the fins that work as heat sinks) are consequently derived thanks to the data provided by phase 2 tests.

The same approach is used to evaluate the effectiveness of the proposed BiPV prototype configuration, in terms of PV performance related to the integration characteristics. The results measured for the BiPV wall prototype are compared with monitored data of two BiPV systems (one façade and one roof integrated PV system) located in South Tyrol (North of Italy).

In particular, the BiPV wall prototype performance is compared with the monitored façade BiPV system (Ex-Post building) and the expression of  $\Delta P_{\text{Ex-Post - WF}}$  is formulated.  $\Delta P_{\text{Ex-Post - WF}}$  is defined as the additional power ( $P_{\text{mppt}}$ ) that the WF module produces being integrated as it is, with respect the hypothetical power that it would produce if it was integrated in the same way as the Ex-Post building modules (according to  $\Delta T_{\text{Ex-Post - WF}}$ ).

## 5.2 “Bi” performance

The thermal transmittance measured by the hot box method according to UNI EN ISO 12567, is **0.204 W/(m<sup>2</sup>K)**.

This value can be considered as a satisfying result in terms of building energy performance, and it is index of a well-insulated wall as its thermal transmittance is below, by an extent of 23%, the limit of 0.26 W/(sqm\*K) required by the actual Italian law referring to the worst case scenario (“zona climatica F”) [5.1].

In fact, the concept that lead to the development of this BiPV prototype, as explained in the previous chapters, foresees the idea of a building component which is first of all “energy saving” and only afterwards “energy producing”.

Energy saving is considered the first inescapable step toward an energy efficient BiPV system.

The measured value of thermal transmittance resulting from the test is coherent with that calculated according to the Standard UNI EN ISO 6946.

In fact, the discrepancy between the measured and calculated value (which is 0.188 W/(m<sup>2</sup>K)) falls within the accepted uncertainty (8,5%).

In addition, it is evaluated that the PV modules themselves do not affect in a significant way the value of thermal transmittance of the whole component, as calculated in the previous chapters according to the calculation method of the Standard UNI EN ISO 6946.

### 5.3 PV” performance

In order to evaluate the effectiveness of the proposed BiPV prototype configuration, in terms of PV performance related to the integration characteristics, the results of the prototype experiments (as reported in chapter 4) are compared with monitored data of two BiPV systems located in South Tyrol (North of Italy). The first system is a façade PV integration (Ex-post building, Bolzano-South Tyrol), while the second one is a PV roof integration (Milland Church, Bressanone-South Tyrol). Additional comparisons are then carried out with ground mounted PV systems, considering two technologies installed at the ABD PV plant (described in paragraph 5.3.3).

#### 5.3.1 BiPV façade system: Ex-Post Building

##### BiPV system description

The three-storey Post building was built in 1954 and refurbished as well as enlarged with two new storey in 2006 for the relocation of the Environmental Department. It is located in the city centre of Bolzano (North of Italy), next to the rail station. Energy efficiency has been a key point for the renovation process and a retrofit BIPV system has been integrated into two façades that face South East and South West [Figure 5.2].

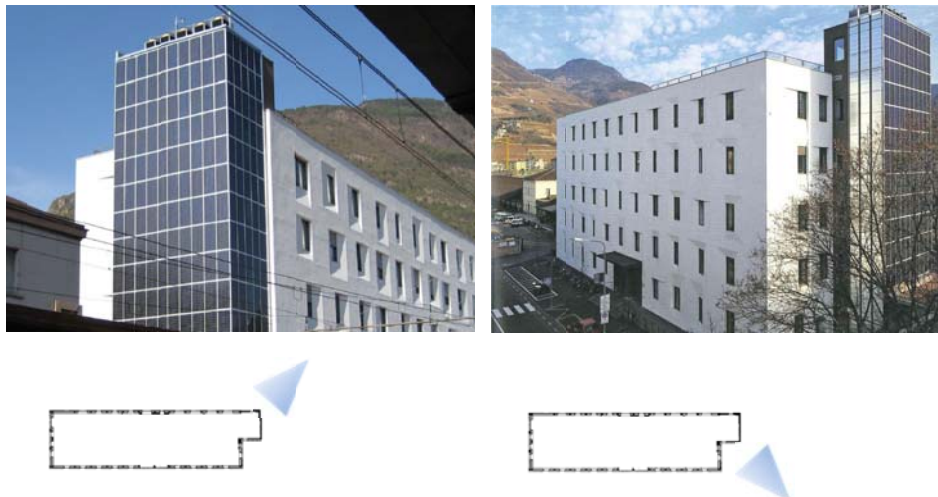


Figure 5.2: Pictures of Ex Post Building with a schema of the building plant showing the pictures point of view [source of pictures: [www.expost.it](http://www.expost.it)]

The PV modules have been applied on the existing façade through a metallic structure as a cladding of the wall [as shown in Figure 5.3]. The modules are not retro-ventilated and even if there is a 15 cm gap between the modules and the wall, a frame surrounding the PV system obstructs the air flow in the gap. Consequences of this lack of ventilation on the PV performance are discussed and analysed by L. Maturi et al. [5.7], which shows that, as for many BiPV façade applications, the PV module temperature increase is one critical aspect causing losses in PV power production: it was calculated that, with reference to one single day, the power production could be enhanced of 3.5% if the system was ventilated.



Figure 5.3: mounting system of the modules integrated in the Ex Post building façade [source: Elpo]

### **BiPV system monitored data**

Eurac is monitoring this BiPV system since 2010. The monitoring system is divided in two main parts: one for the collection of meteorological data and the other one for the registration of the PV system output.

The meteorological data system includes one reference cell mounted vertically on the SE façade and one thermocouple Pt100-M positioned on the back side of a module next to the reference cell.

Monitoring data are registered with 15 minutes intervals. Figure 5.4 shows the monitored values of the difference between  $T_{\text{mod}}$  (i.e. PV module working temperature) and  $T_{\text{air}}$  (i.e. ambient temperature) against irradiation. The difference between  $T_{\text{mod}}$  and  $T_{\text{air}}$  is a parameter very often used to evaluate, against irradiance values, the module working conditions.

The plotted set of data in Figure 5.4 refers to three months monitoring (April-June 2012). A reference cell were installed to measure irradiance and air temperature but data were acquired only for a limited period due to an

electrical fault. An alternative method to provide values of irradiance and  $T_{\text{air}}$  was therefore sought and it is described in details by Moser et al. [5.10] where the validity of satellite derived irradiance and the translational algorithm to the module plane is studied: shading correction was applied using measured on site shading diagrams.

$T_{\text{mod}}$  is measured with one thermocouple Pt100-M positioned on the back side of a module next to the reference cell placed on the SE façade.

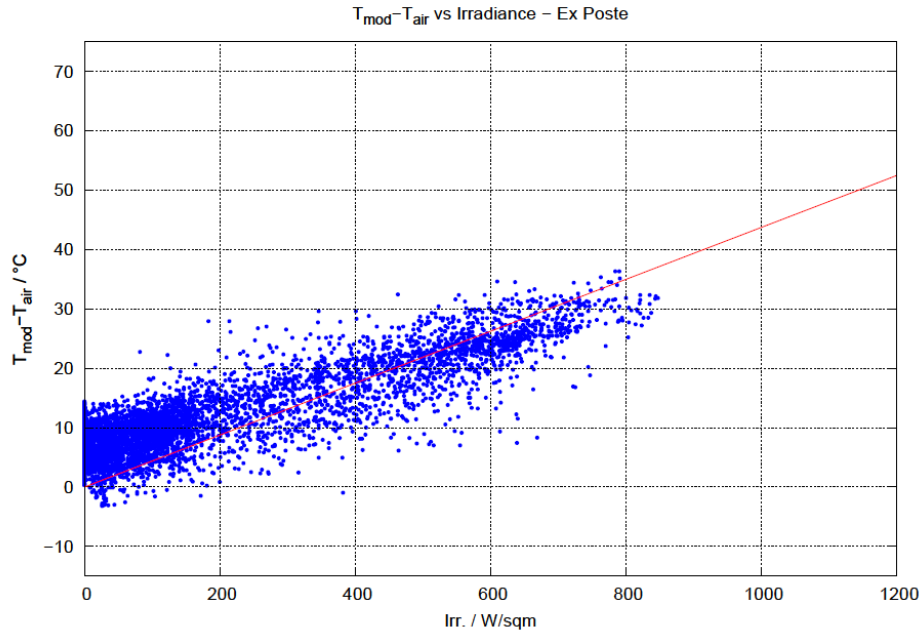


Figure 5.4: Module ( $T_{\text{mod}}$ ) and air ( $T_{\text{air}}$ ) temperature difference against Irradiance values and least-squares-fit line through the set of data (with additional constraint  $T_{\text{mod}}-T_{\text{air}}=0$  when  $\text{Irr}=0$ ), referred to Ex-Post BiPV system

The least-squares-fit line through the set of data (see Equation 5.1 and Figure 5.4) is evaluated with an additional constraint, such as  $T_{\text{mod}}-T_{\text{air}}=0$  when  $\text{Irr}=0$ , for the physical meaning related to the thermal equilibrium, in steady state conditions, when no irradiance is present. The resulting equation follows:

$$T_{\text{mod,Ex-Post}}-T_{\text{air}}= 0.0437*\text{Irr} \quad [^{\circ}\text{C}]$$

Equation 5.1

degrees of freedom (FIT\_NDF): 8732

rms of residuals (FIT\_STDFIT) =  $\sqrt{\text{WSSR}/\text{ndf}}$ : 6.58062

variance of residuals (reduced chisquare) =  $\text{WSSR}/\text{ndf}$ : 43.3046



### 5.3.2 BiPV roof system: Milland Church

#### BiPV system description

The Millan Church was designed by Arch. O. Treffer and built in 1984-85 and it is located in the city of Bressanone (South Tyrol, North of Italy). In 2008, a PV plant has been integrated into the roof. Respecting the original building shape, composition and main colours, this BiPV system is an interesting example of retrofit solution.

The PV system is integrated into the South-West facing roof, and it is made of 87 monocrystalline modules (17.83 kWp) based on monocrystalline technology with black rear side base in order to keep homogeneity in surface and colours.

The PV modules are installed on the existing metal roof, and are placed about 14 cm far from the outside roof layer, allowing a slight ventilation.

On the other hand, some obstacles are present in the inlet and outlet of the air gap reducing its section (as shown in Figure 5.6). In addition the air gap section on the top (see Figure 5.6) is quite small compared with the section on the bottom (it is around 1/3 of section 2 dimensions), and this could obstacle the proper ventilation of the whole PV system.



Figure 5.5: Picture of the roof integrated PV system of the Milland Church in Bressanone (North of Italy)



Figure 5.6: On the left: picture of the BiPV system highlighting the inlet and outlet air gap sections. On the right: zoom which shows the reduced air gap section

### **BiPV system monitored data**

Eurac is monitoring this BiPV system since 2010. The monitoring system includes a meteorological station (1 minute interval averaged over 15 minutes) and a data logger for the registration of the PV system output (15 minutes interval). The former includes one humidity and temperature sensor, one c-Si reference cell (installed in August 2011) and two thermocouples (type K) which are positioned on the back side of two modules placed in the right side of the PV system.

Figure 5.7 shows the monitored values of the difference between  $T_{\text{mod}}$  (i.e. PV module working temperature) and  $T_{\text{air}}$  (i.e. ambient temperature) against irradiation.

Values plotted in Figure 5.7 refer to averaged 15 minutes values. The plotted set of data refers to nine months monitoring (September 2011-May 2012). The considered irradiance is measured on the module plane with a c-Si reference cell.  $T_{\text{air}}$  is measured with a dedicated humidity/temperature weather station.  $T_{\text{mod}}$  is measured with two Pt100 (type K) positioned on the back side of two PV modules placed in the right side of the PV system.

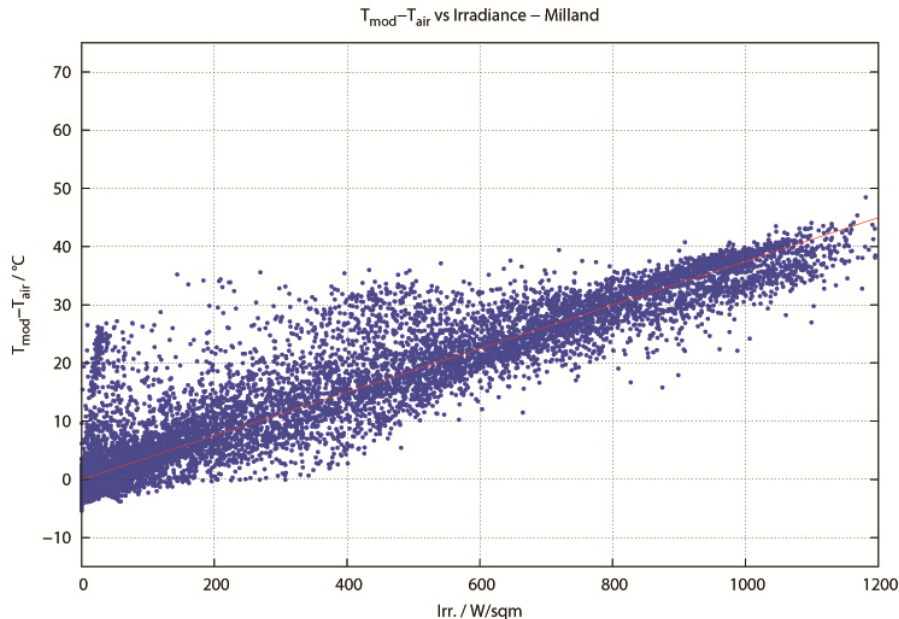


Figure 5.7: Module ( $T_{\text{mod}}$ ) and air ( $T_{\text{air}}$ ) temperature difference against Irradiance values and least-squares-fit line through the set of data (with additional constraint  $T_{\text{mod}} - T_{\text{air}} = 0$  when  $\text{Irr} = 0$ ), referred to Milland Church BiPV system.

Following the same procedure as for the BiPV system of paragraph 5.3.1, the least-squares-fit line through the set of data (see Equation 5.2) is evaluated with an additional constraint, such as  $T_{\text{mod}} - T_{\text{air}} = 0$  when  $\text{Irr} = 0$ , for the physical meaning related to the thermal equilibrium, in steady state conditions, when no irradiance is present. The resulting equation follows:

$$T_{\text{mod,Milland}} - T_{\text{air}} = 0.0375 * \text{Irr} \quad [^{\circ}\text{C}]$$

Equation 5.2

degrees of freedom (FIT\_NDF) : 24844  
 rms of residuals (FIT\_STDFIT) =  $\sqrt{\text{WSSR}/\text{ndf}}$  : 3.77109  
 variance of residuals (reduced chisquare) =  $\text{WSSR}/\text{ndf}$  : 14.2211

### 5.3.3 Ground mounted PV system: ABD PV plant

#### PV system description: PV plant at ABD

The ABD (AeroportoBolzanoDolomiti) PV plant is located in the South of the city of Bolzano (North of Italy) at the airport “Aereoporto Bolzano Dolomiti” (ABD) and it is operating since August 2010. The European Academy of Bozen/Bolzano (EURAC) is the scientific responsible for monitoring and performance and degradation evaluation of the plant, owned by ABD and developed with a co-financing of the European Regional Development Fund (ERDF) [5.2]. On an area of 205 m x 92 m = 18860 sqm the plant contains 10 different PV technologies subdivided into 24 different types of modules. The whole PV plant (Figure 5.8) is divided into a commercial field and an experimental field. The commercial field is made of 8538 CdTe-modules (662 kW<sub>p</sub>), which are installed on a rack with a fixed inclination of 30°. The experimental field contains 24 different types of modules (about 1kW<sub>p</sub> for each type), most of the which are installed on a rack with a fixed tilt of 30°. Some types are also installed on a monoaxial and a biaxial tracker.



Figure 5.8: ABD PV Plant. Experimental plant on the left and commercial part on right

#### Measurement sensors at the ABD plant

Characteristic data regarding PV modules and meteorological parameters are acquired and logged automatically every 15 min. In fact, besides the parameters from the module, such as the current  $I_{mpp}$ , voltage  $V_{mpp}$  or power  $P_{mpp}$  at the maximum power point (mpp), also data from a meteo station installed at the airport are collected [5.3].

The meteo station at ABD include a number of quite accurate tools to measure irradiance, ambient temperature, module temperature and wind values.

Irradiance values are acquired with:

- Two pyranometers (Kipp & Zonen CMP) to measure the diffuse and the global horizontal radiation. To measure the diffuse radiation one pyranometer is shadowed by a sphere (Figure 5.9, on the left). The system is mounted on a 2-axis sun tracker;
- a pyr heliometer (Kipp & Zonen CHP1) (Figure 5.9, on the left);
- an additional pyranometer (Kipp & Zonen CMP) for measuring the global irradiance at tilt of  $30^\circ$  (same plane as the modules) (Figure 5.9, in the centre);
- four reference cells for measuring the global irradiance: one c-Si reference cell on the horizontal plane, one c-Si reference cell at tilt of  $30^\circ$ , one KG5 on the horizontal plane, one KG5 at tilt of  $30^\circ$  (Figure 5.9, in the centre);
- one albedometer to determine the albedo ( $\alpha_{\text{albedo}} = \text{Irr}_{\text{refl}} / \text{Irr}_{\text{global},0}$ ). It consists of two pyranometer: one facing the sky and measuring the global radiation ( $\text{Irr}_{\text{global},0}$ ) and the other one facing the ground and measuring the reflected radiation ( $\text{Irr}_{\text{refl}}$ ) (Figure 5.9, on the right).

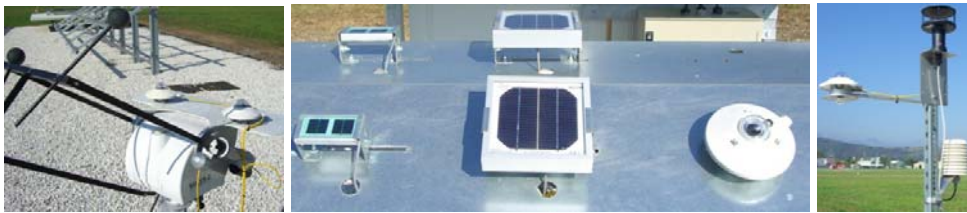


Figure 5.9: meteo station at ABD PV Plant, respectively: two pyranometers with a pyr heliometer; a pyranometer and four reference cells (KG5 on the left and c-Si ref. cell on the right); one albedometer on the left, one anemometer on the top, a PT100 covered by a weather and radiation protection on the right.

The modules and the air temperature are acquired with PT100 resistance temperature sensors. The PT100 that measures the air temperature is covered by a weather and radiation protection (Figure 5.9, on the right); while the PT100 that measure the modules temperature is attached on the back side of the modules (at least one PT100 for each module type).

The wind velocity and direction are measured with a sonic anemometer (Figure 5.9, on the right).

### PV system monitored data

Among the PV technologies at ABD plant, there is the same module technology which is the same as the one integrated in the system described in paragraph 5.3.2, i.e. mono-crystalline back contact technology (same technology and manufacturer of the Milland Church roof integrated system) (Figure 5.10).

This paragraph thus presents the monitored parameter  $T_{\text{mod}}-T_{\text{air}}$  against irradiance, referred to this technology installed on a fixed rack in an open field.

This allows to compare the monitored working conditions of integrated and not-integrated PV modules.



Figure 5.10: The analysed PV systems at ABD: mono-crystalline back-contact technology [source:Eurac].

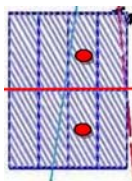


Figure 5.11: schema of the positioning of the two PT100 on the back side of the modules [source:Eurac].

Figure 5.12 shows the monitored values of the difference between  $T_{\text{mod}}$  (i.e. PV module working temperature) and  $T_{\text{air}}$  (i.e. ambient temperature) against irradiation referred to the considered technology.

Values plotted in Figure 5.12 refers to averaged 15 minutes values. The plotted set of data refers to one year monitoring (January-December 2012). The

considered irradiance is measured on the module plane (i.e.  $30^\circ$ ) with a pyranometer Kipp&Zonen CMP11.  $T_{\text{air}}$  is measured with a Pt100 covered by a weather and radiation protection (see Figure 5.9).

$T_{\text{mod}}$  is measured with two Pt100 positioned as indicated in Figure 5.11 on the back side of the PV modules, fixed with silicone and a thermal compound between the module and the sensor.

The plotted data include only conditions such that  $I_{\text{rr}} > 0$  and  $P_{\text{dc}} > 0$  ( $P_{\text{dc}}$  is the power produced by the modules, as direct current), thus when the PV system is operating.

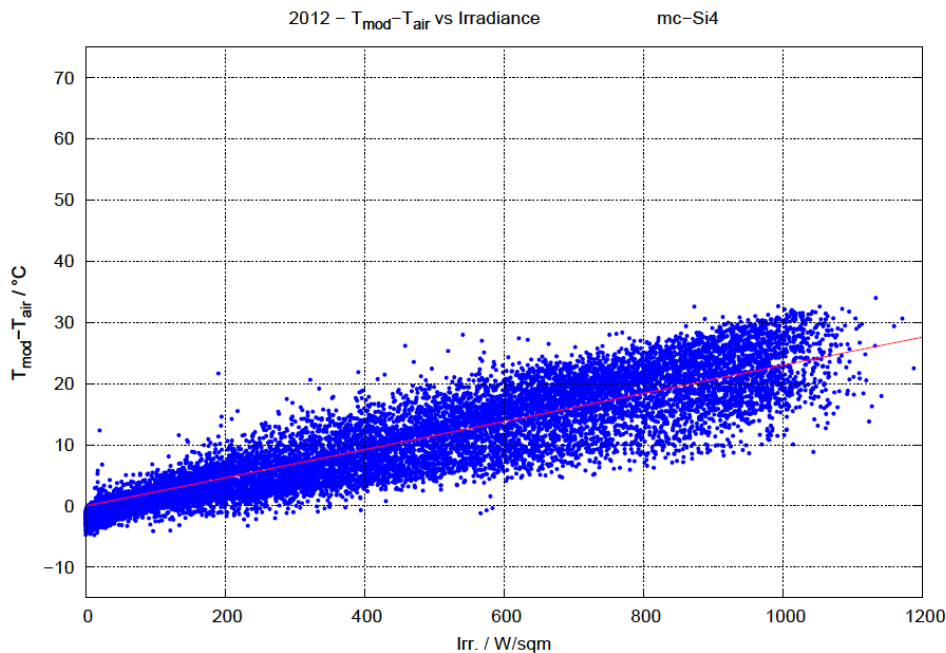


Figure 5.12: Module ( $T_{\text{mod}}$ ) and air ( $T_{\text{air}}$ ) temperature difference against Irradiance values and least-squares-fit line through the set of data (with additional constraint  $T_{\text{mod}} - T_{\text{air}} = 0$  when  $I_{\text{rr}} = 0$ ), referred to the mono-crystalline back-contact technology at ABD plant.

Following the same procedure as for the BiPV systems of paragraph 5.3.1 and 5.3.2, the least-squares-fit lines through the set of data (see Equation 5.3) are evaluated with an additional constraint, such as  $T_{\text{mod}} - T_{\text{air}} = 0$  when  $I_{\text{rr}} = 0$ . The resulting equation follows:



$$T_{\text{mod,m-Si}} - T_{\text{air}} = 0.0230 \cdot I_{\text{rr}} \quad [^{\circ}\text{C}]$$

Equation 5.3

Degrees of freedom = 16581; rms of residuals =  $\sqrt{\text{WSSR}/\text{ndf}} = 3.39886$

variance of residuals (reduced chisquare) =  $\text{WSSR}/\text{ndf} = 11.5523$

### 5.3.4 BiPV wall prototype

This paragraph presents the measured parameter  $T_{\text{mod}} - T_{\text{air}}$  against irradiance, referred to the BiPV wall prototype developed in this thesis.

Figure 5.13 and Figure 5.14 show the measured values of the difference between  $T_{\text{mod}}$  (i.e. PV module working temperature) and  $T_{\text{air}}$  (i.e. ambient temperature) against irradiation referred respectively to the NF and WF modules integrated in the BiPV wall prototype.

Values plotted in Figure 5.13 and Figure 5.14 refer to indoor measurement conditions are described in detail in chapter 4 (see boundary conditions listed below Equation 4.7).

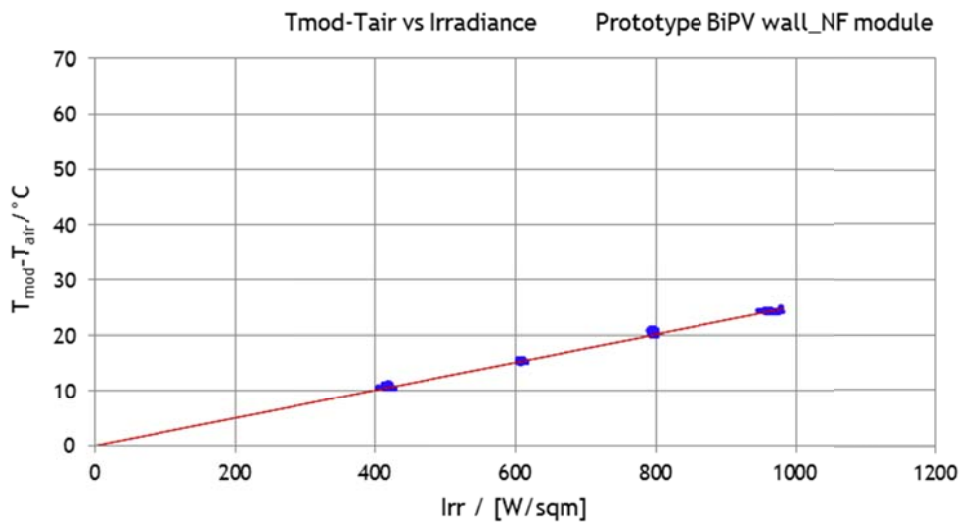


Figure 5.13: Module ( $T_{\text{mod}}$ ) and air ( $T_{\text{air}}$ ) temperature difference against Irradiance values and least-squares-fit line through the set of data (with additional constraint  $T_{\text{mod}} - T_{\text{air}} = 0$  when  $I_{\text{rr}} = 0$ ), referred to the NF module of the BiPV wall prototype.



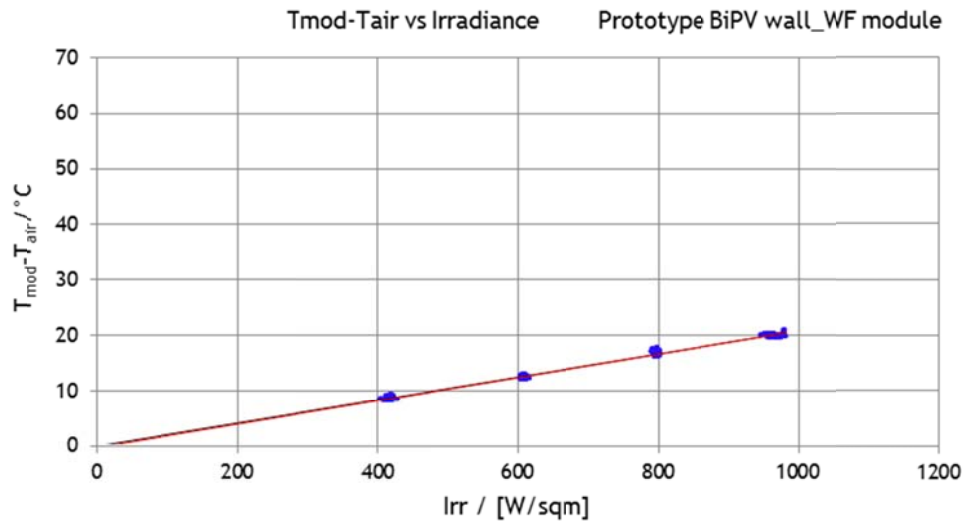


Figure 5.14: Module ( $T_{\text{mod}}$ ) and air ( $T_{\text{air}}$ ) temperature difference against Irradiance values and least-squares-fit line through the set of data (with additional constraint  $T_{\text{mod}}-T_{\text{air}}=0$  when  $I_{\text{rr}}=0$ ), referred to the WF module of the BiPV wall prototype.

The least-squares-fit lines through the set of data (see Equation 5.4 and Equation 5.5) are evaluated with the additional constraint, such as  $T_{\text{mod}}-T_{\text{air}}=0$  when  $I_{\text{rr}}=0$ . The resulting equations follow:

$$T_{\text{mod,NF}}-T_{\text{air}}= 0.0253*I_{\text{rr}} \quad [^{\circ}\text{C}]$$

Equation 5.4

Coefficient of determination ( $R^2$ )= 0.9950

Equation 5.4 refers to the NF module integrated in the BiPV wall prototype.

$$T_{\text{mod,WF}}-T_{\text{air}}= 0.0208*I_{\text{rr}} \quad [^{\circ}\text{C}]$$

Equation 5.5

Coefficient of determination ( $R^2$ )= 0.9932

Equation 5.4 refers to the WF module integrated in the BiPV wall prototype.

### 5.3.5 Performance comparison with BiPV wall prototype

#### Comparison Prototype-BiPV monitored systems

Ex-Post and Milland Church BiPV systems, are two interesting case studies which offer examples of typical problems related, respectively, to PV façade and roof integrated systems.

For many applications in fact, it is a common practice to integrate PV systems in the building envelope without foreseeing a proper ventilation and this leads to the achievement of higher PV module temperatures.

The performance comparison among the Ex-Post facade system, the Milland Church roof system and the BiPV wall prototype developed in this thesis, is thus focused on the PV working temperature conditions, which is related of course to the PV performance as explained in the previous paragraphs and chapters.

The parameters  $T_{\text{mod}}-T_{\text{air}}$  against irradiance, evaluated for the two BiPV systems (as described in paragraph 5.3.1 and 5.3.2), are compared with the one measured for the BiPV wall prototype (as described in paragraph 5.3.4).

Equation 5.1, Equation 5.2, Equation 5.4, Equation 5.5 are plotted and compared in Figure 5.15.

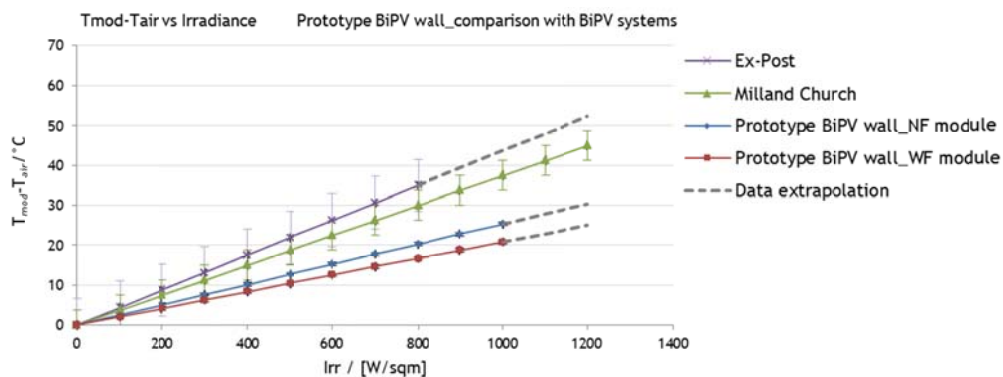


Figure 5.15: plots of Equation 5.1, Equation 5.2, Equation 5.4 and Equation 5.5.

Figure 5.15 shows the comparison of the parameter  $T_{\text{mod}}-T_{\text{air}}$  against irradiance between the two analyzed BiPV systems and the BiPV wall prototype.

It is clearly visible that, as expected, the Ex-Post BiPV system is the worst performing while the WF module of the wall prototype is the best performing. Modules integrated in the Ex-Post building in fact (as shown in paragraph 5.3.1) are not retro-ventilated and this of course affects the module operating temperatures. On the contrary, the WF module of the wall prototype is very well retro-ventilated and in addition it was specifically designed with the heat-sink system to additionally decrease its temperature.

According to the monitored data, the PV modules integrated in the Ex-Post building are operating at a temperature which is  $2.3\%I_{rr}$  higher with respect the best performing WF module integrated into the BiPV wall prototype.

This means that, e.g. at a top irradiance of  $1000\text{W}/\text{sqm}$ , the Ex-Post PV modules would work at a temperature which is  $23^\circ\text{C}$  higher with respect the BiPV wall prototype WF module.

This temperature difference is quite significant and thus affects the PV performance in a significant way. This would be particularly emphasized for those PV technologies which present important temperature coefficients (e.g. crystalline technology, for which the power temperature coefficient  $\gamma_{rel}$  is typically around  $-0.5\%/^\circ\text{C}$ ).

This confirms that different integration configurations can strongly influence the working module temperatures and thus the PV performance.

It also confirms the importance to design for proper ventilation behind the BiPV elements, which, as demonstrated, can enable a temperature reduction of up to  $23^\circ\text{C}$  to be achieved. Similar values were found by Norton et al. in [5.11], which formulated a possible temperature reduction up to around  $20^\circ\text{C}$  to be achieved thanks to natural ventilation.

Figure 5.15 also shows that the PV modules integrated in the Milland Church roof present working temperature conditions which are in between the not-ventilated Ex-Post building and the well ventilated BiPV wall prototype.

This result is also in agreement with expectations: in fact the modules in this case are retro-ventilated but still some obstacles and problems are present as shown in paragraph 5.3.2. The Milland Church PV modules operate at a temperature which is  $1.2\%I_{rr}$  higher with respect the NF module integrated in the BiPV wall prototype.

This means that, e.g. at a top irradiance of 1000W/sqm, the Milland PV modules work at a temperature which is 12 °C higher with respect the BiPV wall prototype NF module. The temperature difference in this case is not that significant as in the previous case. The temperature difference between the NF and WF modules of the BiPV wall modules is extensively discussed in paragraphs 0. The WF module operates at a temperature which is 0.45%\*Irr lower than the NF module, which means a decrease of around 4.5 °C at top irradiance conditions of 1000W/sqm.

This confirms that, as already discussed in paragraphs 5.3 and 5.4.2, the applied heat sink system (i.e. the fins) provide an additional slight increase in PV power performance.

### Comparison Prototype-PV ground mounted system

An additional comparison between the PV working temperature conditions of the BiPV wall prototype and of a ground mounted PV system (described in paragraph 5.3.3) is carried out. Figure 5.16 shows that the PV working temperatures of the modules integrated in the BiPV wall prototype are quite close with the ones of the ground mounted PV system. A limitation to this analysis is given by the fact that the plotted equations reported in Figure 5.16 and in Figure 5.15 refer to outdoor monitored data (for the ground-mounted system) and to indoor experimental data (for the BiPv prototype) and we are thus comparing indoor measured data (with constant wind velocity) with outdoor monitored data.

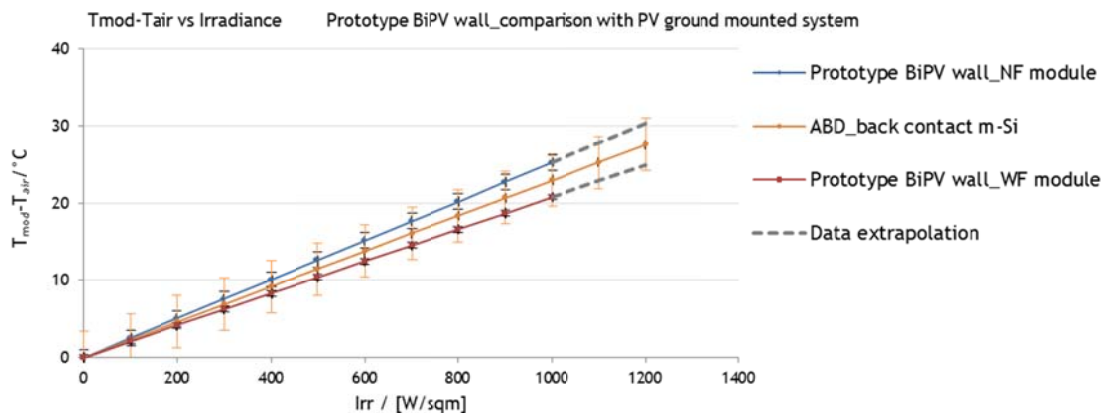


Figure 5.16: plots of Equation 5.3, Equation 5.4 and Equation 5.5

### Comparison conclusions

Concluding, Figure 5.17, which summarizes all results together, shows that the temperature working conditions of the BiPV prototype modules are closer to the conditions reported for the ground-mounted PV systems (i.e. CIGS and m-Si at ABD plant) than the ones reported for the BiPV not retro-ventilated façade system (i.e. Ex-Post building).

These results highlight the effectiveness of the proposed BiPV prototype configuration, in terms of PV performance related to the integration characteristics.

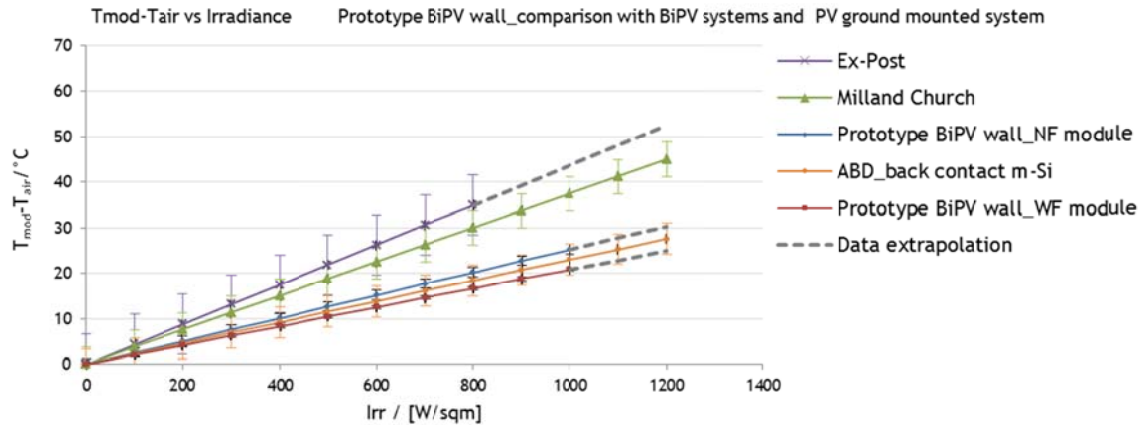


Figure 5.17: plots of Equation 5.1, Equation 5.2, Equation 5.3, Equation 5.4 and Equation 5.5.

### 5.3.6 Generalization of results over one year time period

Results reported in paragraph 5.3.5 regarding the comparison between the BiPV wall prototype and the Ex Post building, are here generalized over one year time period considering the ambient conditions of two different locations in Northern and Southern Italy, i.e. Bolzano and Agrigento.

According to Figure 5.15, the Ex-Post BiPV system is the worst performing while the WF module of the wall prototype is the best performing, in terms of PV operating temperatures.

By subtracting Equation 5.5 (which provides the values of  $T_{mod,Wf}$  as a function of  $T_{air}$  and  $Irr$ ) to Equation 5.1 (which provides the values of  $T_{mod,Ex-Post}$  as a function of  $T_{air}$  and  $Irr$ ), the value of  $\Delta T_{Ex-Post - Wf}$  is obtained:

$$\Delta T_{\text{Ex-Post} - \text{WF}} = 0.0229 * I_{\text{rr}} \quad [^{\circ}\text{C}]$$

Equation 5.6

$\Delta T_{\text{Ex-Post} - \text{WF}}$  is defined as the working temperature difference, as function of Irradiance, between the WF module integrated in the BiPV wall prototype and the modules integrated in the Ex-Post façade, according to measured and monitored data as explained in paragraphs 5.3.4 and 5.3.1.

By multiplying Equation 4.2 (i.e. the value of the CIGS module power temperature coefficient as function of irradiance) with Equation 5.6, the value of  $\Delta P_{\text{Ex-Post} - \text{WF}}$ , for each condition of Irradiance, is evaluated.

$\Delta P_{\text{Ex-Post} - \text{WF}}$  is defined as the additional power ( $P_{\text{mppt}}$ ) that the WF module produces being integrated as it is, with respect the hypothetical power that it would produce if it was integrated in the same way as the Ex-Post building modules (according to  $\Delta T_{\text{Ex-Post} - \text{WF}}$ ).

$$\Delta P_{\text{Ex-Post} - \text{WF}} = (0.0229 * I_{\text{rr}}) * (-0.0003 * I_{\text{rr}} - 0.0123) \quad [\text{W}]$$

Equation 5.7

Equation 5.7 allows to calculate the value of  $\Delta P_{\text{Ex-Post} - \text{WF}}$  for each ambient condition, according to the measured data of  $T_{\text{mod,WF}}$  (see Equation 5.5, and measurement boundary conditions listed below Equation 4.7) and to the monitored data of  $T_{\text{mod,Ex-Post}}$  (see Equation 5.1).

Considering the ambient conditions of two different locations in Northern and Southern Italy, i.e. Bolzano and Agrigento, the hourly based values of  $\Delta P_{\text{Ex-Post} - \text{WF}}$  are evaluated for one reference year. The final value of the annual  $\Delta E_{\text{Ex-Post} - \text{WF}}$  (i.e. the annual energy production difference due to  $\Delta T_{\text{Ex-Post} - \text{WF}}$ ) is then assessed.

### **Meteo data**

The data of ambient temperature and Irradiance used in this analysis are taken from the CTI (Comitato Termotecnico Italiano) database which provides the characteristic climate year of all the Italian provinces, referred to the calculation model of the UNI EN ISO 15927 - 4:2005 "Hygrothermal performance

of buildings - Calculation and presentation of climatic data - Part 4: Hourly data for Assessing the annual energy use for heating and cooling".

Every characteristic year data-set is made of 12 characteristic months selected from a database of weather data actually measured for a period of at least 10 years and contains hourly records of meteorological variables, among which there is the ambient temperature and the global solar irradiance on the horizontal plane.

The values of irradiance on the horizontal plane are then transposed on the vertical plane through the algorithm of the commercial software Valentine PV-SOL Expert. Figure 5.18 shows the resulting average monthly values of irradiance onto a vertical south facing façade for the two locations Agrigento and Bolzano. As expected, the peak of solar radiation is not during summer, as it would happen for an horizontal surface, because it is referred to a vertical surface facing South.

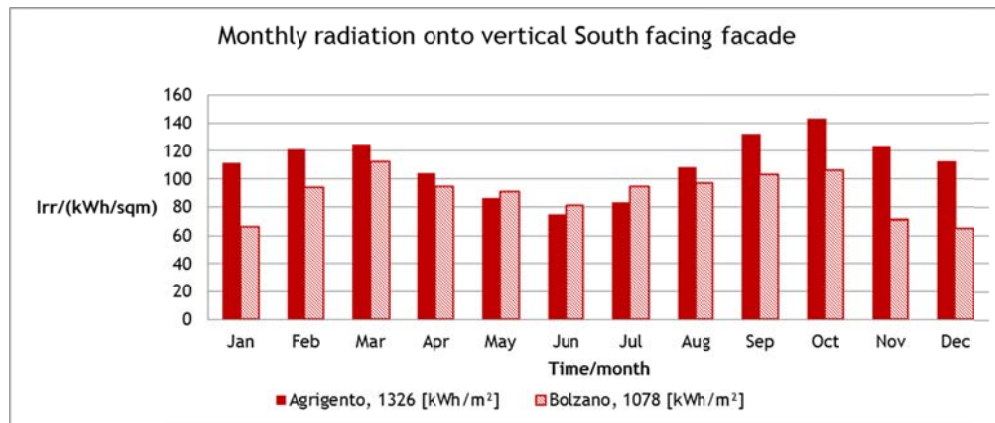


Figure 5.18: average monthly values of irradiance onto a vertical south facing façade for the two locations Agrigento and Bolzano.

## Results

The results reported in this paragraph refers to an hypothetical positioning of the two compared systems on a vertical plane (tilt=90°) South facing (azimuth=0°).

### Bolzano

Based on hourly calculation, the total annual amount of difference of energy production  $\Delta E_{\text{Ex-Post} - \text{WF}}$ , due to  $\Delta T_{\text{Ex-Post} - \text{WF}}$ , results to be 43.70 kWh/(kWp y) for

the city of Bolzano. This value is evaluated summing the  $\Delta E_{\text{Ex-Post} - \text{WF}}$  calculated for each hour, over the whole year.

The reference specific annual yield of a BiPV façade system of Wuerth CIGS modules South facing [Figure 5.19], is calculated through the commercial dynamic simulation software PV-SOL and results to be 818.2 kWh/kWp.

Considering this reference yield, the  $\Delta E_{\text{Ex-Post} - \text{WF}}$ , as related to the integration characteristics, accounts thus for 5.34% of the annual energy production.

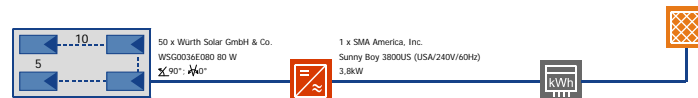


Figure 5.19: Schema of the reference South facing BiPV façade simulated with the commercial software PV-SOL.

Moreover, the average working temperature difference between the WF module and the Ex-Post modules (average calculated on hourly values over one year when  $I_{rr} > 100 \text{ W/sqm}$ ) results to be  $8.2^\circ \text{C}$  (WF module:  $23.8^\circ \text{C}$ , Ex-Post module:  $32^\circ \text{C}$ ).

Reliability research states that the PV degradation rate doubles for every  $10^\circ \text{C}$  increase in temperature [5.9], implying that an array design that ran e.g.  $10^\circ \text{C}$  hotter than another could be expected to last only half as long.

Hypothesizing a direct linear correlation for the degradation rate, a first estimation would thus lead to the consideration that in the climate of Bolzano, the “best integrated” WF module could potentially last around 4/5 longer than the “worst integrated” Ex-Post modules.

### Agrigento

For the city of Agrigento, the total annual amount of difference of energy production  $\Delta E_{\text{Ex-Post} - \text{WF}}$ , due to  $\Delta T_{\text{Ex-Post} - \text{WF}}$ , results to be 59.60 kWh/(kWp y), i.e. 15.9 kWh/(kWp y) more than the value referred to Bolzano.

The reference specific annual yield of a BiPV façade system of Wuerth CIGS modules South facing [the same reference system shown in Figure 5.19], is calculated also for the city of Agrigento through the commercial dynamic simulation software PV-SOL and results to be 993.8 kWh/kWp.

Considering this reference yield, the  $\Delta E_{\text{Ex-Post} - \text{WF}}$ , due to  $\Delta T_{\text{Ex-Post} - \text{WF}}$ , accounts thus for 6.00% of the annual energy production.



Moreover, the average working temperature difference between the WF module and the Ex-Post modules (average calculated on hourly values over one year when  $I_{rr} > 100 \text{ W/sqm}$ ) results to be  $11.4^\circ\text{C}$  (WF module:  $30^\circ\text{C}$ , Ex-Post module:  $41.4^\circ\text{C}$ ).

According to [5.9] as mentioned for the city of Bolzano, a first estimation leads to the consideration that in the climate of Agrigento, the “best integrated” WF module could potentially last more than twice longer than the “worst integrated” Ex-Post modules.

### **Conclusions**

The module working temperature difference  $\Delta T_{\text{Ex-Post} - \text{WF}}$ , which is related to the integration characteristics, leads to an energy production difference  $\Delta E_{\text{Ex-Post} - \text{WF}}$  which accounts for the 6.00% of the annual energy production in the Agrigento climate (South of Italy) and for the 5.34% of the annual energy production in the Bolzano climate (North of Italy).

This means that a proper design for natural ventilation in a BiPV system, leads to an energy gain which can be considered as significant.

In addition, it has also to be taken into account that decreasing the module temperature could also lead to other positive effects, i.e. the opportunity to prolong the life time of an operating PV array due to lower thermal stress.

This effect has been roughly estimated for the two cities: the “well integrated” WF module could potentially last around 4/5 longer than the “bad integrated” Ex-Post modules in Bolzano and more than twice longer in Agrigento.

These results highlight the importance of a proper design for integration of PV systems in the building envelope.

## 5.4 Further PV performance improvement due to fins application

The results of the experimental phases 2 and 3 are discussed in this paragraph in order to evaluate the influence of the fins applied on one module of the specimen, on the PV performance.

Test carried out in phase 3, provides the  $\Delta T_{NF-WF}$  value (i.e. the average temperature difference between the module NF and WF) for each condition of ambient temperature ( $T_{air}$ ) and irradiance ( $I_{rr}$ ), as given below:

$$\Delta T_{NF-WF} = 0.0051 * T_{air} + 0.0044 * I_{rr} \quad [^{\circ}C]$$

Equation 5.8

Equation 5.8 refers to the measured conditions listed in the previous chapter (see boundary conditions listed below Equation 4.7).

Equation 5.9, as found in chapter 4 (i.e. Equation 4.2), provides the  $\gamma$  value (i.e. the temperature coefficient of  $P_{mppt}$ ) of the NF module, which is taken as reference module, for each condition of irradiance ( $I_{rr}$ ), as given below:

$$\gamma = - 0.0003 * I_{rr} - 0.0123 \quad [W / ^{\circ}C]$$

Equation 5.9

By multiplying Equation 5.8 and Equation 5.9, the value of “ $\Delta P_{NF-WF}$ ”, for each condition of  $T_{air}$  and  $I_{rr}$ , is evaluated. “ $\Delta P_{NF-WF}$ ” is defined as the additional power ( $P_{mppt}$ ) produced by the PV module thanks to the influence of the fins that work as heat sinks.

The resulting equation is thus:

$$\begin{aligned} \Delta P_{NF-WF} &= (0.0051 * T_{air} + 0.0044 * I_{rr}) * (- 0.0003 * I_{rr} - 0.0123) \quad [W] \\ \Delta P_{NF-WF} &= -1.32E-06 * I_{rr}^2 - 5.412E-05 * I_{rr} - 6.273E-05 * T_{air} - 1.53E-06 * T_{air} * I_{rr} \end{aligned}$$

Equation 5.10

Equation 5.10, refers to the measured conditions listed in the previous chapter (see boundary conditions listed below Equation 4.7).

Figure 5.20 shows the interpolation surface of  $\Delta P_{NF-WF}$  in different condition of  $T_{air}$  and  $I_{rr}$ , as calculated by Equation 5.10.

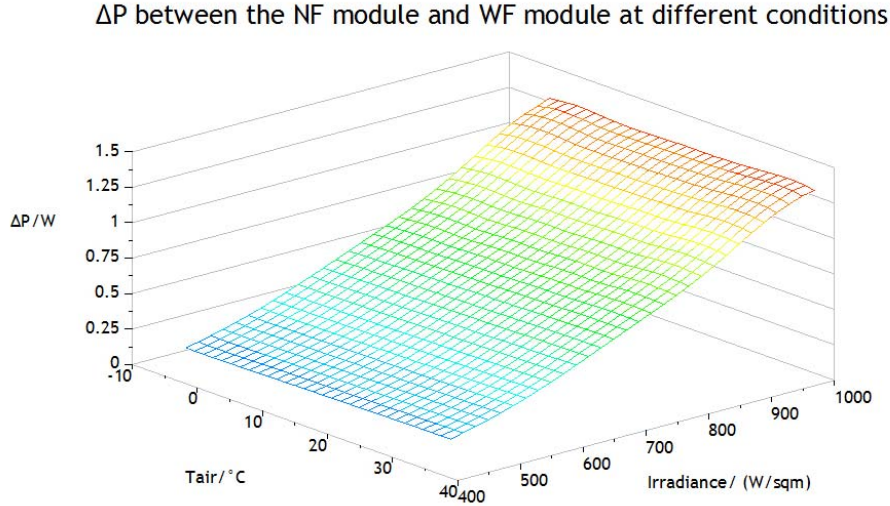


Figure 5.20: interpolation surface of  $\Delta P_{NF-WF}$  (as absolute value) in different condition of  $T_{air}$  and  $I_{rr}$ , as calculated by Equation 5.10

Equation 5.10 can be simplified by fitting the measured data referred to that formula, with a planar surface and thus obtaining the following equation:

$$\Delta P_{NF-WF} = 0.001192 \cdot I_{rr} - 0.001925 \cdot T_{air} \quad [W]$$

RMS (root mean squared) of residuals = 0.1657855;  $R^2 = 0.819689$

Equation 5.11

Equation 5.10 provides the value of  $\Delta P_{NF-WF}$  for each condition of ambient temperature and irradiance.

Figure 5.20 and Equation 5.10, in agreement with what discussed in chapter 4 for the equation 4.7, show that the influence of  $T_{air}$  on  $\Delta P_{NF-WF}$  is much lower than the irradiance's one.

Reporting again the example discussed in chapter 4 for equation 4.7, a peak temperature of  $50^{\circ}C$  would affect the value of  $\Delta P_{NF-WF}$  for an extent of 0.003W, while a peak irradiance of 1100 W/sqm would affect the value of  $\Delta P_{NF-WF}$  for an extent of 1.657 W, i.e. more than 500 times the value due to  $T_{air}$ .

Thus, the influence of  $T_{air}$  on  $\Delta P_{NF-WF}$  can be considered as negligible.

Considering the city of Aswan in Egypt as a limit example, the highest irradiance on a best oriented module (i.e. azimuth of  $0^{\circ}$  and tilt of  $23^{\circ}$ ) is 1172

W/sqm and the corresponding  $T_{air}$  is  $28.8^{\circ}\text{C}$ , happening on the 7<sup>th</sup> of March at noon referring to the meteorological database of the commercial software PV-SOL.

In these peak conditions ( $I_{rr}=1172$  W/sqm and  $T_{air}=28.8^{\circ}\text{C}$ ), the resulting  $\Delta T_{NF-WF}$  evaluated in chapter 4 was  $5.3^{\circ}\text{C}$ , which was considered as a limit value of the maximum contribution that can be provided by the fins to decrease the module temperature in the considered conditions (as listed below the Equation 5.10). According to Equation 5.10, the corresponding  $\Delta P_{NF-WF}$  at these peak conditions results to be  $1.93$  W (as absolute value) referred to one module.

Normalizing this value to the module nominal power  $P_n$ , it results to be  $0.024$  W/ $W_p$ . This means that, in these conditions, the presence of fins leads to an increase in power of the 2.4% of the nominal power installed.

This number can be considered as a limit value of the maximum contribution that can be provided by the fins, to increase the module power in the considered conditions (as listed below the Equation 4.7).

### 5.4.1 Generalization of results to other PV technologies

The results obtained for the prototype, which is made of two Würth CIGS modules, are generalized taking into consideration other PV technologies.

Among the 24 types of modules monitored by Eurac at ABD-PV plant (as described in paragraph 5.3.3), 6 of them are selected for this analysis as they present a similar section, in terms of materials and thickness, compared with the Würth CIGS module tested in the prototype.

In fact, the generalization of the results is based on the hypothesis that the presence of fins on the module would affect the module temperature with the same extent of the tested CIGS modules, and thus the  $\Delta T$  values resulting from the phase 2 tests are assumed to be the same as for the selected PV technologies.

The selection of 6 glass-glass module types (see Table 5.1), which present similar characteristics of materials and thickness as the Würth CIGS modules, is meant to be as coherent as possible with the above mentioned hypothesis.

The dependence of the  $P_{mppt}$  on the module temperature is evaluated, for each of the 6 analyzed technologies, through monitored data acquired in the outdoor ABD-PV field (see description in paragraph 5.3.3).

### **Outdoor temperature characterization**

Values of outdoor temperature coefficient for the 6 selected technologies at different irradiances are evaluated from the data monitored at the ABD plant. The considered time period for the following results starts with January 2012 and ends with December 2012, i.e. one entire year to avoid overestimating or underestimating the role of a season. On the other side, by measuring every 15 min, this long time period provides a huge amount of data, which includes all possible outdoor conditions. To exclude the non-reliable and non-comparable data, a filtering method, which was applied by M. Pichler et al. [5.3], is implemented.

The filtering method considers of three parameters: turbidity, performance ratio and wind speed.

#### **Turbidity**

The turbidity ( $t$ ) is a measure for the clearness of the sky for a single day. It is defined as the ratio of the sum of the diffuse ( $I_{day\ diff}$ ) and of the global ( $I_{day\ global}$ ) irradiance over one day [5.4]. Days with a low turbidity tend to be at clear sky condition, while increasing the turbidity leads to more cloudy days. The problem with cloudy days is the fact that clouds can shadow the module but not the pyranometer, or vice versa. In such a case the data is not coherent. Additionally, the spectrum during days with a high turbidity or high diffuse irradiance can be different to the spectrum of bright days, which are closer to AM1.5 (definition of STC). This difference is hard to determine and therefore overcast days have to be excluded. In the results reported in this paragraph, a turbidity of  $t < 0.25$  is used for the sorting procedure. The choice of  $t < 0.25$  leads to the selection of days at clear sky condition.

#### **Performance Ratio**

The Performance Ratio (PR) is the ratio of the normalized value of the produced energy and the normalized value of the incoming solar energy:

$$PR = \frac{Y_f}{Y_r}, \quad Y_f = \frac{E}{P_n}, \quad Y_r = \frac{G_{sum}}{G_n}$$

Equation 5.12

where  $Y_f$  is the final PV system yield,  $Y_r$  is the reference yield,  $E$  is the net energy output in a certain period of time,  $P_n$  is the nominal power of the PV array,  $G_{sum}$  is the total in-plane irradiance over time,  $G_n$  is the PV's reference irradiance.

The turbidity is not enough to exclude the points coming from shading effects. Also on days with clear sky it can happen that the module is producing no energy while the pyranometer is measuring some irradiance or that the pyranometer is measuring very low irradiance while the module is still producing energy. These situations arise in the morning and in the afternoon, i.e. at sunrise and at sunset. The reason for shading at these times is due to the mountains around the PV-plant and the fact that the plant has only one pyranometer and not one per array. To exclude these points, the performance ratio at a 15 min-interval  $PR_{15min}$  is used. Due to the definition from Equation 5.12, PR is too small when only the module is shadowed and too high when only the pyranometer is shadowed. To have an adequate range for all modules for the sorting by  $PR_{15min}$ , the average ( $\overline{PR}_{15min}$ ) and the standard deviation of  $PR_{15min}$  ( $\sigma_{PR15min}$ ) are calculated as follows:

$$\overline{PR}_{15min} = \frac{1}{N} \sum_{i=1}^N PR_{15min}^i$$

$$\sigma_{PR15min} = \sqrt{\frac{1}{N-1} \sum_{i=1}^N (\overline{PR}_{15min} - PR_{15min}^i)^2}$$

where  $N$  is the number of the data points. The sorting range is then given by  $\overline{PR}_{15min} \pm \sigma_{PR15min}$ . This method ensures that 68 % of the data points are in this range.

### Wind speed

The PT100 used for measuring the module temperature are not sufficiently insulated against influences of the weather and therefore the wind has an

effect on the measured temperature. Too windy days have to be sorted out to ensure the assumption that  $T_{mod} \approx T_{BoM}$  (where  $T_{mod}$  is the module temperature and  $T_{BoM}$  is the temperature measured on the back side of the module).

For the following results, a wind speed of  $V_{wind} < 2$  m/s is used for the sorting procedure.  $V_{wind} < 2$  m/s decreases the influence of the cooling effect of the wind on the measured module temperature.

## Results

The outdoor temperature coefficients for the selected PV technologies are evaluated for each irradiance value (from 500 W/sqm to 900 W/sqm, with a step of 100W/sqm) and the expression  $\gamma_{out}$  as function of irradiance is then derived through the least-squares-fit method (all graphs are reported in annex A). By multiplying the equation of  $\gamma_{out}$  of each technology (as reported in Table 5.1) with Equation 5.8, the expression of  $\Delta P$  can be derived as follows:

$$\Delta P = (0.0051 * T_{air} + 0.0044 * Irr) * \gamma_{out} \quad [W]$$

Equation 5.13

It has to be underlined that the calculated temperature coefficients  $\gamma_{out}$  are still subjected to various external effects such as LS, TA, spectrum etc. which are not considered by the methodology used for their calculation (as proposed by [5.3]), thus care must be taken in the consideration of the following outcomes.

Reference nr.	Technology	$\gamma_{out}$ [W/°C]	R <sup>2</sup>	P <sub>n</sub> [kW]
1	mc-Si	-0.0143*Irr + 7.4975	0.8225	1.98
2	mc-Si	-0.0112*Irr + 5.8644	0.7600	1.96
3	a-Si	-0.0024*Irr + 5.0136	0.5286	1.00
4	a-Si/a-Si	-0.0034*Irr + 4.8651	0.6169	0.97
5	a-Si/ $\mu$ c-Si	-0.0045*Irr + 5.3529	0.5972	1.15
6	a-Si/ $\mu$ c-Si	-0.0047*Irr + 5.0143	0.8049	1.10

Table 5.1: outdoor temperature coefficients as function of irradiance for each PV technology, referred to the installed nominal power P<sub>n</sub>

### Amorphous silicon technology

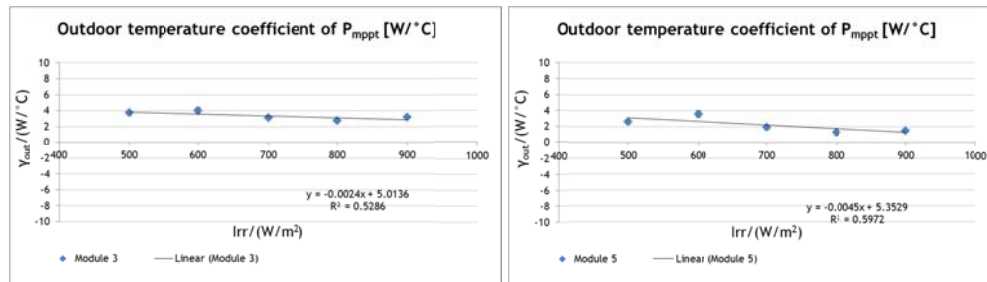


Figure 5.21: Outdoor temperature coefficients evaluated with the methodology explained in the previous paragraph, referred to a-Si (on the left, Module 3) and a-Si/ $\mu$ c-Si (on the right, Module 5) technologies.

Figure 5.21 shows that the temperature coefficients  $\gamma_{out}$  are positive for the considered range of irradiances. On the other hand, the values of relative temperature coefficient reported on the module datasheets are negative (i.e. a-Si module =  $-0.19\%/^{\circ}\text{C}$  and a-Si/ $\mu$ c-Si Module 5 =  $-0.25\%/^{\circ}\text{C}$ ). They refer to an irradiance of  $1000\text{W}/\text{sqm}$  and are measured indoor.

Indoor measurements of temperature coefficients (measured according to the standard [4.4]) are in fact always negative because, with temperature increasing, the PV energy gap ( $E_g$ ) decreases and thus the voltage decreases. This phenomena is immediate and can be measured according to the standard procedure for temperature coefficient evaluation [4.4].

The temperature coefficient which is evaluated in this way, do not take into considerations other phenomena, such as the thermal annealing which is typical of a-Si modules and which leads instead to power recovery of the modules. This typical behavior of a-Si module is part of the well-known Staebler-Wronski effect. Annealing in particular, mainly depends on the module temperature: the higher the temperature, the more effective the defects recovery in the PV module [5.5].

This phenomena may explain the positive value of the outdoor temperature coefficients (as shown in Figure 5.21), evaluated as explained in the previous chapter.

The positive value of the temperature coefficients for a-Si technology, according to Equation 5.13, would result in a positive  $\Delta P$ , meaning a negative influence of the fins attached on the module.



This means that for PV module based on amorphous silicon technology, the presence of fins, that would reduce their operating temperature, would have a negative impact on the module power production.

#### Crystalline silicon technology

It is well known that the relative temperature coefficients of  $P_{mppt}$  of crystalline silicon modules (referred to standard conditions of 1000W/sqm), are among the highest of all technologies and are usually in the range of  $-0.41\%/^{\circ}\text{C}$  and  $-0.57\%/^{\circ}\text{C}$  [5.6]. This is confirmed by A. Virtuani et al. in [5.6], who compared indoor measured temperature coefficients values of several thin film technologies (a-Si based single or multi-junctions, CdTe, CIS, thin-film silicon) with typical temperature coefficients of a conventional c-Si wafer-based module. In that study is confirmed that, with the only exception of the thin film Si device ( $\gamma_{rel}=-0.48\%/^{\circ}\text{C}$ ), all thin film technologies have lower values for the  $\gamma_{rel}$  compared to the c-Si wafer-based module ( $\gamma_{rel}=-0.45\%/^{\circ}\text{C}$ ), with the amorphous silicon single-junction ( $\gamma_{rel}=-0.13\%/^{\circ}\text{C}$ ) device showing the less pronounced decrease with temperature.

This means that crystalline silicon modules, are the most affected by the temperature increasing and thus the influence of fins attached on the back side of these module types could be more effective than as it is for e.g. the CIGS modules.

Considering, as an example, a crystalline silicon module with a relative temperature coefficient  $\gamma_{rel} = -0.57\%/^{\circ}\text{C}$  at an irradiance of 1000W/sqm and an air temperature of  $50^{\circ}\text{C}$ , according to Equation 5.13 (but considering  $\gamma_{rel}$  instead than  $\gamma_{out}$ ), the absolute value of  $\Delta P$ , normalized on the nominal power, would result  $0.027\text{ W}/W_p$ .

If we consider instead, at the same conditions (irradiance of 1000W/sqm and air temperature of  $50^{\circ}\text{C}$ ), the  $\gamma_{out}$  of module 1 and 2 (both mono crystalline) as given in Table 5.1, the absolute value of  $\Delta P$  normalized on the nominal power results to be, respectively,  $0.016\text{ W}/W_p$  and  $0.013\text{ W}/W_p$ . This is due to the fact that the outdoor temperature coefficients  $\gamma_{out,rel}$  of the two modules (respectively:  $-0.287\%/^{\circ}\text{C}$  and  $-0.201\%/^{\circ}\text{C}$ ) are lower than those considered above (which refers to indoor measurements). The outdoor temperature coefficients, evaluated with the methodology discussed in the previous

paragraph, result in fact to be lower than the values reported on the datasheets which refer to indoor measurements: for an extent of 43% for Module 1 and of 62% for Module 2.

Reporting again the limit example of a best tilted module at Aswan, already discussed in paragraph 5.3, and considering the outdoor temperature coefficients  $\gamma_{out}$  of module 1 and 2, the resulting absolute value of  $\Delta P$  normalized on the nominal power would be, respectively, 0.024 W/W<sub>p</sub> and 0.019 W/W<sub>p</sub>.

### 5.4.2 Generalization of results over one year time period

Equation 5.10 allows to calculate the value of  $\Delta P_{NF-WF}$  (i.e. the power production difference of WF and NF module, due to the  $\Delta T_{NF-WF}$  between them) for each ambient condition (i.e. air temperature and irradiance), according to the settings listed below Equation 4.7 (which means that spectral effects, angle of incidence, reflection losses and wind velocity variations are not considered). Considering the ambient conditions of two different locations in Northern and Southern Italy, i.e. Bolzano and Agrigento, the hourly based values of  $\Delta P_{NF-WF}$  are evaluated for one reference year. The final value of the annual  $\Delta E_{NF-WF}$  (i.e. the annual energy production difference of WF and NF module, due to the  $\Delta T_{NF-WF}$  between them) is then assessed.

The results reported in this paragraph refers to the prototype positioned on a vertical plane (tilt=90°) South facing (azimuth=0°).

#### Bolzano

Based on hourly calculation, the total annual amount of difference of energy production  $\Delta E_{NF-WF}$  between the WF and NF modules, due to their  $\Delta T_{NF-WF}$ , results to be 8.82 kWh/(kWp y) for the city of Bolzano (see meteo data description in paragraph 5.3.6). This value is evaluated by summing the  $\Delta E_{NF-WF}$  calculated for each hour over the whole year.

Considering the reference specific annual yield of a BiPV façade system in Bolzano (as described in paragraph 5.3.6 and shown in [Figure 5.19]), the  $\Delta E_{NF-WF}$  due to the presence of fins accounts thus for 1.08% of the annual energy production.

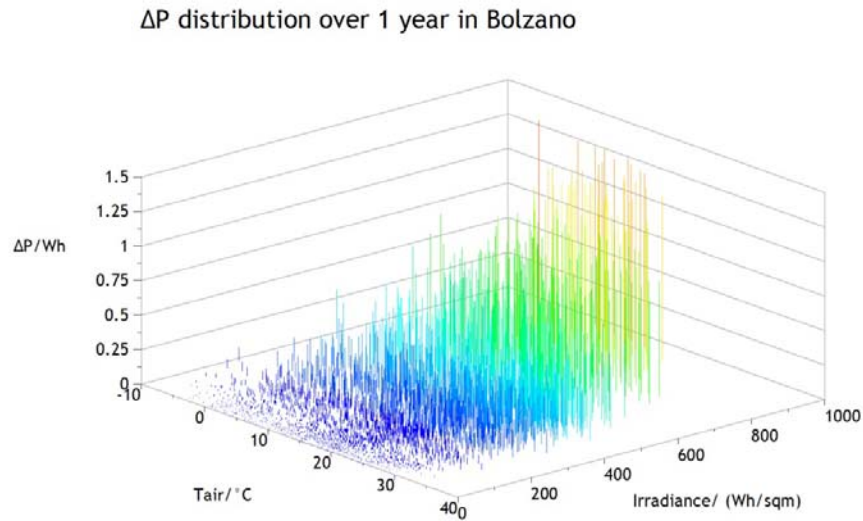


Figure 5.22:  $\Delta P_{NF-WF}$  distribution over 1 year referred to the prototype positioned South facing (azimuth =  $0^\circ$ , tilt =  $90^\circ$ ) in Bolzano.  $\Delta P_{NF-WF}$  is the hourly energy production difference of the WF and NF module, due to the  $\Delta T_{NF-WF}$  between them;  $T_{air}$  is the ambient temperature and Irradiance is the irradiance on the vertical plane of the modules.

The average working temperature of the NF module is  $25.5^\circ\text{C}$  (average calculated on hourly values over one year when  $Irr > 100\text{W/sqm}$ ), while the average working temperature of the WF module is  $23.8^\circ\text{C}$  (average calculated on hourly values over one year when  $Irr > 100\text{W/sqm}$ ). This means that in operative conditions (considered as  $Irr > 100\text{W/sqm}$ ) the WF module operates with an average temperature which is  $1.7^\circ\text{C}$  lower than the NF module.

As already mentioned in paragraph 5.3.6, reliability research states that the PV degradation rate doubles for every  $10^\circ\text{C}$  increase in temperature [5.9], implying that an array design that ran e.g.  $10^\circ\text{C}$  hotter than another could be expected to last only half as long.

Hypothesizing a direct linear correlation for the degradation rate, a first estimation would thus lead to the consideration that the WF module could potentially last around 1/6 longer than the NF module in Bolzano.

### Agrigento

For the city of Agrigento (see meteo data description in paragraph 5.3.6), the total annual amount of difference of energy production  $\Delta E_{NF-WF}$  between the WF

and NF modules, due to their  $\Delta T_{NF-WF}$ , results to be 12.12 kWh/(kWp y), which is 3.3 kWh more than the value referred to Bolzano.

Considering the reference specific annual yield of a BiPV façade system in Agrigento (as described in paragraph 5.3.6 and shown in [Figure 5.19]), the  $\Delta E_{NF-WF}$  due to the presence of fins accounts thus for 1.22% of the annual energy production.

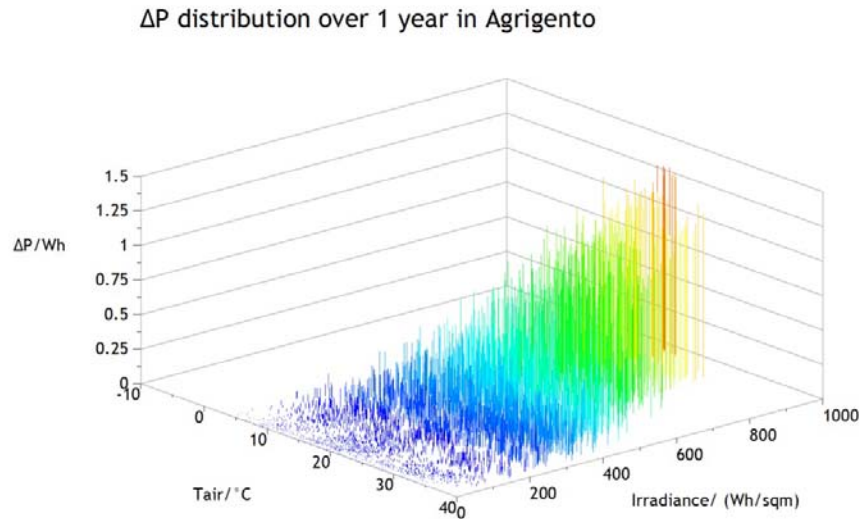


Figure 5.23:  $\Delta P_{NF-WF}$  distribution over 1 year referred to the prototype positioned South facing (azimuth =  $0^\circ$ , tilt =  $90^\circ$ ) in Agrigento.  $\Delta P_{NF-WF}$  is the hourly energy production difference of the WF and NF module, due to the  $\Delta T_{NF-WF}$  between them;  $T_{air}$  is the ambient temperature and Irradiance is the irradiance on the vertical plane of the modules.

The average working temperature of the NF module is  $31.9^\circ\text{C}$  (average calculated on hourly values over one year when  $Irr > 100\text{W/sqm}$ ), while the average working temperature of the WF module is  $30.0^\circ\text{C}$  (average calculated on hourly values over one year when  $Irr > 100\text{W/sqm}$ ). This means that in operative conditions (considered as  $Irr > 100\text{W/sqm}$ ) the WF module operates with an average temperature which is  $1.9^\circ\text{C}$  lower than the NF module.

According to [5.9] as mentioned for the city of Bolzano, a first estimation leads to the consideration that in the climate of Agrigento the WF module could potentially last around 1/5 longer than the NF module.

### **Conclusions**

Concluding, the presence of fins on the CIGS module for the considered prototype, would slightly enhance the PV output energy production over one year time: for an extent of 1.08% in the climate of Bolzano and for an extent of 1.22% in the climate of Agrigento.

Consequently, even if the cost of the proposed heat sink system (metal fins + thermal adhesive) is marginal, the net energy gain they would provide in the considered conditions results probably to be too low to be an interesting solution for the market.

On the other hand, it has also to be taken into account that decreasing the module temperature could also lead to other positive effects, i.e. the opportunity to prolong the life time of an operating PV array due to lower thermal stress, considering that presence of fins would ensure a lower working module temperature over time.

This effect has been roughly estimated for the two cities: the WF module could potentially last around 1/5 longer than the NF module in Agrigento and it could potentially last around 1/6 longer in Bolzano.

## References

- [5.1] Decreto Ministeriale 26 gennaio 2010. Aggiornamento del decreto 11 marzo 2008 in materia di riqualificazione energetica degli edifici. G.U. n. 35, 12/01/2010
- [5.2] A.Colli, W.Sparber, M. Armani, B. Kofler and L.Maturi, 2010. Performance monitoring of different PV technologies at a PV field in Northern Italy. Proceedings of the 25th European Photovoltaic Solar Energy Conference and Exhibition / 5th World Conference on Photovoltaic Energy Conversion, Valencia, Spain. 4344 - 4349
- [5.3] M. Pichler, 2012. Outdoor temperature coefficient of different PV module technologies at ABD-plant in a one-year period. Master Thesis at the Vienna University of Technology.
- [5.4] S. Krauter and A. Preiss, 2010. Performance comparison of aSi, a-Si, c-si as a function of air mass and turbidity. Proceedings of the 25th European Photovoltaic Solar Energy Conference and Exhibition / 5th World Conference on Photovoltaic Energy Conversion, Valencia, Spain. 3141 - 3144.
- [5.5] L. Fanni, A. Virtuani, D. Chianese, 2011. A detailed analysis of gains and losses of a fully-integrated flat roof amorphous silicon photovoltaic plant. Solar Energy 85, 2360-2373.
- [5.6] A. Virtuani, D. Pavanello, G. Friesen, 2010. Overview of Temperature Coefficients of Different Thin Film Photovoltaic Technologies. Proceedings of the 25th European Photovoltaic Solar Energy Conference and Exhibition / 5th World Conference on Photovoltaic Energy Conversion, Valencia, Spain. 4248 - 4252.
- [5.7] L. Maturi et al., 2010. Analysis and monitoring results of a BiPV system in Northern Italy. Proceedings of the 25<sup>th</sup> European Photovoltaic Solar Energy Conference and Exhibition / 5th World Conference on Photovoltaic Energy Conversion, Valencia, Spain. 3141 - 3144.
- [5.8] R. Gottschalga et al., 2003. Experimental study of variations of the solar spectrum of relevance to thin film solar cells. Solar Energy Materials & Solar Cells 79. 527-537.
- [5.9] Flat-Plate Solar Array Project Final Report, 1986. Volume VI: Engineering Sciences and Reliability, report prepared by JPL (Jet Propulsion Laboratory,

California Institute of Technology, Pasadena) for U.S. Department of Energy with NASA, JPL Publication 86-31.

[5.10] D. Moser et al., 2012. Evaluation of the performance of façade mounted photovoltaic modules. Do we need a sensor when we have satellite derived irradiance?. Proceedings of the 27<sup>th</sup> European Photovoltaic Solar Energy Conference and Exhibition 3723 - 3726.

[5.11] B. Norton et al., 2011. Enhancing the performance of building integrated photovoltaics, Solar Energy 85(8) 1629-1664.

## CHAPTER 6

### Summary, conclusions and future development

#### *Abstract*

The prototype of a wooden prefabricated BIPV wall has been conceived, designed, built and finally tested.

This chapter summarizes the main steps of the prototype development process and presents the main related outcomes and conclusions.

The last paragraph highlights the research limitations, which could represent the starting point for future developments of this work.





## 6.1 Summary

This paragraph summarizes the main step of the prototype development process and presents the main related outcomes, according to each step of Figure 6.1.

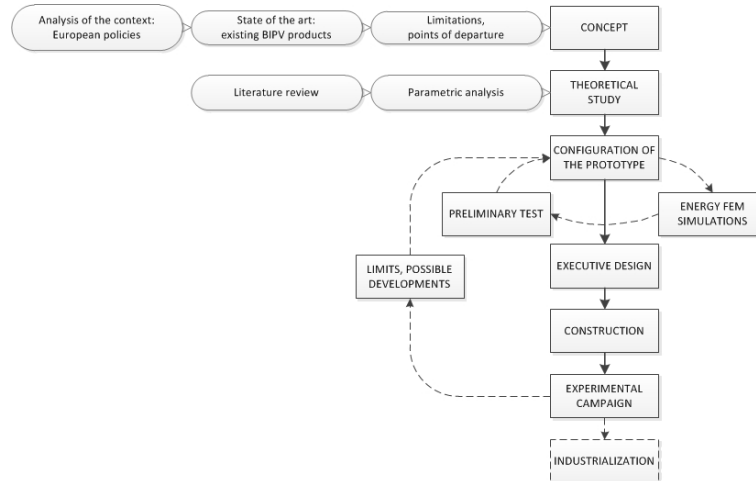


Figure 6.1: (from chapter 3) Process that guided the development of the BiPV prototype, from the concept to the experimental campaign.

### 6.1.1 Concept

Given the recommendations provided by the IEA Task 41 project for the development of new BiPV products related to architects and designers' needs (as highlighted from the results of an international survey which involved about 600 architects/designers [3.1]), an innovative BiPV façade component is conceived and developed.

According to these recommendations, four main concepts have been identified as key-points for the prototype development:

- multi-functionality concept: the prototype is conceived to satisfy several building requirements and to produce electricity;
- sustainability concept: the prototype foresees the coupling of the PV technology, which exploits a renewable energy source, with wood, which is an autochthonous material considering the Alpine region where it has been developed;

- integration concept: the PV system is not conceived as an element added as an additional layer to the building envelope, but as a part of it;
- prefabrication concept: to allow a costs reduction, implementation effectiveness, lean construction site and quality enhancement.

Identification of these concepts constitute the motivation and background for the prototype development.

### **6.1.2 Theoretical study**

The configuration of the prototype is the result of a theoretical study which takes into account both architectural integration aspects (as described in paragraph 3.4.1) and energy performance issues.

The latter in particular, is based on the evaluation and improvement of both PV and building-related aspects.

The “PV” performance is improved taking into consideration passive strategies to keep the module temperature as low as possible (thus increasing the PV efficiency) and the “Bi” (i.e. building) performance is evaluated, considering different possible materials, taking into account the thermal transmittance value of the whole BiPV system.

#### **“PV” Performance**

The prototype has been designed foreseeing an air gap for the natural ventilation of the modules.

This is a crucial aspect for the correct integration of PV modules, since the increase of the operating temperature is one of the critical points which affect the BiPV systems performance [see literature review: 3.9, 3.12, 3.14, 3.17, 3.21].

The optimal thickness of the air gap to keep the operating module temperature as low as possible, has been calculated to be 10 cm, according to a procedure formulated by Brinkworth et al. [3.19, 3.20, 3.21].

In order to further minimise efficiency loss due to temperature rise, a passive low-cost strategy is experimented and investigated, with the aim to further

enhance the advantages provided to the PV module performance by the ventilation.

A strategy which is very often used in the ICT sector for electronic device cooling, is implemented in the prototype: metal fins are applied on the back side of the PV module to work as a heat sink (see Figure 3.15).

In order to define the configuration of the system module-heat sink, because no much experimental data or examples are available, preliminary tests on a small sample and several energy simulations with finite elements method are carried out. The main results of the energy FEM simulations regarding the fins application show that:

- There is no significant improvement in using Silver based technology ( $\lambda=8.89$  W/mK) as thermal compound between fin and module instead than Epoxy based technology ( $\lambda=1.4$  W/mK), which is cheaper;
- A 8 cm-long fin could decrease the cell temperature of  $8.2^{\circ}\text{C}$  with respect to a 3 cm-long fin, which means, in the considered conditions (see paragraph 3.4.2), an increase in the PV power output of about 3%;
- The effect of the fins application on the PV module is beneficial and could lead to a slight enhancement of the PV power production (+1.3% in typical summer conditions, +2.2% in typical winter conditions referred to Northern Italy latitudes).

These energy simulations were carried out to support the prototype design phase. However, in order to comprehensively quantify the influence of fins on the performance of the PV module integrated in a façade, further experimental investigation were carried out, providing monitored data to describe this phenomena in an exhaustive and reliable way.

### **“Bi” Performance**

The “Bi” (i.e. building) performance is evaluated taking into account the thermal transmittance value of the whole BiPV system.

Four different thermal insulation materials are compared and among them, a natural wood fibres insulation was selected as the best option for this prototype.

Moreover, in order to understand the impact of the PV system on the energy performance of the building envelope in steady-state conditions, the value of the thermal transmittance of the prototype was calculated in accordance with the UNI EN ISO 6946 [3.1] considering two situations: the building component with and without the PV system.

The results show that the presence of PV do not affect in a significant way the total thermal resistance of the component: the thermal transmittance of the component with the integrated PV system (which is 0.188 W/sqm K) is slightly lower than the one without it (which is 0.191 W/sqm K).

Therefore, according to this calculation schema, the PV system does not affect the building envelope performance in a negative way.

### **6.1.3 Prototype design and application**

The final prototype design is the result of the theoretical study carried out as described in the previous paragraph. The prototype [see Figure 3.27] is conceived as a standardized modular unit with dimensions of 442 x 1310 x 1240 mm, characterized by a nominal power of 160Wp and with a calculated thermal transmittance value of 0,188 W/sqm K.

This BiPV wall prototype was used in the design of an elementary school of 200 sqm entirely made of prefabricated wood framed panels (within a wider research project entitled “Chi Quadrato: building construction of certified green buildings designed for training activities”), providing an example of possible application of the BiPV prototype in a building design.

### **6.1.4 Experimental campaign**

A specimen of the designed prototype was built by a network of enterprises called “Chi Quadrato” (see paragraph 4.5.2). The specimen is a modular unit with dimensions of 442 x 1400 x 1310 mm, with two PV modules integrated in a wooden structure (see Figure 4.6). One of the two PV modules has eleven fins attached on the back side (as shown in Figure 4.6 and Figure 4.7).

This configuration allows us to get measurements of temperature in both PV configurations (with and without fins) and thus permits the data comparability between the two modules which works in identical controlled conditions.

A new experimental approach, based on three phases and combining different test facilities (i.e. INTENT lab and SoLaRE-PV lab), was defined to properly test this BiPV prototype.

The experimental campaign is divided into three phases to evaluate both the “Bi” (i.e. the building) and the “PV” (i.e. the photovoltaic system) performance: the first phase focuses on the characteristics related to the “Bi” side and in particular on the thermal characterization of the prototype with the measurement of its thermal transmittance; the second phase deals with the “PV” side, and in particular with the electrical characterization of the modules through the measurements of the I-V characteristic curve at different conditions; the goal of the last phase is to merge together the “Bi” and the “PV” sides, focusing on the thermal-energy characterization of the integrated PV modules.

### **Phase 1 results: “Bi” characterization**

In the first test phase the steady-state thermal transmission properties of the prototype are measured and its global thermal transmittance is assessed in accordance with the UNI EN ISO 8990 [4.1] and UNI EN ISO 12567-1 [4.2].

The thermal transmittance of the whole BiPV wall prototype measured by the hot box method results to be 0.204 W/(m<sup>2</sup>K). The discrepancy between the measured and calculated values (which is 0.188 W/(m<sup>2</sup>K), as reported in the previous paragraph) lies in the 8.5% measurements error.

### **Phase 2 results: “PV” characterization**

The second test phase is carried out to measure the PV-related characteristics of the CIGS modules (I-V characteristic curve, Voc, Isc, Pmppt values at different conditions).

Before carrying out the measurements, the modules were pre-conditioned, through controlled Light-Soaking by means of simulated solar irradiation, to stabilize their electrical features. Preconditioning is in fact strongly

recommended for CIGS technology, which is known for its metastability and light-induced change behaviour [4.4, 4.6, 4.7, 4.8].

According to the procedure of the International Standard IEC 61646 [4.4], the stabilization for the two CIGS modules, occurred after three light soaking periods (as shown in Figure 4.11).

The values of  $P_{mppt}$  of the NF module, which is used as reference module, are measured in SoLaRE-PV lab, at different conditions of temperature and irradiation with a step respectively of 5°C and 100 W/sqm, over a range of 70°C and 1100W/sqm.

From these measured data, a mathematical expression (i.e. Equation 4.1) is derived, using the least error squares method and considering  $P_{mppt}$  linear to both irradiance and temperature, which provides the values of  $P_{mppt}$  as a function of irradiance and module temperature.

$$P_{mppt,NF}=0.0818*Irr-0.1085*T_{mod} \quad [W]$$

Equation 4.1

After that, the power temperature coefficients ( $\gamma$ ) of the NF module are assessed at each irradiance value from the measured data (according to IEC 61646 [4.4] and IEC 60891 [4.5]), and the mathematical expression (i.e. Equation 4.2) which provides the values of  $\gamma$  as a function of irradiance is derived, using the least error squares method.

$$\gamma = - 0.0003*Irr - 0.0123 \quad [W/^{\circ}C]$$

Equation 4.2

### **Phase 3 results: “PV in Bi” characterization**

The temperature distribution of the two modules (NF and WF) integrated in the wooden wall is measured, in INTENT Lab, in different environmental conditions (i.e. air temperature from 0°C to 40°C with a step of 10°C and irradiance from 400 W/sqm to 1000 W/sqm with a step of 200 W/sqm) and the averaged  $\Delta T_{NF-WF}$  (temperature difference) between the two modules is assessed for each condition.

From these measured data, two mathematical expressions (i.e. Equation 4.3 and 4.4) are derived, using the least error squares method and considering  $T_{mod}$  linear to both irradiance and air temperature, which provide the values of  $T_{NF}$  (i.e. average NF module working temperature) and  $T_{WF}$  (i.e. average WF module working temperature) as a function of irradiance and air temperature.

$$T_{NF} = 1.0122 * T_{air} + 0.0250 * Irr \quad [^{\circ}C]$$

Equation 4.3

$$T_{WF} = 1.0071 * T_{air} + 0.0206 * Irr \quad [^{\circ}C]$$

Equation 4.4

Consequently, the mathematical expression of  $\Delta T_{NF-WF}$  between the two modules is derived, as a function of irradiance and air temperature (Equation 4.7).

$$\Delta T_{NF-WF} = 0.0051 * T_{air} + 0.0044 * Irr \quad [^{\circ}C]$$

Equation 4.7

Equation 4.7 allows to evaluate the contribution provided by the fins to decrease the module temperature in each condition of irradiance and air temperature.

### **Phase 2 and 3 results: further outcomes**

By multiplying Equation 4.2 and Equation 4.7, the value of  $\Delta P_{NF-WF}$ , for each condition of  $T_{air}$  and  $Irr$ , is evaluated.  $\Delta P_{NF-WF}$  is defined as the additional power ( $P_{mppt}$ ) produced by the PV module thanks to the influence of the fins that work as heat sinks. The resulting equation is thus:

$$\Delta P_{NF-WF} = (0.0051 * T_{air} + 0.0044 * Irr) * (-0.0003 * Irr - 0.0123) \quad [W]$$

Equation 5.3



## 6.2 Conclusions

### 6.2.1 General achievement

The prototype of a wooden prefabricated BiPV wall was conceived, designed, built and tested. It is a standardized modular unit with dimensions of 442 x 1310 x 1240 mm, characterized by a nominal power of 160 Wp and with a measured thermal transmittance value of 0.2 W/sqm K.

Designed according to the recommendations developed by the IEA Task 41 “Solar Energy and Architecture” project, this prototype is intended to make available to architects, engineers and designers a multifunctional product which is characterized both from the “Bi” and the “PV” point of view and which is able to provide both passive and active functions to the building envelope.

### 6.2.2 Experimental approach

The development of such multifunctional building component entails the need for innovative experimental approaches to be developed in order to properly evaluate its energy performance. In fact, there is a need to monitor and test together its “passive” (e.g. thermal transmission properties) and “active”(e.g. electrical and thermal production) performance and to understand the energy interaction between the active and passive layers.

In this thesis, a new experimental approach, based on three phases with the combination of different test facilities (i.e. INTENT lab and SoLaRE-PV lab) and original experimental set-ups, is defined and applied. Figure 4.1 shows the organization of the experimental campaign in three phases and Figure 4.5 shows the concept behind the coupled use of two different test facilities (i.e. INTENT and SoLaRE-PV Labs): the experimental results obtained as an output in INTENT Lab are used as an input for the test performed in SoLaRE-PV Lab. By coupling the two test facilities together and defining original experimental set-ups (as described in chapter 4) it was possible to characterize the BiPV component as a whole.

### 6.2.3 “Bi” performance

The thermal transmittance of the BiPV wall prototype measured by the hot box method according to UNI EN ISO 12567, results to be 0,204 W/(m<sup>2</sup>K).

This value can be considered as a satisfying result in terms of building energy performance, and it is index of a well-insulated wall as its thermal transmittance is below, for an extent of 23%, the limit of 0.26 W/(sqm\*K) required by the actual Italian law referring to the worst case scenario (“zona climatica F”) [5.1].

The measured value of thermal transmittance resulting from the test is coherent with that calculated according to the Standard UNI EN ISO 6946.

In fact, the discrepancy between the measured and calculated value (which is 0.188 W/(m<sup>2</sup>K)) falls within the accepted uncertainty (8,5%).

### 6.2.4 Effectiveness of the BiPV prototype configuration

The effectiveness of the proposed BiPV prototype configuration, in terms of PV performance related to the integration characteristics, is evaluated by comparing the results of the prototype experiments with monitored data of two BiPV systems (a roof system, i.e. Milland Church and a façade system, i.e. Ex-Post) located in South Tyrol (North of Italy).

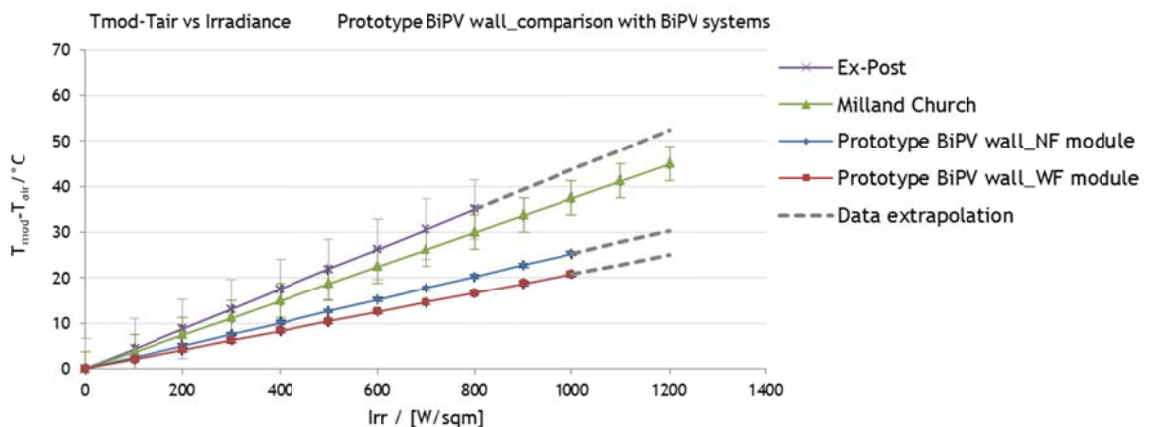


Figure 5.15: plots of Equation 5.1, Equation 5.2, Equation 5.4 and Equation 5.5.

### **General remarks**

Results reported in Figure 5.23 highlight the effectiveness of the proposed BiPV prototype configuration in comparison with the other analyzed BiPV systems: in particular the WF module of the wall prototype results to be the best performing, operating at a temperature which is 2.3%\*Irr lower with respect the worst performing modules integrated in the Ex-Post building (which are not retroventilated).

This means that, e.g. at a top irradiance of 1000W/sqm, the Ex-Post PV modules work at a temperature which is 23°C higher with respect the BiPV wall prototype WF modules.

This confirms that different integration configurations can strongly influence the working module temperatures and thus the PV performance.

It also confirms the importance to design for proper ventilation behind the BiPV elements, which, as demonstrated, could enable a temperature reduction of up to 23°C to be achieved. Similar values were found by Norton et al. in [5.10], which formulated a possible temperature reduction up to around 20°C to be achieved thanks to a proper design.

### **Energy gain over one year time period**

The module working temperature difference  $\Delta T_{\text{Ex-Post} - \text{WF}}$ , which is related to the integration characteristics, leads to an energy production difference  $\Delta E_{\text{Ex-Post} - \text{WF}}$  which accounts for the 6.00% of the annual energy production in the Agrigento climate (South of Italy) and for the 5.34% of the annual energy production in the Bolzano climate (North of Italy).

In addition, it has also to be taken into account that decreasing the module temperature could lead to other positive effects, i.e. the opportunity to prolong the life time of an operating PV array due to lower thermal stress.

This effect has been roughly estimated for the two cities: the “well integrated” WF module could potentially last around 4/5 longer than the “bad integrated” Ex-Post modules in Bolzano and more than twice longer in Agrigento (see Figure 6.2).

These results confirm that different integration configurations can strongly influence the PV performance and highlight the importance to design for proper ventilation behind the BiPV elements.

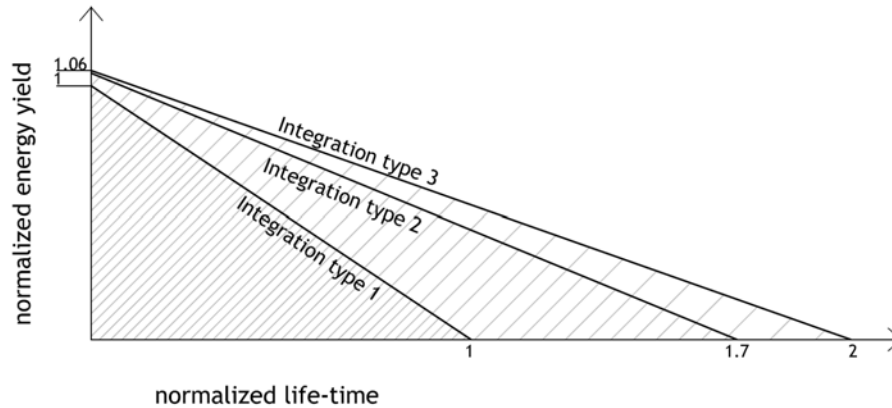


Figure 6.2: energy yield and module life-time, normalized by values referred to integration type 1 referred to the climate of Agrigento. Integration types refer to (1) Ex-Post modules, (2) NF prototype module, (3) WF prototype module.

### 6.2.5 Influence of “PV” on “Bi” and of “Bi” on “PV”

The influence of “Bi” on “PV” is evaluated in terms of PV working temperature conditions. Experimental data obtained for the BiPV wall prototype, are also compared with monitored data of one ground mounted PV system placed at the ABD PV plant (in Bolzano, North of Italy). According to Figure 5.17, the temperature working conditions of the BiPV prototype modules are closer to the conditions reported for the ground-mounted PV system than the ones reported for the BiPV systems (i.e. Ex-Post building and Milland Church system, as described in the paragraph above). Consequently, according to these data, the working temperature conditions of the modules integrated in the BiPV wall prototype, are not significantly affected by the “Bi” side because of the well retro-ventilation of the PV modules.

The influence of “PV” on “Bi” is evaluated in terms of steady-state thermal transmission properties, calculating the thermal transmittance of the prototype considering two situations: the building component with and without the PV system. The results show that the presence of PV do not affect in a significant way the total thermal resistance of the component: the thermal transmittance

of the component with the integrated PV system (which is 0.188 W/sqm K) is slightly lower than the one without it (which is 0.191 W/sqm K).

Therefore, according to this calculation schema, the PV system does not affect the building envelope performance in any significant way.

The resulting negligible influence of “Bi” on “PV” and of “PV” on “Bi”, can be mainly ascribed to a proper PV integration design.

### 6.2.6 Explicit correlation for façade integrated PV operating temperature

The expression of  $T_{\text{mod,NF}}$  as function of  $T_{\text{air}}$  and  $I_{\text{rr}}$  is formulated (Equation 5.4) according to the experimental data. This expression can be generally used to easily predict the operating temperature of façade integrated PV modules, which present similar integration characteristics as the prototype ones (i.e. well retro-natural-ventilation, see boundary conditions listed below).

$$T_{\text{mod,NF}} = T_{\text{air}} + 0.0253 \cdot I_{\text{rr}}$$

Equation 5.4

Coefficient of determination ( $R^2$ )= 0.9950

Equation 5.4 refers to the NF module integrated in the BiPV wall prototype. It is the least-squares-fit line evaluated through the set of data measured at the following boundary conditions:

- Irradiance ranging from 400W/sqm to 1000W/sqm;
- Air temperature ranging from 0 to 40° C;
- Velocity of the air adjacent to the PV modules kept constant at 2m/s (as shown in Figure 4.21);
- Air gap velocity ranging between 1.1 m/s and 1.5m/s (as measured, see Figure 4.22);
- Irradiation referred to the spectrum AM 1.5;
- Additional constraint:  $T_{\text{mod}} - T_{\text{air}} = 0$  when  $I_{\text{rr}} = 0$ .

### 6.2.7 NOCT model vs experimental data

The NOCT model is a very commonly used approach to estimate the cell temperature based on the ambient temperature and the solar irradiance [4.10] [4.11].

According to this model, the module operating temperature can be retrieved by Equation 4.5 (i.e.:  $T_{\text{mod}} = T_{\text{air}} + I_{\text{rr}} * (\text{NOCT} - 20) / 800$ ).

Comparing the results predicted by this model with measured data resulting from the BiPV wall prototype experimental campaign (described by Equation 4.3), significant errors of prediction by this model (without wind corrections) are found: the coefficients of Equation 4.3 (from measured data) differ from the coefficients of Equation 4.6 (from NOCT model) of 1% with regard the  $T_{\text{air}}$  and between 17% and 33% (according to the NOCT value uncertainty given in the module datasheet:  $\text{NOCT} = 47^{\circ}\text{C} \pm 3^{\circ}\text{C}$ ) with regard the  $I_{\text{rr}}$ .

These results show that there are significant limitations in using the NOCT approach (without wind corrections) for predicting cell temperature in BiPV applications as the tested one, i.e. when the two sides of the module are subjected to significantly different environmental conditions due to the mounting characteristics.

It is thus recommended not to rely on this model without wind correction, even if it a very simple and handy one, when dealing with these kind of BiPV applications, but to use more accurate techniques, such as:

- Expressions which include a parameter for BiPV situations depending on the level of integration and (ventilation) gap size, e.g. [4.15],[4.16];
- Expressions which include wind velocity as a parameter, e.g. [4.17],[4.18],[4.19],[4.20];
- More complex heat transfer models, e.g. [4.11], [4.14].

### 6.2.8 Factors influencing effectiveness of fins application

The influence of  $T_{\text{air}}$  on  $\Delta P_{\text{NF-WF}}$  is much lower than the irradiance's one (as shown in Figure 4.18).

For example, a peak temperature of  $50^{\circ}\text{C}$  would affect the value of  $\Delta P_{\text{NF-WF}}$  for an extent of 0.003W, while a peak irradiance of 1100 W/sqm would affect the

value of  $\Delta P_{NF-WF}$  for an extent of 1.657 W, i.e. more than 500 times the value due to  $T_{air}$ . Thus, the influence of  $T_{air}$  on  $\Delta P_{NF-WF}$  can be considered as negligible. The dominating factor which influence  $\Delta P_{NF-WF}$  (i.e. the fins effectiveness in increasing the PV efficiency) is the irradiance. This means that application of fins is more effective for those systems which are exposed to high irradiance levels (i.e. PV modules on movable tracking systems).

### 6.2.9 Effectiveness of fins application in the prototype

#### Limit conditions (upper limits of effectiveness)

Considering a limit example (i.e. the city of Aswan in Egypt, top irradiance of 1172 W/sqm and corresponding  $T_{air}$  of 28.8°C), the maximum contribution that can be provided by the fins to decrease the module temperature in the prototype is evaluated according to the experimental results. In these “limit conditions”, the resulting  $\Delta T_{NF-WF}$  is 5.3°C (see paragraph 4.8.3), and the resulting  $\Delta P_{NF-WF}$  (according to paragraph 5.3) is 1.93 W (as absolute value referred to one module), i.e. 0.024 W/W<sub>p</sub> (as normalized value on the module nominal power P<sub>n</sub>). This means that, in these “limit conditions”, the presence of fins leads to an increase in power of the 2.4% of the nominal installed power.

#### Energy gain over one year time period

Considering the ambient conditions of two different locations in Northern and Southern Italy, i.e. Bolzano and Agrigento, the hourly based values of  $\Delta P_{NF-WF}$  are evaluated for one reference year. The final value of the annual  $\Delta E_{NF-WF}$  (i.e. the annual energy production difference of WF and NF module, due to the  $\Delta T_{NF-WF}$  between them) is then assessed.

According to the experimental results, it is proven that the presence of fins on the CIGS module for the considered prototype, would slightly enhance the PV output energy production over one year time: for an extent of 1.08% in the climate of Bolzano and for an extent of 1.22% in the climate of Agrigento.

Consequently, even if the cost of the proposed heat sink system (metal fins + thermal adhesive) is marginal, the net energy gain they would provide in the

considered conditions results probably to be too low to be an interesting solution for the market.

On the other hand, it has also to be taken into account that decreasing the module temperature could also lead to other positive effects, i.e. the opportunity to prolong the life time of an operating PV array due to lower thermal stress, considering that presence of fins would ensure a lower working module temperature over time.

This effect has been roughly estimated for the two cities: the WF module could potentially last around 1/5 longer than the NF module in Agrigento and it could potentially last around 1/6 longer in Bolzano.

### **6.2.10 Estimated effectiveness of fins application for different PV technologies**

The effectiveness of fins application on different PV technologies is estimated under the hypothesis that the presence of fins on the module would affect the module temperature with the same extent of the tested CIGS modules, and thus the  $\Delta T_{NF-WF}$  values resulting from the phase 2 tests are assumed to be the same as for the selected PV technologies (modules with similar sections to the tested CIGS Würth modules are selected in order to be as coherent as possible with this hypothesis).

Based on the above mentioned hypothesis, two main conclusions can be derived:

- For amorphous silicon modules, according to the measured outdoor temperature coefficients (see paragraph 5.4), the presence of fins would have a negative impact on the module power production. Application of fins is thus a strategy to avoid for this technology.
- For crystalline silicon modules, the influence of fins results to be more effective than as it is for the tested CIGS modules: considering “extreme conditions” (i.e. irradiance of 1000W/sqm and air temperature of 50°C), the power increase due to the influence of fins results to be 1.8% of the nominal power for the CIGS module, and up to 2.7% of the nominal power for a crystalline silicon module (i.e. 0.9% more effective at extreme conditions).



### 6.3 Research limitations and future developments

The research work has been carried out under some significant hypotheses which of course influence and restrict the effectiveness of the obtained results. Nevertheless, such bounds can represent the starting point for future developments of this work.

With regard the experimental results, the major limitations concern the test boundary conditions (as listed in paragraph 4.8.3) which do not take into consideration angle of incidence, spectral effects (that could be neglected as shown in paragraph 5.3) as well as, most important, wind effects. As for the latter in particular, tests were carried out with a constant air velocity value (i.e. 2 m/s, which is an annual average value in the city of Bolzano-North of Italy). Consequently, equations 4.3 ( $T_{NF}$ ), 4.4 ( $T_{WF}$ ), 4.7 ( $\Delta T_{NF-WF}$ ) and 5.10 ( $\Delta P_{NF-WF}$ ) which are derived from the experimental data, are express as a function of only ambient temperature and irradiance. Further investigations could be carried out to extend those equations with a third parameter, i.e. the wind velocity.

Other possible future developments could regard:

1) Experimental evaluation of different prototype configurations

Because of reasons of time and funding, one single prototype was developed and built within this thesis. Anyway, some aspects could be further improved (i.e. from the technological point of view) and other prototype configurations could be investigated, going again through the development procedure as illustrated in Figure 6.1.

Two new configurations are proposed:

- Option 1: development of a system to recover the heat of the air gap, using it to contribute to the building heating demand instead than dissipating it as for the actual prototype configuration.
- Option 2: development and optimization of a mechanical ventilation system for the air gap to further decrease the modules temperature and evaluation of the  $\Delta T$  (temperature difference between NF and WF module) values according to different air gap velocities

2) Further investigation of identified research topics:

- Detailed analysis of module-life duration according to working temperature conditions. As such activity did not fall within the major goals of this thesis, this topic was just briefly treated according to general values found in literature, but it could be interesting to consider a more detailed analysis about the correlation between PV working temperature conditions and module life-time.
- Evaluation of dynamic performance to further investigate the energy influence between the photovoltaic system and the building envelope, considering a whole façade-building approach.

In this thesis the influence of the photovoltaic system on the building envelope performance was mainly evaluated with respect to steady-state parameters. In case of different prototype configurations (such as the one suggested above with air gap heat recovery), it could be of interest to also analyze dynamic parameters.

Despite the mentioned restrictions, the goal to conceive, design, build and test the prototype of a BiPV wall, was achieved.

Along such a development process, many problems were addressed and solved and significant experimental data are finally provided, contributing to a deeper understanding of BIPV systems energy performance.

The impact of this work related to the contributions provided to the IEA Task 41 project “Solar Energy and Architecture” (see annex section) and in the definition of the newly accepted FP7 project “Solar Design - On-the-fly alterable thin-film solar modules for design driven applications” (see annex section), is a further confirmation of the relevance of this thesis outcomes.



---

## BIBLIOGRAPHY

- [1.1] Oliver Morton, 2006. Solar energy: A new day dawning?: Silicon Valley sunrise. *Nature* 443, 19-22. doi:10.1038/443019a
- [1.2] IEA Promoting Energy Efficiency Investments - case studies in the residential sector, Paris 2008. ISBN 978-92-64-04214-8
- [1.3] Directive 2010/31/EU of the European Parliament and of the Council of 19 May 2010 on the Energy Performance of Buildings (EPBD)
- [1.4] Directive 2009/28/CE the European Parliament and of the Council of 23 April 2009 on renewable energy sources (RES)
- [1.5] Piano di Azione Nazionale per le Energie Rinnovabili (with reference to Directive 2009/28/CE), Ministero dello sviluppo economico
- [1.6] <http://www.ecologiae.com/energie-rinnovabili/18808/>
- [1.7] T. Schoen, et al, 2001. Task 7 of the IEA PV power systems program- achievements and outlook, Proceedings of the 17th European Photovoltaic Solar Conference.
- [1.8] <http://www.chiquadrato.org/>
- [1.9] <http://www.eurac.edu/en/research/institutes/renewableenergy/default.html>
- [1.10] K. Farkas, M. Horvat et al., 2012. Report T.41.A.1: Building Integration of Solar Thermal and Photovoltaics - Barriers, Needs and Strategies.
- [2.1] A. Giovanardi, 2012. Integrated solar thermal facade component for building energy retrofit. PhD thesis, Doctoral School in Environmental Engineering Università degli Studi di Trento.
- [2.2] Marcel Gutschner et al., 2002. Report IEA-PVPS T7-4, Potential for building integrated photovoltaic. IEA Task 7 PVPS “Photovoltaic Power Systems in the Built Environment”
- [2.3] Report T.41.A.3, 2013. Designing photovoltaic systems for architectural integration -Criteria and guidelines for product and system developers, in press.

- 
- [2.4] A. Scognamiglio, P. Bosisio, V. Di Dio, 2009. Fotovoltaico negli edifici, Edizioni Ambiente, ISBN 978-88-96238-14-1.
- [2.5] MC Munari Probst, C Roecker et al., 2012. Report T.41.A.2: IEA SHC Task 41 Solar energy and Architecture. Solar energy systems in architecture -Integration criteria and guidelines. (available at: <http://members.iea-shc.org/publications/task.aspx?Task=41>)
- [2.6] F. Frontini, 2009. Daylight and Solar Control in Buildings: General Evaluation and Optimization of a New Angle Selective Glazing, PhD Thesis, Politecnico di Milano, Fraunhofer Verlag, ISBN 978-3839602386.
- [2.7] F. Frontini, T.E. Kuhn, 2010. A new angle-selective, see-through BiPV façade for solar control. In proceedings of Eurosun Conference 2010, Graz.
- [2.8] C. Schittich et al., 2001. Building Skins - Concepts, Layers, Materials, Birkhauser (2001) Edition Detail, pp.8-27.
- [2.9] Karsten Voss, Eike Musall, 2012. Net zero energy buildings, Detail Green Book, ISBN 978-3-920034-80-5.
- [2.10] Directive 2010/31/EU of the European Parliament and of the Council of 19 May 2010 on the Energy Performance of Buildings (EPBD)
- [2.11] K. Farkas, M. Horvat et al., 2012. Report T.41.A.1: Building Integration of Solar Thermal and Photovoltaics - Barriers, Needs and Strategies.
- [2.12] T.T. Chow et al., 2007. An experimental study of façade-integrated photovoltaic/water-heating system. Applied Thermal Engineering 27 (1), 37-45. DOI: 10.1016/j.applthermaleng.2006.05.015
- [2.13] G. Quesada et al., 2012. A comprehensive review of solar facades. Transparent and translucent solar facades. Renewable and Sustainable Energy Reviews 16, 2643-2651.
- [2.14] A. Guardo et al., 2009. CFD approach to evaluate the influence of construction and operation parameters on the performance of Active Transparent Facades in Mediterranean climates. Energy and Buildings 41, 534-42.
- [2.15] S.P. Corgnati et al., 2007. Experimental assessment of the performance of an active transparent facade during actual operating conditions. Solar Energy 81,993-1013.

- 
- [2.16] D.Infield D et al., 2004. Thermal performance estimation for ventilated PV facades. *Solar Energy* 76, 93-8.
- [3.1] UNI EN ISO 6946:2007, Building component and building elements - thermal resistance and thermal transmittance - calculation method
- [3.2] MC.Munari Probst, 2008. Architectural Integration and Design of Solar Thermal Systems. École Polytechnique Fédérale de Lausanne, doctoral thesis n. 4258
- [3.3] K. Farkas, 2011. The Perception of Formal and Symbolic Aesthetics of Photovoltaics. Proceedings of ISES Solar World Congress 2011, ISBN 978 39814659 0 7
- [3.4] M. Wall et al., 2008. IEA Task 41-Solar Energy and Architecture-Annex Plan. (available at: <http://members.iea-shc.org/publications/task.aspx?Task=41>)
- [3.5] MC Munari Probst, C Roecker et al., 2012. Report T.41.A.2: IEA SHC Task 41 Solar energy and Architecture. Solar energy systems in architecture -Integration criteria and guidelines. (available at: <http://members.iea-shc.org/publications/task.aspx?Task=41>)
- [3.6] Report T.41.A.3, in press: Designing photovoltaic systems for architectural integration -Criteria and guidelines for product and system developers, 2013.
- [3.7] K. Farkas, M. Horvat et al., 2012. Report T.41.A.1: Building Integration of Solar Thermal and Photovoltaics - Barriers, Needs and Strategies.
- [3.8] R. Gottschalg et al., 2003. Experimental study of variations of the solar spectrum of relevance to thin film solar cells. *Solar Energy Materials & Solar Cells* 79, 527-537
- [3.9] Energy-efficient buildings ppp - Multi-annual roadmap and longer term strategy-, prepared by the Ad-hoc Industrial Advisory Group, European Commission
- [3.10] J.J. Bloem, 2008. Evaluation of a PV-integrated building application in a well-controlled outdoor test environment. *Building and Environment* 43, 205-216
- [3.11] T. Schoen et al., 2001. Task 7 of the IEA PV power systems program - achievements and outlook, Proceedings of the 17<sup>th</sup> European Photovoltaic Solar Conference.

- 
- [3.12] I. Bergmann, W.Weiss, 2002. Fassadenintegration von thermischen Sonnenkollektoren ohne Hinterlüftung. AEE Intec, Arbeitsgemeinschaft ERNEUERBARE ENERGIE, Institut für Nachhaltige Technologien
- [3.13] P. Funtan et al., 2009. MULTIELEMENT project-PV Elements in Building Services Engineering, (<http://www.pv-multielement.de/>)
- [3.14] J.K. Tonui & Y. Tripanagnostopoulos, 2008. Performance improvement of PV/T solar collectors with natural air flow operation. Solar Energy 82(1) 1-12
- [3.15] T.T. Chow, 2010. A review on photovoltaic/thermal hybrid solar technology, Applied Energy, 87(2) 365-379
- [3.16] Y. Tripanagnostopoulos et al., 2002. Hybrid photovoltaic/thermal solar systems, Solar Energy 72(3) 217-234
- [3.17] B. Norton et al., 2011. Enhancing the performance of building integrated photovoltaics, Solar Energy 85(8) 1629-1664
- [3.18] P. Batagiannis, C. Gibbons, 2001. Thermal assessment of silicon-based composite materials used in photovoltaics, Conference proceedings of Renewable Energy in Maritime Island Climates, Belfast, 151-157
- [3.19] B.J. Brinkworth & M.Sandberg, 2006. Design procedure for cooling ducts to minimise efficiency loss due to temperature rise in PV arrays, Solar Energy 80(1) 89-103
- [3.20] B.J. Brinkworth, 2006. Optimum depth for PV cooling ducts, Solar Energy 80, 1131-1134
- [3.21] Brinkworth, B.J. et al, 2000. A validated model of naturally ventilated PV cladding. Solar Energy 69, 67-81
- [3.22] Ji Jie et al., 2002. The annual analysis of the power output and heat gain of a PV-wall with different integration mode in Hong Kong, Solar Energy Materials and Solar Cells, Vol 71 Issue 4 435-448
- [3.23] H. Yang et al., 2001. Building-integrated photovoltaics: effect on the cooling load component of building facades, Building Serv Eng Res Technol 22 (3), 157-165
- [3.24] B. van Kampen, 2008. Actual Temperatures of Building Integrated PV Modules. Study in the framework of the EU IP Performance project, September 2008 (available at: [www.pv-performance.org](http://www.pv-performance.org))

- 
- [3.25] L. Fanni et al., 2011. Maximum production conditions of a c-Si module in three different Italian locations. Proceedings of the 26th European Photovoltaic Solar Energy Conference and Exhibition. 3446 - 3449
- [3.26] Y. A. Cengel, 2006. Heat and Mass Transfer -A Practical Approach- 517-518
- [3.27] L. Maturi, R. Lollini, P. Baldracchi, W. Sparber, 2011. Building skin as electricity source: the prototype of a wooden BiPV façade component. Proceedings of the 26<sup>th</sup> European Photovoltaic Solar Energy Conference and Exhibition. 3991 - 3999
- [3.28] N. Friling et al., 2009. Modelling the heat dynamics of building integrated and ventilated photovoltaic modules. Energy and Buildings 41 (10), 1051-1057
- [3.29] L. Maturi et al., 2010. Analysis and monitoring results of a BiPV system in Northern Italy. Proceedings of the 25th European Photovoltaic Solar Energy Conference and Exhibition, 5131-5134
- [3.30] UNI EN ISO 10456:2008. Materiali e prodotti per edilizia - Proprietà igrometriche - Valori tabulati di progetto e procedimenti per la determinazione dei valori termici dichiarati e di progetto.
- [3.31] Flat-Plate Solar Array Project Final Report, 1986. Volume VI: Engineering Sciences and Reliability, JPL Publication 86-31.
- [3.32] B. Weller et al., 2010. Detail Practice: Photovoltaics, ed. Detail, ISBN 978-3-0346-0369-0.
- [3.33] [www.natureplus.org](http://www.natureplus.org)
- [3.34] [www.fsc.org](http://www.fsc.org)
- [3.35] S. Wittkopf et al., 2011. Testing a design methodology for building integration of photovoltaics (PV) using a PV demonstration site in Singapore. Architectural Science review 54, 192-205.
- [3.36] Directive 2010/31/EU of the European Parliament and of the Council of 19 May 2010 on the Energy Performance of Buildings (EPBD)
- [3.37] RES Directive 2009/28/CE the European Parliament and of the Council of 23 April 2009 on renewable energy sources



- 
- [3.38] Graeme Auld et al., 2008. Certification Schemes and the Impacts on Forests and Forestry, Annual Review of Environment and Resources. Vol. 33: 187-211. DOI: 10.1146
- [3.39] V.A. Sample, 2003. Certification on Public and University Lands: Evaluations of FSC and SFI by the Forest Managers. Journal of Forestry, Volume 101 (8), 21-25(5)
- [3.40] G. Makrides et al., 2009. Temperature behaviour of different photovoltaic systems installed in Cyprus and Germany. Solar Energy Materials and Solar Cells 93, 1095-1099.
- [3.41] E. Skoplaki, J.A. Palyvos, 2009. On the temperature dependence of photovoltaic module electrical performance: A review of efficiency/power correlations. Solar Energy 83, 614-624.
- [3.42] P. Trinuruk et al., 2009. Estimating operating cell temperature of BIPV modules in Thailand. Renewable Energy 34, 2515-2523.
- [3.43] A. Buchanan A, B. Levine, 1999. Wood-based building materials and atmospheric carbon emissions. Environmental Science and Policy 2, 427-37.
- [3.44] L. Gustavsson et al, 2006. Carbon dioxide balance of wood substitution: comparing concrete- and wood-framed buildings. Mitigation and Adaptation. Strateg for Glob Change 11, 667-91.
- [3.45] R.J. Cole, P.C. Kernan, 1996. Life-cycle energy use in office buildings. Building and Environment 31(4), 307-17.
- [3.46] A.K. Petersen, B. Solberg, 2005. Environmental and economic impacts of substitution between wood products and alternative materials: a review of micro-level analyses from Norway and Sweden. Forest Policy and Economics 7, 249-59.
- [4.1] International Standard UNI EN ISO 8990, 1999. Thermal Insulation - Determination of steady-state thermal transmission properties - Calibrated and guarded hot box.
- [4.2] International Standard UNI EN ISO 12567, 2002. Thermal performance of windows and doors - Determination of thermal transmittance by hot box method.
- [4.3] International Standard IEC 60904-9, 2007. Photovoltaic devices -Part 9: Solar simulator performance requirements.

- 
- [4.4] International Standard IEC 61646, 2008. Thin film terrestrial photovoltaic (PV) modules - Design qualification and type approval.
- [4.5] International Standard IEC 60891, 2009-12. Photovoltaic devices - Procedures for temperature and irradiance corrections to measured I-V characteristics.
- [4.6] Robert P. Kenny, Anatoli I. Chatzipanagi and Tony Sample, 2012. Preconditioning of thin-film PV module technologies for calibration. Progress in Photovoltaic: research and applications, DOI: 10.1002/pip.2234.
- [4.7] N. Taylor et al., April 2011. Guidelines for PV Power Measurement in Industry. Report of Performance FP6 Integrated Project.
- [4.8] M. Gostein & L. Dunn, 2011. Light Soaking Effects on Photovoltaic Modules: Overview and Literature Review. Proceedings of the 37th IEEE Photovoltaic Specialists Conference (PVSC), Seattle, Washington. 003126-003131.
- [4.9] D. L. King, J. A. Kratochvil and William E. Boyson, 1997. Temperature Coefficients for PV Modules and Arrays: Measurement, Methods, Difficulties and Results. Proceedings of the 26th IEEE Photovoltaic Specialists Conference, Anaheim, California, 1183-1186.
- [4.10] P. Trinuruk, C. Sorapipatana, D. Chenvidhya, 2009. Estimating operating cell temperature of BIPV modules in Thailand. Renewable Energy 34, 2515-2523.
- [4.11] M.W. Davis, B.P. Dougherty, A.H. Fannery, 2001. Prediction of Building integrated Photovoltaic Cell Temperatures. ASME Transactions the journal of Solar Energy Engineering, Vol. 123, No.2, 200-210.
- [4.12] R. Gottschalga et al., 2003. Experimental study of variations of the solar spectrum of relevance to thin film solar cells. Solar Energy Materials & Solar Cells 79. 527-537.
- [4.13] E. Skoplaki et al., 2008. A simple correlation for the operating temperature of photovoltaic modules of arbitrary mounting. Solar Energy Materials & Solar Cells 92, 1393-1402.
- [4.14] E. Skoplaki et al., 2008. Operating temperature of photovoltaic modules: a survey of pertinent correlations. Renewable Energy 34, 23-29.

- 
- [4.15] T. Nordmann T, L. Clavadetscher, 2003. Understanding temperature effects on PV system performance. In Proceedings of the third world conference on photovoltaic energy conversion, Osaka, Japan. 2243-6.
- [4.16] S.C.W. Krauter, 2004. Development of an integrated solar home system. *Solar Energy Materials and Solar Cells* 82, 119-30.
- [4.17] R. Chenni et al., 2007. A detailed modelling method for photovoltaic cells. *Energy* 32, 1724-30.
- [4.18] V.V. Risser, M.K. Fuentes, 1983. Linear regression analysis of flat-plate photovoltaic system performance data. In: Proceedings of the fifth E.C. photovoltaic solar energy conference, Athens. 623-7.
- [4.19] D.L. King, 1997. Photovoltaic module and array performance characterization methods for all system operating conditions. In Proceedings of the NREL/SNL photovoltaic program review meeting, Lakewood, CO, 1-22.
- [4.20] J.M. Servant, 1985. Calculation of the cell temperature for photovoltaic modules from climatic data. In Proceedings of the 9<sup>th</sup> biennial congress of ISES - Intersol 85, Montreal, Canada, extended abstracts, p. 370.
- [5.1] Decreto Ministeriale 26 gennaio 2010. Aggiornamento del decreto 11 marzo 2008 in materia di riqualificazione energetica degli edifici. G.U. n. 35, 12/01/2010
- [5.2] A.Colli, W.Sparber, M. Armani, B. Kofler and L.Maturi, 2010. Performance monitoring of different PV technologies at a PV field in Northern Italy. Proceedings of the 25th European Photovoltaic Solar Energy Conference and Exhibition / 5th World Conference on Photovoltaic Energy Conversion, Valencia, Spain. 4344 - 4349
- [5.3] M. Pichler, 2012. Outdoor temperature coefficient of different PV module technologies at ABD-plant in a one-year period. Master Thesis at the Vienna University of Technology.
- [5.4] S. Krauter and A. Preiss, 2010. Performance comparison of aSi, a-Si, c-si as a function of air mass and turbidity. Proceedings of the 25th European Photovoltaic Solar Energy Conference and Exhibition / 5th World Conference on Photovoltaic Energy Conversion, Valencia, Spain. 3141 - 3144.

- 
- [5.5] L. Fanni, A. Virtuani, D. Chianese, 2011. A detailed analysis of gains and losses of a fully-integrated flat roof amorphous silicon photovoltaic plant. *Solar Energy* 85, 2360-2373.
- [5.6] A. Virtuani, D. Pavanello, G. Friesen, 2010. Overview of Temperature Coefficients of Different Thin Film Photovoltaic Technologies. *Proceedings of the 25th European Photovoltaic Solar Energy Conference and Exhibition / 5th World Conference on Photovoltaic Energy Conversion, Valencia, Spain.* 4248 - 4252.
- [5.7] L. Maturi et al., 2010. Analysis and monitoring results of a BiPV system in Northern Italy. *Proceedings of the 25<sup>th</sup> European Photovoltaic Solar Energy Conference and Exhibition / 5th World Conference on Photovoltaic Energy Conversion, Valencia, Spain.* 3141 - 3144.
- [5.8] R. Gottschalga et al., 2003. Experimental study of variations of the solar spectrum of relevance to thin film solar cells. *Solar Energy Materials & Solar Cells* 79. 527-537.
- [5.9] Flat-Plate Solar Array Project Final Report, 1986. Volume VI: Engineering Sciences and Reliability, report prepared by JPL (Jet Propulsion Laboratory, California Institute of Technology, Pasadena) for U.S. Department of Energy with NASA, JPL Publication 86-31.
- [5.10] D. Moser et al., 2012. Evaluation of the performance of façade mounted photovoltaic modules. Do we need a sensor when we have satellite derived irradiance?. *Proceedings of the 27<sup>th</sup> European Photovoltaic Solar Energy Conference and Exhibition* 3723 - 3726.
- [5.11] B. Norton et al., 2011. Enhancing the performance of building integrated photovoltaics, *Solar Energy* 85(8) 1629-1664.

---

## ANNEXES



## **Annex A**

Annex A includes:

- construction drawings of the prototype
- drawing of the INTENT calorimeter
- sensors positioning -phase 1-
- sensors positioning -phase 3-
- measurements of phase 2

**A**

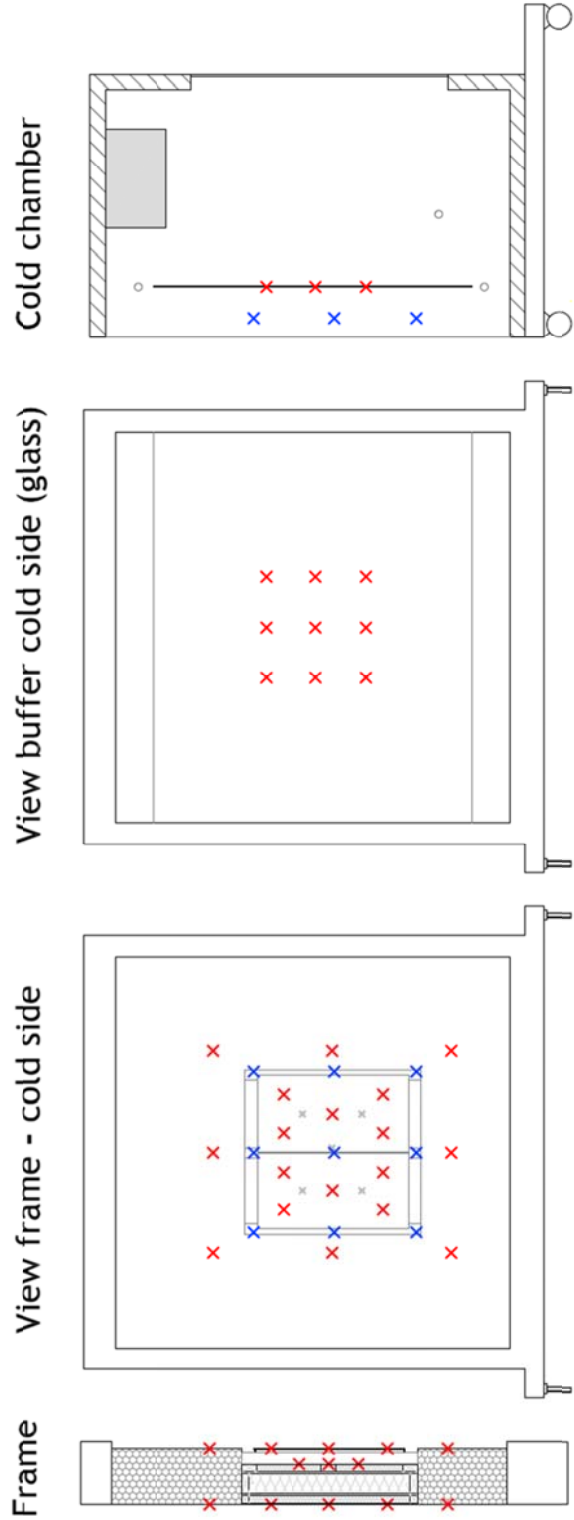




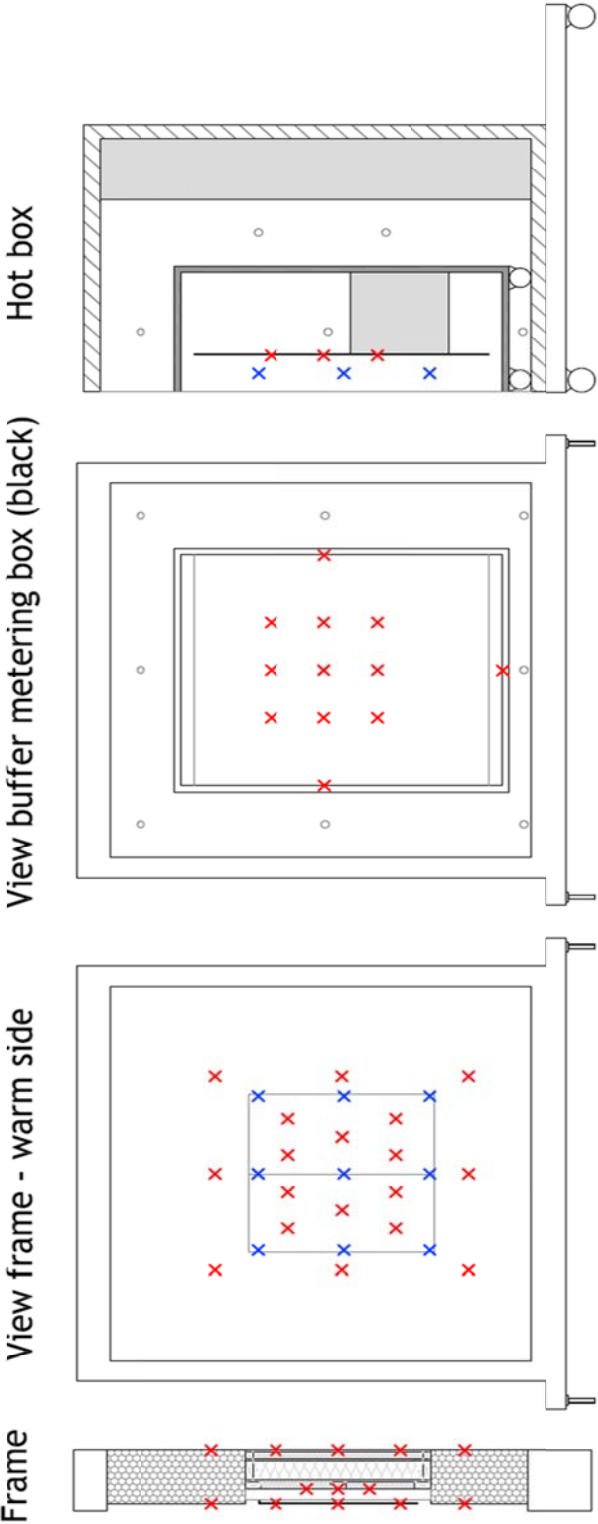




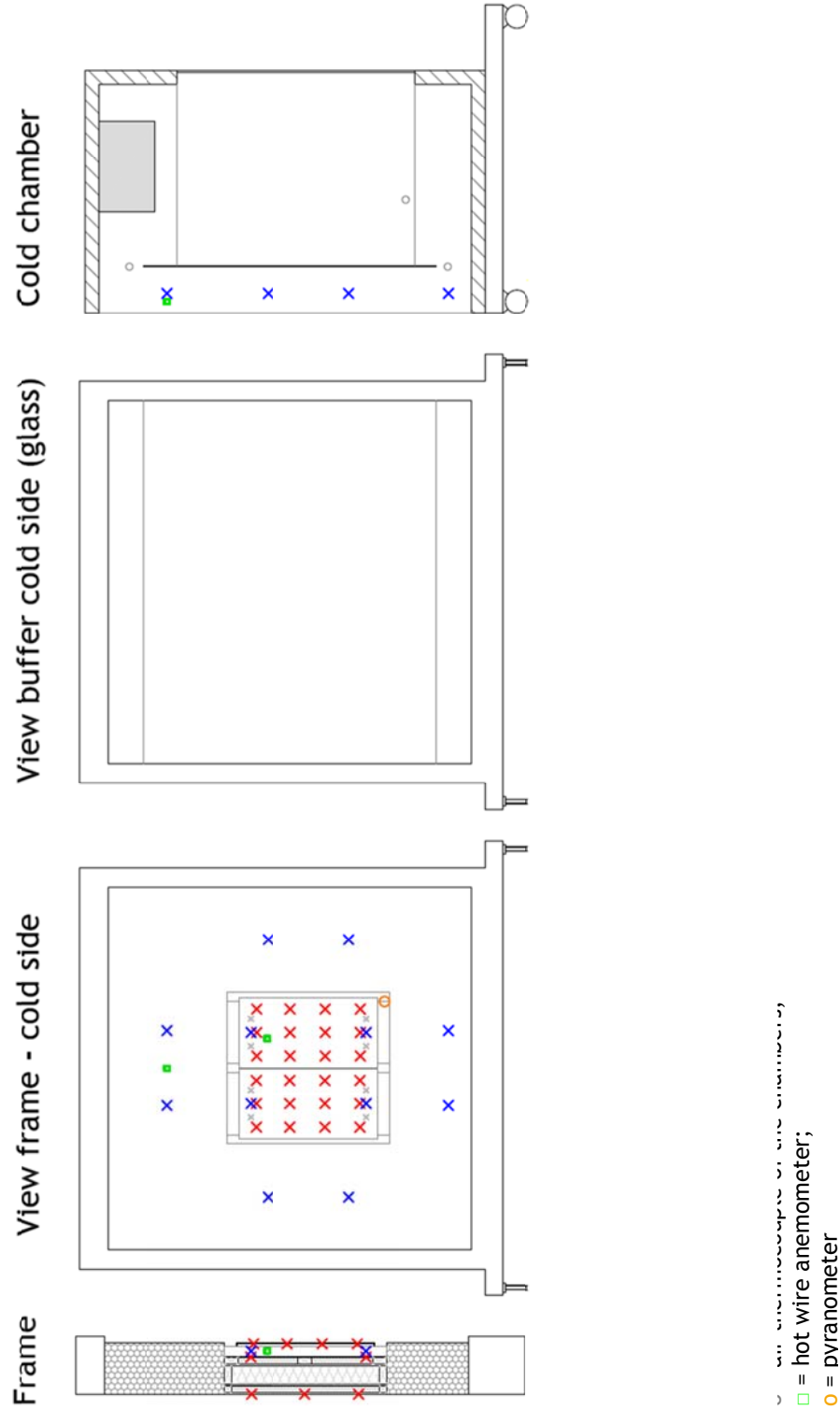
### Sensors positioning -phase 1-

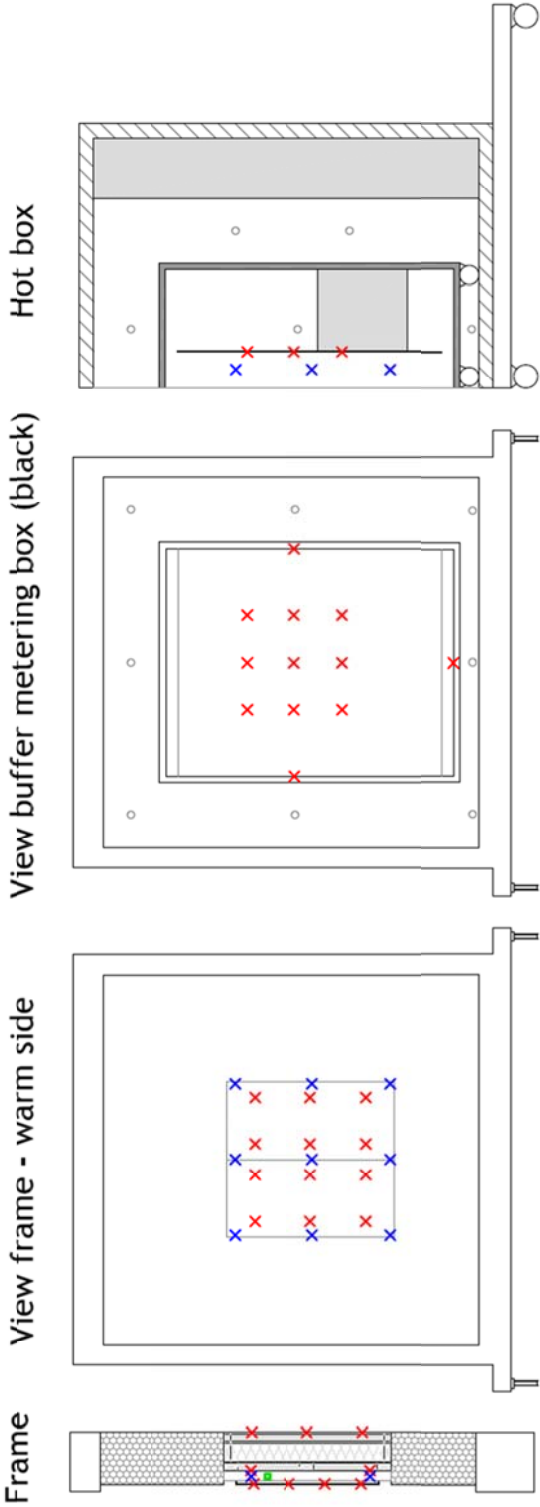


U - 011 UNIVERSITÄT DE BIE BRUNNEN



### Sensors positioning -phase 3-





- x = hot wire anemometer;
- = hot wire anemometer;
- = pyranometer

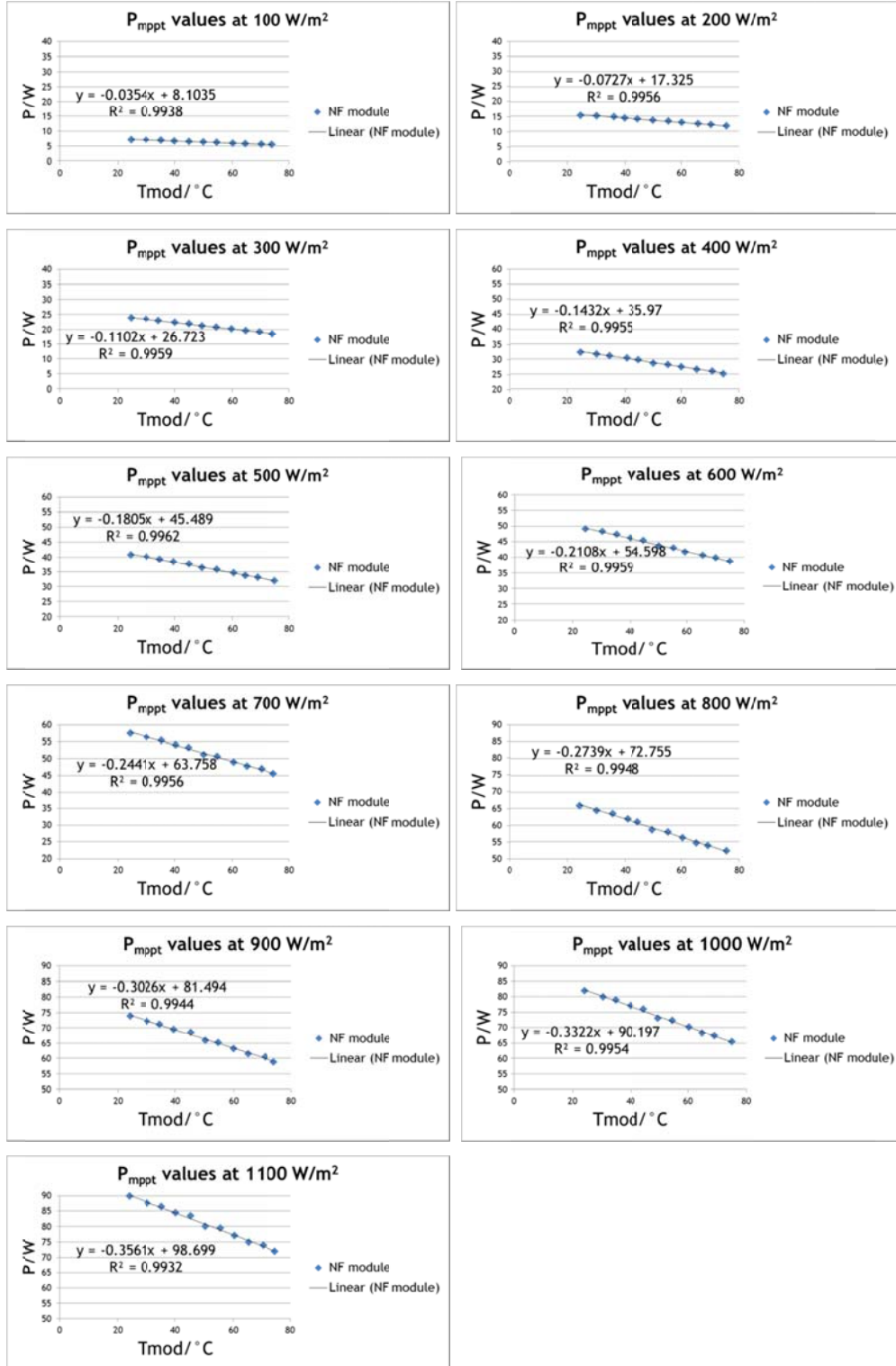
## Measurements of phase 2

Measurements carried out in phase 2, include:

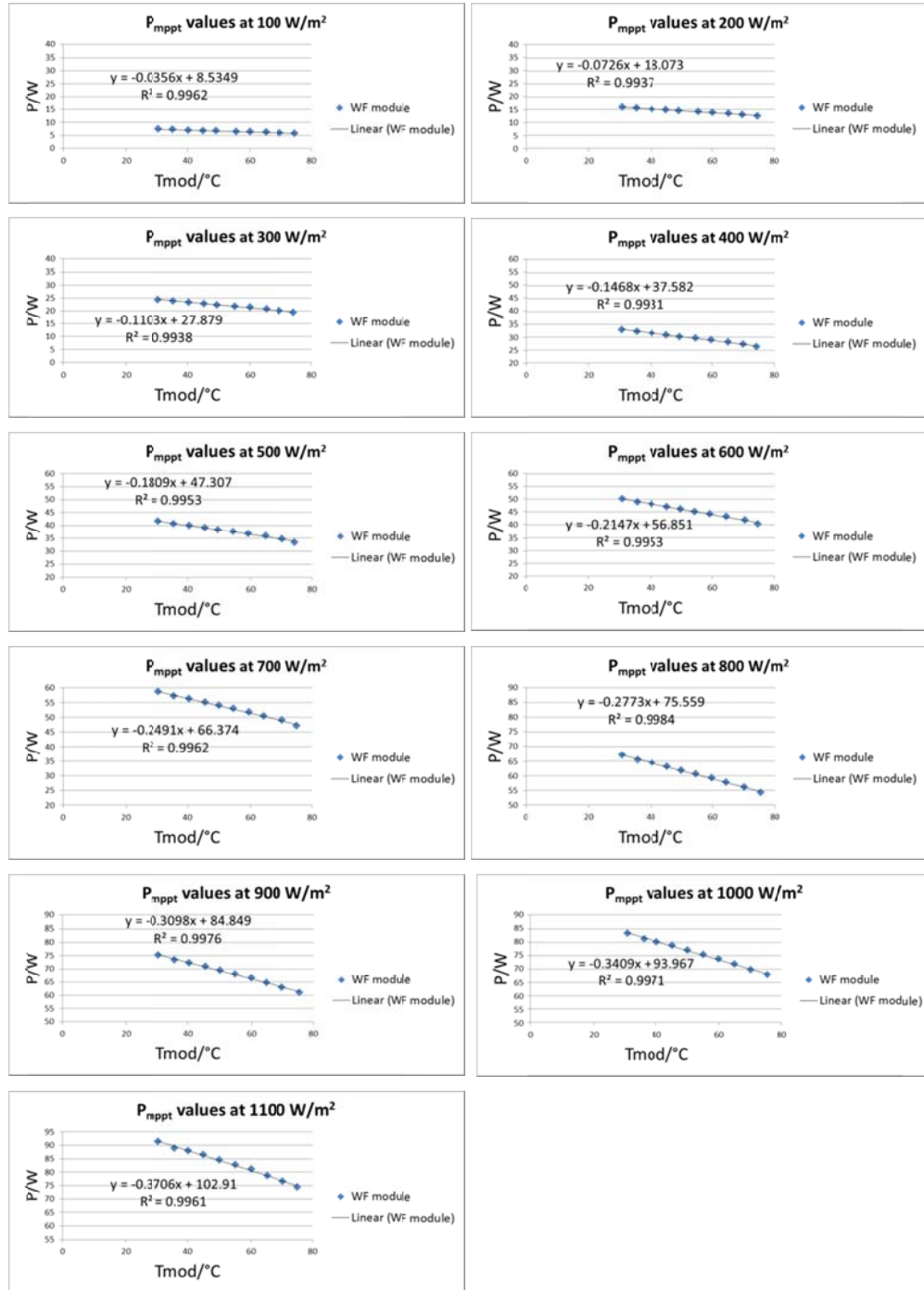
- Measured Pmppt values at different Irradiances and module temperatures (module no fins);
- Measured Pmppt values at different Irradiances and module temperatures (module with fins):



Measured  $P_{mppt}$  values at different Irradiances and module temperatures  
(module no fins):



Measured P<sub>mppt</sub> values at different Irradiances and module temperatures (module with fins):





## **Annex B**

Outdoor temperature coefficients of six different technologies

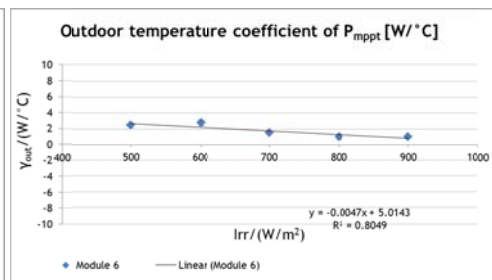
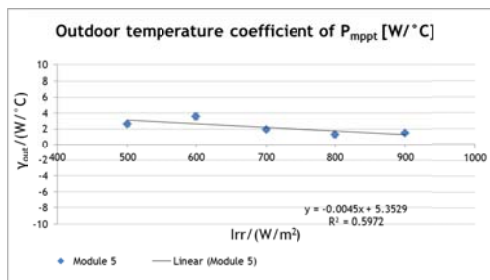
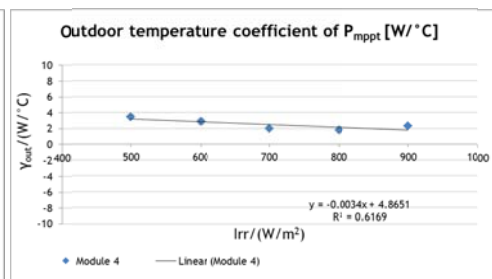
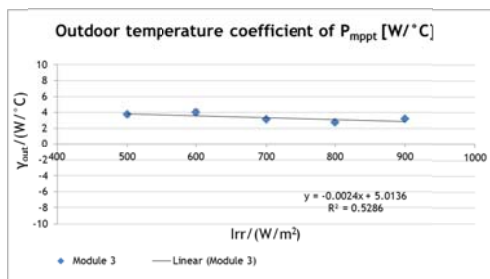
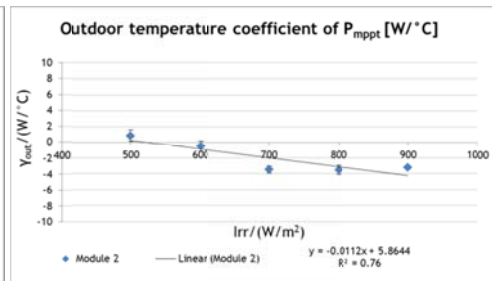
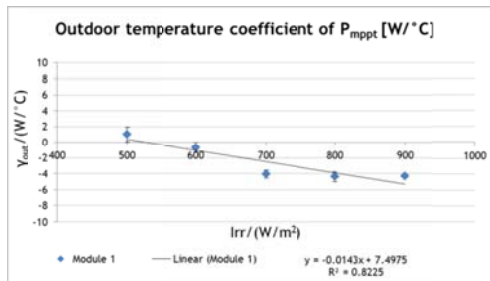
**B**



## Outdoor temperature coefficients of six different technologies

The graphs show the dependence of the outdoor temperature coefficients on irradiance for each module typology. The data refer to monitored data collected over one year time period at the experimental PV plant of the airport “Aereoporto Bolzano Dolomiti” of Bolzano.

Reference nr.	Technology
Module 1	mc-Si
Module 2	mc-Si
Module 3	a-Si
Module 4	a-Si/a-Si
Module 5	a-Si/ $\mu$ c-Si
Module 6	a-Si/ $\mu$ c-Si





## **Annex C**

Annex C includes:

- IEA Task 41 project “Solar Energy and Architecture”
- FP7 project “Solar Design - On-the-fly alterable thin-film solar modules for design driven applications”

**C**





## IEA Task 41 project “Solar Energy and Architecture”

IEA Task 41 “Solar Energy and Architecture” is an international research project of the International Energy Agency carried out in the Framework of the SHC (Solar Heating and Cooling) Programme. It started in May 2009 and finished in April 2012, involving around 70 experts coming from 14 different countries (for more details visit IEA Task 41 website: <http://members.iea-shc.org/task41/index.html>).

Main goals of this project were to help achieving high quality architecture for buildings integrating solar energy systems, improving the qualifications of the architects, their communications and interactions with engineers, manufactures and clients, making architectural design a driving force for the use of solar energy.

The author of this thesis was member of Task 41 project, and she contributed in the following publications:

- Report T.41.B.1 of IEA-SHC Task 41, State-of-the-art of digital tools used by architects for solar design, published on the IEA-SHC Task 41 web site [<http://www.iea-shc.org/publications/task.aspx?Task=41>], September 2010.

Abstract of the report: This report presents a review of existing digital tools widely used today, as part of the Subtask B: Methods and Tools for Solar Design of the IEA SHC Task 41 “Solar Energy and Architecture”. The review covers a total of 56 computer programs, classified according to three categories: 1) CAAD (computer-aided architectural design), 2) visualization, 3) simulation tools. The aim of this review is to analyse the current software landscape for building projects with a focus on early design phase (EDP).

- Report T.41.B.2. of IEA-SHC Task 41, *International Survey About Digital Tools Used by Architects for Solar Design*, published on the IEA-SHC Task 41 web site [<http://www.iea-shc.org/publications/task.aspx?Task=41>], July 2011.

Abstract of the report: This report forms part of IEA-SHC Task 41: Solar Energy and Architecture, specifically Subtask B: Methods and Tools for Solar Design. After a literature review of former studies made between

1993 and 2011, the international survey Design Process for Solar Architecture, conducted in 2010 within Task 41 is presented and analyzed. Professionals in 14 countries were contacted and questioned about their use of digital tools for solar design and related themes, such as, barriers for the use of digital tools or their design process. In addition, general data concerning the firm (size, type of buildings) and personal facts (age, experience, profession) was collected. The response rate was less than hoped; nevertheless, this report points out that there is a high awareness of the importance of solar energy use in buildings, but that there are still a number of barriers to the widespread application of digital tools during the design process. The survey affirms results of former investigations by others presented in literature review that widely accepted solar design software packages adequate for use by architects in the early design phase are still lacking. The identification of opportunities and obstacles, special requirements expressed by professionals and suggestions for improvements will help formulate the next program of work, which will involve the development of guidelines for both professionals and software tool developers in order to support design methods and enhance the use of solar energy in building projects.

- Report T.41.A.1 of IEA-SHC Task 41, *Building Integration of Solar Thermal and Photovoltaics - Barriers, Needs and Strategies*, published on the IEA-SHC Task 41 web site [<http://www.iea-shc.org/publications/task.aspx?Task=41>], May 2012.

Abstract of the report: This report describes the results of a large international survey on the reasons why architects do not use or rarely use solar technologies, and gives proposals to help overcome these barriers by identifying the architect's needs in this area.

- Report T.41.C.1 of IEA-SHC Task 41, *Communication Guideline*, published on the IEA-SHC Task 41 web site [<http://www.iea-shc.org/publications/task.aspx?Task=41>], July 2012.

Abstract of the report: In order to stimulate an increased use of solar in energy conscious building design, the Task 41 participants have developed a Communication Guideline as a tool to support architects in

their communication process with especially clients, authorities and contractors. Today the energy performance of solar solutions is well documented and well known especially in the “technical environment”. This knowledge, however, needs to be communicated in a convincing way to the decision makers in order to ensure a broad implementation of sustainable solar solutions in future building design. The Communication Guideline includes convincing arguments and facts supporting the implementation of solar based design solutions. The Communication Guideline is divided in three main parts:

- Part 1: Convincing clients to request and commission solar buildings
- Part 2: Communication strategies at the design/ construction team level

- Part 3: Tools and References

- Contributor in Report T.41.C.2 of IEA-SHC Task 41, *Product Developments and Dissemination Activities*, published on the IEA-SHC Task 41 web site [<http://www.iea-shc.org/publications/task.aspx?Task=41>], September 2012.

Abstract of the report: This document shows product developments and dissemination activities carried out within the framework of, or in close relation to, the project IEA SHC Task 41 Solar Energy and Architecture. This Task gathered researchers and practicing architects from 14 countries in the three year project whose aim was to identify the obstacles architects are facing when incorporating solar design in their projects, to provide resources for overcoming these barriers and to help improving architects’ communication with other stakeholders in the design of solar buildings. Participating countries were Australia, Austria, Belgium, Canada, Denmark, Germany, Italy, Norway, Portugal, Republic of Korea, Singapore, Spain, Sweden and Switzerland. The report gives not a complete list of activities, but shows the different types of activities to spread the findings in Task 41 and to initiate product developments in participating countries.

- Contributor in Report T.41.A.2 of IEA-SHC Task 41, *Solar energy systems in architecture -Integration criteria and guidelines*, published on the

IEA-SHC Task 41 web site [<http://www.iea-shc.org/publications/task.aspx?Task=41>], September 2012.

Abstract of the report: This document is conceived for architects and intended to be as clear and practical as possible. It summarizes the knowledge needed to integrate active solar technologies (solar thermal and photovoltaics) into buildings, handling at the same time architectural integration issues and energy production requirements. Solar thermal and photovoltaics are treated separately, but the information is given following the same structure: 1- Main technical information; 2- Constructive/functional integration possibilities in the envelope layers; 3- System sizing and positioning criteria; 4- Good integration examples; 5- Formal flexibility offered by standard products; 6 - Innovative market products. To complete the information the manual ends with a short section dedicated to the differences and similarities between solar thermal and photovoltaic systems, with the purpose to help architects make an energetic and architecturally optimized use of the sun exposed surfaces of their buildings.

In order to further disseminate IEA Task 41 outcomes and to help increasing public awareness with regard the use of solar energy in architecture, the author of this thesis contributed in the scientific organization of several events and workshops (see Fig. 1, Fig. 2, Fig. 3, Fig. 4):

1. “Progettazione integrata e architettura solare - Verso edifici a bilancio energetico nullo”, 19/3/2010, Bolzano;
2. “Forms of Energy”, 10/6/2010, Roma, in collaboration with ENEA;
3. “Energia solare ed architettura - casi studio nazionali di edifici ed aree urbane”, in the context of Klimaenergy fair 2010, 23/9/2010, Bolzano;
4. “Fotovoltaico integrato: la sfida per gli edifici del futuro”, in the context of Klimahouse fair 2012, 26/01/2012, Bolzano.

**Contatti:**  
Istituto per le Energie Rinnovabili  
dell'EURAC  
Viale Druso 1, 39100 Bolzano

**Roberto Lolini:**  
tel. 0471 055650  
roberto.lolini@eurac.edu

**Alessia Giovanardi:**  
tel. 0471 055653  
alessia.giovanardi@eurac.edu

**Laura Maturi:**  
tel. 0471 055633  
laura.maturi@eurac.edu

**www.eurac.edu**




L'Istituto per le Energie Rinnovabili dell'EURAC organizza la conferenza  
**PROGETTAZIONE INTEGRATA E ARCHITETTURA SOLARE  
VERSO EDIFICI A BILANCIO ENERGETICO NULLO**  
EURAC, Conferenza (hall - Viale Druso 1, 39100 Bolzano)  
**19.03.2010 - ore 9.30**

La conferenza è rivolta a progettisti, produttori di facciate complesse, costruttori, ricercatori, amministratori pubblici e a tutti gli interessati all'argomento delle applicazioni di tecnologie solari, di tipo fotovoltaico ed a solare termico, negli edifici. Obiettivo del convegno è trasferire nozioni di base sul tema degli edifici a bilancio energetico nullo e dell'integrazione e gestione dell'energia solare. Questo trasferimento di conoscenze si propone di stimolare un nuovo e più consapevole approccio progettuale e la cooperazione tra i diversi attori del mercato. La conferenza vuole essere anche occasione per scambiare esperienze e approcci metodologici tra i diversi attori che partecipano alla definizione delle soluzioni progettuali e alla realizzazione dell'edificio.

**Programma**

**9.30** – Introduzione alla conferenza  
Wolfram Sparber, direttore Istituto per le Energie Rinnovabili dell'EURAC

**9.40** – Cos'è un NZEB (Net Zero Energy Building).  
Attività del task 40/annex52 IEA e posizione della EC  
Assunta Napolitano, Istituto per le Energie Rinnovabili dell'EURAC

**10.00** – Problematiche dell'integrazione architettonica delle tecnologie solari e attività del task 41 IEA  
Maria Cristina Munari Probst, Laboratorio d'energia solare et physique du bâtiment – Ecole Polytechnique Fédérale de Lausanne, Svizzera

**10.20** – Procedure di progettazione integrata (IDP: Integrated Design Process)  
Andrea Costa, Istituto per le Energie Rinnovabili dell'EURAC


**10.40** – Coffee break e networking

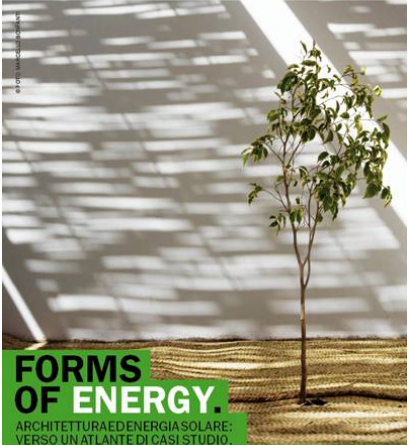
**11.00** – Integrazione di sistemi fotovoltaici negli edifici (BIPV: Building Integrated Photovoltaics)  
Kim Nagel, Istituto di Sostenibilità applicata all'Ambiente Costruito - Scuola Universitaria Professionale della Svizzera Italiana (SUPSI)

**11.20** – Simulazione e strategie di controllo solare di facciate complesse  
Francesco Frontini, Fraunhofer Institute for Solar Energy Systems (ISE), Germania

**11.40** – Dibattito e chiusura

Fig. 1: Flyer of the workshop “Progettazione integrata e architettura solare - Verso edifici a bilancio energetico nullo” held in Bolzano on the 19<sup>th</sup> of March 2010





**FORMS OF ENERGY.**  
ARCHITETTURA ED ENERGIA SOLARE:  
VERSO UN ATLANTE DI CASI STUDIO.

Roma, 10 giugno ore 17.30 - Biblioteca IED - Via Casilina n. 51 / 00182, Roma

Incontro promosso da ENEA (Agenzia nazionale per le nuove tecnologie, l'energia e lo sviluppo economico sostenibile) ed Eurac (Accademia europea di Bolzano), in collaborazione con Domus. Organizzato da IED Roma Master in Environmental Design, con il supporto di INARCH Master di Architettura Digitale. A cura di Maralusa Palumbo ed Alessandra Scognamiglio.

**Rolf Pantaleo TAMACCOR:**  
Realizzazione e coordinamento dell'iniziativa Energy

**Laura Maturi IED:**  
Coordinamento internazionale di ricerca per le città e gli edifici del futuro: le attività della IEA (International Energy Agency)

**Alessandra Scognamiglio ENEA e Simona Bordoni Domus:**  
Roma ed Energy Call for government

**Coordinatore Maralusa Palumbo**  
tel. 067024025 | e-mail: p.palumbo@ied.it

Fig. 2: Flyer of the launch of initiative “Forms of Energy”, Rome, held on the 10<sup>th</sup> of June 2010





**23/9/2010 KlimaEnergy, Bolzano**

**Seminario su ENERGIA SOLARE ED ARCHITETTURA**  
Casi studio nazionali di edifici ed aree urbane

**Obiettivi**  
Il workshop è finalizzato alla presentazione di casi studio di edifici e quartieri che integrino soluzioni per la gestione dell'energia solare sia passive (daylighting, vernici/guaine riflettenti, ...) che attive (fotovoltaico e solare termico). È prevista una "call for case studies" per una selezione dei casi più significativi da presentare all'interno del progetto internazionale "Solar Energy and Architecture" del task 41 IEA. Il seminario vuole stimolare un nuovo e più consapevole approccio progettuale e la cooperazione tra i diversi attori del mercato che partecipano alla realizzazione dell'edificio, oltre che essere un'occasione per scambiare esperienze e approcci metodologici.

**Agenda**  
14:00-14:15  
Introduzione al seminario: IEA task 41 "Solar Energy and Architecture"  
Roberto Lollini  
14:15-14:30  
Forms of energy/dsmuivweb.it: raccogliere, discutere, innovare  
Simone Ardore  
14:30-15:30  
Il fotovoltaico in Architettura: idee innovative ed esempi realizzati  
Paola Bellio  
15:30-16:00  
Sistemi BIPV (Building Integrated PhotoVolitics): opportunità e problematiche  
Laura Maturi  
16:00-16:15  
Discussione  
16:15-16:30  
Pausa  
16:30-17:00  
Integrazione di solare termico nell'involucro edilizio  
Alessio Giovannardi  
17:00-17:30  
Presentazione di soluzioni progettuali  
Marco Azzurli  
17:30-18:00  
Discussione  
**Destinatari**  
Il seminario è rivolto a progettisti, produttori di componenti di involucro, faccisti, costruttori, ricercatori e a tutti gli interessati all'argomento dell'integrazione di tecnologie solari negli edifici.

**Seminario - Energia solare ed architettura - casi studio nazionali di edifici ed aree urbane**  
23. 09. 2010, ore 14 - 18



Foto: Palms, Pala Innovazione Strategica, Portogruaro, Arch. Marco Acerbis

Il workshop è finalizzato alla presentazione di casi studio di edifici e quartieri che integrino soluzioni per la gestione dell'energia solare sia passive che attive. È stata lanciata una "call for case studies" in occasione della conferenza "Forms of Energy" a Roma nello scorso mese di giugno, in collaborazione con ENEA e la rivista DONUS, per una selezione di casi significativi da presentare all'interno del progetto internazionale "Solar Energy and Architecture", task 41 dell'IEA.

Fig. 3: Flyer of the seminar “Energia solare ed architettura - casi studio nazionali di edifici ed aree urbane” organized in the context of Klimaenergy fair in Bolzano on the 23<sup>rd</sup> of September 2010







**26/01/2012 Klimahouse 2012, Bolzano**  
Quando: 9:00-12:30  
Dove: TIS Innovation Park, via Siemens 19 Bolzano



**Seminario**  
**"FOTOVOLTAICO INTEGRATO: LA SFIDA PER GLI EDIFICI DEL FUTURO"**

**Obiettivi**  
I forti consumi energetici dovuti al settore edile (il 40% dei consumi energetici totali in Europa), hanno spinto la Comunità Europea ad approvare importanti direttive come l'EPBD recast e la RES, al fine di promuovere l'uso di energie rinnovabili negli edifici.  
Secondo tali direttive, infatti, in futuro gli edifici non dovranno solamente puntare sul risparmio energetico ma dovranno anche essere in grado di produrre, da fonte rinnovabile, una parte di energia che essi consumano.  
Il seminario vuole pertanto stimolare un nuovo e più consapevole approccio progettuale e la cooperazione tra i diversi attori del mercato che partecipano alla realizzazione dell'edificio, facendo dialogare il mondo del fotovoltaico e dell'edilizia.

**Agenda**  
**Chairman:** Wolfram Sparber  
**9:00-9:10**  
Saluto e introduzione al seminario  
Wolfram Sparber, EURAC  
**09:10-09:30**  
Fotovoltaico in sito adige: la ricerca applicata al territorio  
Matteo Del Buono, EURAC  
**09:30-10:00**  
BIPV, verso la Zero Energy House  
Niccolò Aste, POLITECNICO DI MILANO  
**10:00-10:20**  
Integrare, risparmiare, produrre. Il prototipo di un nuovo componente di facciata BIPV.  
Laura Maturi, EURAC  
**10:20-10:40**  
Discussione  
**10:40-11:00**  
Coffee break  
**11:00-11:30**  
Moduli BIPV: il punto di vista del produttore  
Mauro Rizzotti, SolarDay  
**11:30-12:00**  
Occasioni internazionali di ricerca: il progetto IEA "Task 41 Solar Energy and Architecture"  
Francesco Frontini, ISAAC-D4CD-SUPSI  
**12:00-12:30**  
Tavola rotonda

**Quota di partecipazione:** €70 (include biglietto ingresso alla Fiera Klimahouse)  
**Destinatari**  
Il seminario è rivolto a progettisti nel campo dell'ingegneria e dell'architettura, aziende, produttori di elementi edili di facciata, coperture, installatori, costruttori, committenti pubblici e privati, centri di ricerca.  
**Organizzazione scientifica:** Istituto per le Energie Rinnovabili, Eurac  
**Responsabili del corso:**  
Ing. Matteo Del Buono, [matteo.delbuono@eurac.edu](mailto:matteo.delbuono@eurac.edu)  
Ing. Laura Maturi, [laura.maturi@eurac.edu](mailto:laura.maturi@eurac.edu)  
**Iscrizioni e informazioni:**  
Francesca Gallinetta, [francesca.gallinetta@eurac.edu](mailto:francesca.gallinetta@eurac.edu)  
0471 055 442

Fig. 4: Flyer of the seminar “FOTOVOLTAICO INTEGRATO: la sfida per gli edifici del futuro” organized in the context of Klimahouse fair in Bolzano on the 26<sup>th</sup> of January 2012

## **FP7 project “Solar Design - On-the-fly alterable thin-film solar modules for design driven applications”**

### **Objective of the project:**

The demand for aesthetically integrated photovoltaic materials is increasing steadily in many industries. A growing number of designers, architects and industrial manufacturers across the world share a common interest in using Photovoltaics (PV) as a decentralized and sustainable source of energy in their product designs. Developing markets such as sustainable housing, temporary building structures, outdoor activities, electro-mobility and mobile computing will drive the demand for decentralized, attractive energy solutions. For solar powered products are customisable shapes, sizes, colours, transparencies or specific electrical properties required, which have a decisive influence on the acceptance on the market. Therefore a new breed of solar technologies is necessary. To achieve this goal new flexible production processes and materials need to be developed.

A novel manufacturing process will enable the adjustment of all properties of a thin-film module on-the-fly and facilitate the production of customized photovoltaic modules with the desired voltage, size and shape. Combined with the material characteristics given by the underlying thin-film solar cell technology a new-breed of design-led, sustainable and decentralised energy solutions can be realized. Furthermore the designer or architect who wants to incorporate solar electricity into his work needs a service environment to be assisted in the creative process. Tools should support the designer in conceiving, planning and producing the solar design products. This project will address the above mentioned challenges by exploring and developing new materials, manufacturing and business processes in PV powered product design and architecture.

### **Project duration:**

1.1.2013- 31.12.2015

### **Project participants:**

Technische Universitaet Wien (Austria), Sunplugged - Solare Energiesysteme GmbH (Austria), Faktor 3 (Denmark), Innovatec Sensorizacion Y Comunicacion (Spain), Studio Itinerante Arquitectura (Spain), Rhp-Technology GmbH & Co



(Austria), Euskal Herriko Elektronika Eta Informazio Gaia (Spain), Fachhochschule Munchen (Germany), Accademia Europea Bolzano (Italy), Universita' Degli Studi Di Milano-Bicocca (Italy), Commissariat a l Energie Atomique et aux Energies Alternatives.

**Further information available at:**

[http://cordis.europa.eu/search/index.cfm?fuseaction=proj.document&PJ\\_RCN=13384701](http://cordis.europa.eu/search/index.cfm?fuseaction=proj.document&PJ_RCN=13384701)